NUMERICAL MODELING OF ICE-STRUCTURE INTERACTION

Annual Progress Report No. 1

September 28, 1984 - September 30, 1985

Research Supported By
MINERALS MANAGEMENT SERVICE
United States Department of the Interior

Contract No. 14-12-0001-30219
Duration of Contract: 09/28/1984 - 09/30/1987
Contract Amount: $110,000
COTR: Mr. Charles E. Smith

Prepared By
Prof. S. Shyam Sunder - Principal Investigator
Prof. Jerome J. Connor - Co-Principal Investigator

Department of Civil Engineering
MASSACHUSETTS INSTITUTE OF TECHNOLOGY
Room 1-274
Cambridge, Massachusetts 02139

September 30, 1985

TABLE OF CONTENTS

1. INTRODUCTION

OBJECTIVE OF PROPOSED WORK

The objective of this project is to systematically investigate using numerical models the mechanics of deformation and progressive failure in ice for the purpose of predicting global forces and local pressures on offshore structures proposed for deployment in the Arctic. The focus is on ice sheets interacting with rigid cylindrical indenters. The project involves the following three major areas of study:

1. Development of constitutive models to characterize the mechanical behavior of sea ice.
2. Development of finite element methods of analysis to account for the simultaneous occurrence of viscous (rate dependent) and fracture behavior in ice, and time varying contact between ice and structure.
3. Numerical solution of ice-structure interaction processes for selected ice features and structural configurations to predict global forces and local pressures.

BACKGROUND

As much as 30-40 percent of the U.S. undiscovered hydrocarbon recoverable reserves, comparable in magnitude to those of the Persian Gulf, are estimated to lie in the Arctic. The extraction of these resources in an economical and safe manner poses many technical challenges to offshore engineering. At the root of these problems is the severe environment created by perennial ice features that impart global forces and local pressures on structures which are several times greater than those from waves

in non-Arctic environments. Typically, two levels of ice loading are considered for design purposes. Global ice loads govern the overall structural geometry and dimensions as well as the foundation design, while local ice pressures are likely to dictate wall thicknesses and local framing, and may well govern structural cost.

Most of the emphasis in research has been on predicting global forces. Only during recent years, as the focus changed from overall feasibility to preliminary and detailed design, has the importance of local pressures emerged. It is widely recognized that significant uncertainties exist in the ice load models in use today and that some design loads may be overestimated by an order of magntidue. Research is necessary to quantify the uncertainties in ice loads and to develop improved load prediction models for the safe and economical design of structures.

Uncertainties in existing ice load models arise primarily from five sources:

- Incomplete modeling of the mechanical behavior of ice, including temperature and fracture effects.
- Empiricism in existing theoretical models resulting from the use of approximate analysis methods.
- Inadequate modeling of the contact forces at the ice-structure interface.
- Neglecting the effect of scale/size on material strength.
- Not accounting for the finiteness of environmental and other forces driving the ice features.

In order to quantify these uncertainties and to better predict global and local ice loads, numerical models are necessary for computer simulation

of ice-structure interaction processes. In contrast to analytical methods, such models can realistically simulate the interaction accounting for spatial-temporal variability in the mechanical behavior of ice and for multiple modes of failure in ice.

The complexity of sea ice behavior is due mainly to:

- Strong dependence on rate of loading, which is spatially and temporally variable in ice features.
- Simultaneous occurrence of ductile, strain-softening, and brittle modes of deformation.
- Pressure sensitivity leading to different strengths in compression and tension (at moderate-to-high rates of loading) and to melting point depression.
- Material anisotropy leading to strength variation by a factor of three.
- Strong dependence on temperature, varying in first year ice from melting point at the water interface to perhaps -50°F at the air interface.
- Strong dependence on internal structure of ice (grain size, fabric, brine volume, salinity, porosity), which is spatially varying particularly in multi-year ice features.

A key aspect in the development of constitutive models is the need for accurate and consistent experimental data on ice, especially to characterize its behavior relating to tensile loading, cyclic loading, multiaxial loading, nucleation and interaction of cracks, material anisotropy, thermal and structural gradients, and fracture toughness. Currently available data is in many cases sufficient to postulate approximate constitutive models.

Numerical simulations can help to establish the importance of more extensive experimentation in quantifying ice-structure interaction processes.

Finite element methods of analysis for simulating ice-structure interaction processes are affected by the following research concerns:

- Rate dependent material behavior with negligible elastic deformation.
- Initiation and propagation of cracks due to fracture.
- Simultaneous occurrence of rate dependent and fracture behavior.
- Adfreeze bond and friction at ice-structure interface.
- Time-varying contact between ice and stucture and between fractured ice features.
- Strain-softening of ice.

STAFFING

Dr. S. Shyam Sunder, Winslow Associate Professor of Civil Engineering, is Principal Investigator for this project while Dr. Jerome J. Connor, Professor of Civil Engineering, is Co-Principal Investigator. In addition, two full-time graduate Research Assistants are participating in this research. They are Mr. S-K Ting, a doctoral student with considerable experience in concrete testing and dynamic behavior of offshore structures (9/1/84 - 8/31/85); Mr. F.S. Chehayeb, a doctoral student whose background is in numerical analysis and finite element methods (9/1/84 -5/31/85); and Mr. Jaideep Ganguly, a master's student with expertise in computational mechanics (6/1/85 - 8/31/85).

2. SUMMARY OF RESEARCH ACTIVITIES

The principal technical developments during this reporting period have been:

(1) The study of sea ice indentation in the creeping mode of deformation.

(2) Initiation of research to study sea ice indentation accounting for fracture behavior.

Specific accomplishments and current research directions are discussed below.

SEA ICE INDENTATION IN THE CREEPING MODE

A study of ice indentation in the creeping mode is important for two reasons: (a) creep is the predominant mode of deformation for artificial islands in the Arctic nearshore region during "breakout" and/or steady indentation conditions occurring in the winter, and (b) stresses, strains, and strainrates within the continuum resulting from creep are necessary to predict the initiation and propagation of cracks when viscous effects influence fracture.

Global and local pressures generated during sea ice indentation in the creeping mode are being studied, accounting for the spatial variation of strainrates. Two methods of analysis are being considered: (a) approximate methods, i.e., upper-bound method and strain path method, and (b) "exact" method based on the finite element method. In both cases, a two-dimensional idealization of the indentation process is considered. In order to provide continuity with previous work, the isotropic, incompressible three-dimensional extension of the uniaxial power-law creep model has been extensively studied. Pressures predicted with this model are being compared

with those from previously published formulas, e.g., API Bul. 2N, Ponter et al., and Bruen & Vivatrat. In addition, ice pressures have been obtained with the approximate methods for a new uniaxial model that accounts for the stress-strain-strainrate behavior of sea ice, including its strain-softening behavior. The current emphasis is on the development of an orthotropic power law creep model for sea ice and its implementation within a finite element analysis framework to quantify the effect of material anisotropy on ice loads.

The key difference in the two approximate methods of analysis is that point stresses within the continuum can be obtained with the strain path method. As a result, local stresses at the ice-structure interface can be estimated, unlike the upper bound method which only yields the global pressure. However, both methods rely on an adequate specificiation of the velocity field in the ice sheet. This is obtained through a combination of theoretical modeling based on fluid mechanics and field ice movement survey data from an artificial island in the Beaufort Sea. In particular, two theoretical kinematic models are considered: one resulting from the superposition of a point source and a uniform flow (Kinematic Model A) that has been proposed by Bruen & Vivatrat; and the other resulting from the superposition of a doublet and a uniform flow (Kinematic Model B).

The results of the approximate methods indicate that:

(a) Kinematic Model B better models the ice movement survey data used here than Kinematic Model A.

(b) In the creeping mode of ice deformation, local ice pressures are of the same order of magnitude as the global pressures.

(c) Under the same conditions, Kinematic Model B, the API model, and the Ponter et al. model predict similar global pressures.

(d) The variation in global pressures for different power-law model parameters (Wang, Sanderson, Ting & Shyam Sunder) is on the order of 30%.

A key finding of the work is that for rate-dependent material models describing sea ice behavior, interface adfreeze and friction stresses can significantly influence both local and global ice pressures. The only realistic way to study these effects is through numerical models based on the finite element method of analysis.

This research has been summarized in a paper entitled "Sea Ice Indentation Accounting for Strain-Rate Variation", published in the proceedings of the ASCE Specialty Conference: ARCTIC '85 - Civil Engineering in the Arctic Offshore held at San Francisco, CA, March 25-27, 1985 (Appendix A).

A finite element formulation for general viscoplastic behavior including creep (nonlinear viscoelasticity) has been developed and implemented in a computer code called DECNEC (Discrete Element Computational NEtwork Controller). A new bi-level solution algorithm has been developed for fast convergence in problems where permanent deformations dominate. This algorithm is based on a secant type iteration on the global equations of motion and a Newton-Raphson (tangent type) iteration, combined with an implicit numerical time integrator, on the rate-dependent constitutive relations at each integration point within an element. A post-processor, originally written at the Lawrence Livermore Laboratory, can be used in conjunction with the computer code to produce graphical displays. The program has the ability to simulate a free or frictional contact between two deformable bodies, i.e., no contact stresses due to adfreeze bond, by defining the interface as a "slideline". The current implementation is a two-dimensional version for plane stress problems. A four noded quadri-

lateral element is currently available. Although an eight-noded quadratic element is often preferred (and may be included in the future), accurate results can and have been obtained with the four-noded element using a finer finite element mesh. An isotropic power-law creep material model was implemented first.

The accuracy of the computer code has been verified in two ways; through the solution of simple test problems, and by comparing the variability in predicted global pressures due to indenter diameter, material model parameters, and ice sheet velocity with that predicted by approximate methods of analysis. In both cases, the numerical solutions are accurate to within specified tolerances typically achievable in finite element analyses.

Numerical simulations have been performed under plane stress conditions to assess the influence of interface adfreeze and friction, material constants for a multi-axial power law creep model, grounded rubble pile, and ice sheet velocity on predicted global forces and local pressures. The results have been compared with those based on approximate methods of analysis. Stress, strainrate, and strain countours have been obtained in addition to the distribution of interface pressures.

The numerical simulations show that:

1. Global forces vary by a factor of 2.5 depending upon whether the interface condition is fixed (infinite adfreeze bond strength), roller, or free (no adfreeze bond strength or interface friction). The fixed condition is about 1.3 times and the free condition about 0.5 times the roller condition.

2. Finite element analysis predictions of global pressure differ from a modified form of the upper bound solution for Kinematic Model B by less than 10% for varying velocity, indenter diameter, and material constants. The modification is necessary since the two-dimensional nature of the kinematic models makes the approximate solutions strictly apply to plane strain conditions, and not to the plane stress condition of interest.

3. The ratio of maximum normal interface pressure to global pressure approximately varies in the range 0.35-1.10 depending upon the interface condition. It is 0.35 for the fixed condition, 0.55 for the roller condition, and 1.10 for the free condition.

4. The maximum (peak) normal interface pressures vary by a factor of 1.26 depending upon the interface condition. The fixed condition is about 0.83 times and the free condition about 1.04 times the roller condition. The maximum interface shear stress for the fixed condition is about 0.81 times the corresponding maximum normal pressure. However, a different boundary value problem involving a smaller contact area, as opposed to contact over half the perimeter in the free condition, will lead to higher interface pressures.

5. Pressure-area curves should be considered as providing the maximum normal interface pressure for a given indenter area of contact (form area), rather than the average integrated normal pressure over a tributary loaded area for a structural component. It is conservative to assume a uniform or rectangular distribution of the local pressure over the indenter area of contact for purposes of design.

6. Tensile stresses, strains and strainrates occur almost all over the ice sheet, and may be the key to explaining fracture behavior during indentation. While biaxial compression and tension states tend to occur for stress on the upstream and downstream sides, respectively, the state of strain is almost always compression-tension. The levels of tensile strain are often sufficient to cause cracking even before steady state creep is reached.

The possible effect of a grounded rubble pile or accreted ice foot on ice pressures was assessed by defining an effective indenter equal to a multiple (2.85) of the structural diameter. This resulted in a factor of 1.97 increase in global force. In the case of a grounded rubble pile, it would be over conservative to consider that all this force is transmitted to the foundation by the structure. On the other hand, the force transmitted to the foundation by the structure would decrease by a factor of 4.14 if both the structure and the grounded rubble pile could transmit a force proportional to the contact area of each with the foundation. This may be reasonable only if the rubble pile is consolidated and grounded fimly in the foundation soil such as in the case of constructed ice packs. Further research is necessary to quantify the level of force that can be directly transmitted to the foundation by a grounded rubble pile.

The numerical simulations also showed that (i) even a factor of two uncertainty in velocity will affect ice pressures only by about 20-30%, and (ii) uncertainties in material constants for an isotropic power law creep model may yield ice pressures that vary by about 15-30%. However, improved material models that include fracture and temperature effects in addition to the transversely isotropic behavior of sheet ice can have a major influence

on ice pressure predictions.

This research has been summarized in a paper entitled "Sea Ice Indentation in the Creeping Mode", published in the proceedings of the 17th Annual Offshore Technology Conference, Houston, TX, May 6-9, 1985 (Appenidx B).

Sea ice, however, is not an isotropic material. Field observations have shown that this type of ice, which is predominantly columnar, has two sources of anisotropy: (a) the c-axis is oriented perpendicular to the axis of crystal growth, and (b) the c-axes of different crystals may show preferred azimuthal orientation in the plane on which they lie. The anisotropy of sea ice strongly influences the macromechanical behavior of first year sheet ice, while its influence on the behavior of multi-year floes, though less well studied, may be less. In first year sheet ice, the first source of anisotropy leads to a ratio of vertical to horizontal stress at constant strainrate varying from 2-5, while the second source of anisotropy leads to stress ratios of 0.25-0.60 at a 45 degree angle to the c-axis and 0.50-0.95 at a 90 degree angle.

Two theoretical models have been developed for predicting indentation pressures assuming the ice sheet to be transversely isotropic. They are: (1) the upper and lower bound, plasticity based solution of Ralston, and (2) the upper bound, power-law creep solution of Vivatrat and Chen. The first model assumes the material behavior to be pressure sensitive while the second formulation is pressure-insensitive. Ralston's model has been incorporated in the API Bulletin 2N guidelines.

A general orthotropic elastic - power law model for sea ice has been developed assuming pressure insensitivity. This model predicts very well the plane strain uniaxial compression tests conducted by Frederking. Further,

experimental data of Richter-Menge et al. on first-year sea ice and that of Hausler on saline ice indicate that sea ice is only moderately pressure sensitive in comparison with pure polycrystalline ice which is highly pressure sensitive.

A finite element method of analysis has been developed for studying the effect of sea ice anisotropy on indentation in the creeping mode. Numerical simulations of ice-structure interaction for a rigid cylindrical indenter under plane stress conditions and a tranversely isotropic version of the above material model showed that:

1. Anisotropy, as represented by the vertical stress ratio varying between 1 and 5, can cause global forces to increase by almost 15 percent depending upon whether the interface condition is fixed (infinite adfreeze bond strength), roller, or free (no adfreeze bond strength or interface friction). The factor is 1.10 for the fixed condition, 1.12 for the roller condition, and 1.13 for the free condition.
2. Anisotropy can cause maximum (peak) normal interface pressures to increase by almost 20 percent depending upon the interface condition. The factor is 1.07 for the fixed condition, 1.16 for the roller condition, and 1.19 for the free condition. The interface shear stress for the fixed condition essentially remains unchanged.
3. Finite element predictions of global forces and local pressures differ from a (approximate) modified upper bound solution by less than about 10 percent for varying velocity, indenter diameter, and material constants.
4. Theoretical predictions of pressure area curves provide an excellent match to measured local pressures.

5. Anisotropy leads to an increase in the size of the compression-compression and tension-tension states of stress on the upstream and downstream sides, respectively, of the indenter.
6. Anisotropy leads to decreasing strains for the roller and free conditions but to almost no change for the fixed condition. This is associated with the increase in lateral confinement near the upstream and downstream tips of the indenter which in turn significantly affects the behavior of transversely isotropic sea ice. Lateral confinement effects are smaller for the fixed condition since the influence of anisotropy is more evenly distributed over the interface due to the presence of interface shear stresses.

The numerical simulations also showed that (i) even a factor of two uncertainty in velocity will affect ice pressures only by about 20-30 percent, and (ii) the uncertainties in pressures resulting from variability in the degree of anisotropy is approximately two or three times less important than the variability in the power law constants in the reference direction.

This research has been summarized in a paper entitled "Anisotropic Sea Ice Indentation in the Creeping Mode" to be presented at the Fifth International Symposium on Offshore Mechanics and Arctic Engineering, Tokyo, Japan, April 13-17, 1986 (Appendix C).

SEA ICE IDENTATION ACCOUNTING FOR FRACTURE

Field observations of sea ice identation on offshore structures in the Arctic show that fracture processes are a major factor in ice-structure interaction.

Fracture manifests itself in terms of tensile cracking and crushing in

compression. Numerical simulations of ice-structure interaction processes in the creeping mode of deformation have indicated that the ice sheet consists of three regimes of principal stresses and strains; i.e., compression-compression, compression-tension, and tension-tension. The latter two regimes occupy a major fraction of the area of the continuum. Since ice is weaker in tension than in compression once cracks occur, accounting for the differing behavior of ice in tension may help to reduce (or limit) ice force predictions significantly.

A constitutive model for sea ice, applicable to monotonic uniaxial loading in both compression and tension, has been proposed and calibrated with experimental data. The stress-strain-strainrate behavior of sea ice has been modelled accounting for strain softening and for fracture which manifests itself in terms of tensile cracking and crushing in compression. The adequacy of the model has been demonstrated by comparison with experimental data obtained under constant strainrate, creep, and constant stressrate conditions. The model has been used to predict the occurrence of first cracks in ice under uniaxial compressive loading. Tensile strains occur under this loading condition as a result of the Poisson effect and/or incompressibility condition. Once cracks occur, the material continues to sustain compressive load but loses its ability to carry tensile loads in the transverse direction if applied. This is a realistic assumption and has been used often in modeling concrete behavior. A limiting tensile strain criterion dependent on the instantaneous strainrate in tension has been used to predict crack nucleation. The results for compressive creep compare very well with the experimental data of Gold.

This research has been summarized in a paper entitled "Ductile to Brittle Transition in Sea Ice Under Uniaxial Loading" presented at the 8th

International Conference on Port and Ocean Engineering under Arctic Conditions, Narssarssuaq, Greenland, September 7-14, 1985 (Appendix D).

There are many aspects of sea ice behavior which are essential for numerically simulating rate-dependent fracture processes. A rate-sensitive damage model for describing the continuum behavior of sea ice under variable loading conditions has been developed for the purpose. The model, based on a nonlinear generalization of the Maxwell differential formulation, is characterized by its ability to (a) decompose the various recoverable and irrecoverable components of strain, (b) represent continuously damaging or strain-softening material behavior in the ductile to brittle transition region, (c) capture the rate-dependent behavior of sea ice with rate-independent model parameters, and (d) describe materially anisotropic mechanical behavior. Further, the model shows strong dependency of the creep and constant strainrate behavior. Calibration of the model is achieved with several independent sets of data, particularly those for first-year sea ice. The following specific conclusions can be drawn from this work:

1. The uniaxial model developed is described by 9 parameters. For comparable models, i.e., those of Sinha and Michel, the number of parameters is 8 and 10 respectively. It must be recognized that Sinha's model does not capture material damage while calibration of Michel's model with experimental data is very limited.
2. All parameters of the model, i.e., 9 for the uniaxial model and 5 for the orthotropic generalization, can be determined from conventional tests conducted on ice. The experimental data base is generally adequate to determine the model parameters. In particular, normalization of the uniaxial strength data for salinity and temperature is a useful way of including test results for pure

polycrystalline ice in model calibration.

3. Material damage that can be described by the continuum model proposed here is significant in the strainrate range of 2×10^{-4} s^{-1} to 10^{-2} s^{-1}. At higher strainrates the presence of microcracks precludes a solely continuum description of ice behavior.
4. According to the proposed model, an ideal creep test does not lead to primary creep strains. However if the finite rise time required to reach the nominal stress in a creep test is taken into account, primary creep strains are simulated by the model. Experimental evidence appears to support this conclusion.
5. The pressure-insensitive orthotropic model predicts very well the plane strain uniaxial compression test results of Frederking. Further, experimental data of Richter-Menge et al. on first-year sea ice and that of Hausler on saline ice indicate that sea ice is only moderately pressure sensitive in comparison with pure polycrystalline ice which is highly pressure-sensitive.

This work has been summarized in a paper entitled "A Rate Sensitive Damage Model for the Continuum Behavior of Sea Ice" in submission for publication in the Cold Regions Science and Technology Journal (Appendix E).

The quantification of fracture behavior requires two criteria, one for initiation and the other for propagation. Fracture initiation can often be well described by a stress or strain criterion. However, two alternative approaches are available to describe fracture propagation: a tensile limiting strain or strength criterion, and a fracture mechanics criterion. In the case when ice is a load bearing system, a fracture mechanics

criterion for cracking is conservative. However, when ice features act as load transmitting systems, a fracture mechanics approach may lead to unconservative results. To account for tensile cracking and compressive fracture in ice and still be conservative in force and pressure predictions, a rate-dependent limiting strain or stress criterion is preferable to the fracture mechanics approach. The former is adopted in this project.

Several approaches are available to account for cracking in a finite element framework. Two of the more common approaches are the discrete cracking models which follow individual discrete cracks between elements and the smeared cracking models which treat the gross (smeared) effect of cracks in an element. The latter approach has been preferred in finite element analyses of concrete since it is computationally far more convenient, and will be adopted in this project. An added advantage is that smeared crack models can be extended easily to allow for an objective energy release rate criterion for fracture propagation. The resulting theory, called the blunt crack band theory, will require the development of an appropriate modification to the rate-dependent limiting tensile stress fracture criterion.

A major research effort is being undertaken to (1) extend the plane stress finite element analysis computer code to incorporate smeared cracking models, and (2) implement the constitutive model in the program. The influence of fracture on both global forces and local pressure will then be quantified through numerical simulations.

3. NOTABLE NON-TECHNICAL ACTIVITIES

PUBLISHED OR SUBMITTED PAPERS

1. Ting, S-K., and Shyam Sunder,, S., "Sea Ice Indentation Accounting for Strain-Rate Variation," Proceedings of the ASCE Specialty Conference: ARCTIC '85 - Civil Engineering in the Arctic Offshore, San Francisco, CA, March 25-27, 1985, pp. 931-941.

2. Chehayeb, F.S., Ting, S-K., Shyam Sunder, S., and Connor, J.J., "Sea Ice Indentation in the Creeping Mode," Proceedings of the 17th Annual Offshore Technology Conference, Houston, TX, May 6-9, 1985, OTC Paper 5056, pp. 329-341. Paper to be simultaneously reviewed for publication in the Journal of Engineering Mechanics, ASCE.

3. Shyam Sunder, S., and Ting, S-K., "Ductile to Brittle Transition in Sea Ice Under Uniaxial Loading," Proceedings of the 8th International Conference on Port and Ocean Engineering Under Arctic Conditions, Narssarssuaq, Greenland, September 6-13, 1985.

4. Shyam Sunder, S., Ganguly, J., and Ting, S-K., "Anisotropic Sea Ice Indentation in the Creeping Mode," Proceedings of 5th International Symposium on Offshore Mechanics and Arctic Engineering, Tokyo, Japan, April 13-18, 1986. Accepted for publication subject to final review of manuscript. Paper to be simultaneously reviewed for publication in the Journal of Energy Resources Technology, ASME.

5. Ting, S-K., and Shyam Sunder, S., "A Rate-Sensitive Damage Model for the Continuum Behavior of Sea Ice," Cold Regions Science and Technology, In Submission, September 1985.

SEMINARS AND TALKS

1. Both Professors S. Shyam Sunder and Jerome J. Connor participated in the Workshop on Breaking Process of Ice Plates held at M.I.T. on November 1-2, 1984. The title of their presentations are listed below:

   a. Professor S. Shyam Sunder: Sea Ice Indentation Accounting for Strain-Rate Variation.

   b. Professor Jerome J. Connor: Numerical Simulation of the Creep Mode in Ice-Structure Interaction.

   Professor S. Shyam Sunder was invited to talk on the same topic at the weekly seminar of the Constructed Facilities Division of the Department

of Civil Engineering at MIT on December 5, 1984.

2. Professor S. Shyam Sunder was invited to talk on "Sea Ice and Its Mechanical Behavior" at a series of seminars on Engineering in the Arctic organized during MIT's Independent Activities Period, January 1985.

PROFESSIONAL ACTIVITIES

1. Professor S. Shyam Sunder was a member of the Conference Committee for ARCTIC '85 - Civil Engineering in the Arctic Offshore Speciality Conference of the ASCE held in San Francisco, March 25-27, 1985. He was also moderator for a session on Probabilistic Methods in Arctic Offshore Engineering.
2. Professor S. Shyam Sunder is Chairman of ASCE's Subcommittee on Arctic and Frontier Regions. This subcommittee operates under the ASCE Structural Division's Committee on Reliability of Offshore Structures. This Committee met at San Francisco in conjunction with item 3.
3. Professor S. Shyam Sunder has been appointed Vice-Chairman of the ASCE Task Committee on Reliability-Based Techniques for Designing Offshore Arctic Structures which is entrusted with the responsibility of producing a monograph bearing the same name. He attended the Task Committee meetings at San Francisco (March 1985) and Houston (May 1985).
4. Professor S. Shyam Sunder attended the Arctic Energy Technologies Workshop organized by the U.S. Department of Energy as part of a recently initiated Arctic and Offshore Research Program. The workshop was held at Morgantown, West Virginia, on November 14-15, 1984. He also participated in the discussion group on Arctic Offshore Structures which had the task of defining the state-of-the-art, identifying technical issues, listing research and development needs, and recommending topics for research support by the U.S. DOE.

5. Professor S. Shyam Sunder participated in a workshop on "Northern Research Needs in Civil Engineering" organized by the University of Alaska, Fairbanks, in Seattle, WA, February 16-17, 1985. The workshop was sponsored by the National Science Foundation to help formulate a five year plan for Arctic research under its mandate for implementing the Arctic Research & Policy Act of 1984. Professor Shyam Sunder contributed to the Committee on Offshore and Coastal Facilities, Design and Construction.

6. Professor Jerome J. Connor is leading the organization of an International Conference on Ice Technology (ITC '96) to be held at MIT, June 10-12, 1986. An international Scientific Advisory Committee has been set up with Professor Connor and Dr. C.A. Brebbia of Southampton University, England, as Co-Chairmen. This conference will be sponsored by the Center for Scientific Excellence in Offshore Engineering at MIT, the Centre for Advanced Engineering Studies at the University of Southampton, and the MIT Sea Grant Program.

7. Professor S. Shyam Sunder attended a meeting of the Ice Mechanics Committee of ASME's Offshore Mechanics and Arctic Engineering Division of which he is a member at Dallas, TX in February 1985.

8. Professor S. Shyam Sunder attended a meeting of ASCE's Committee on Reliability of Offshore Structures of which he is a member at Houston, TX in May 1985.

9. Professor S. Shyam Sunder has been invited to serve as a member of the Conference Committee for POAC '87, the 9th International Conference on Port and Ocean Engineering under Arctic Conditions. He is organizing technical sessions on Numerical Modeling of Ice-Structure Interaction and Probabilistic Methods in Arctic Offshore Engineering.

EXPERIMENTAL DATA FROM U.S. ARMY CRREL:

An informal agreement has been reached with the U.S. Army Cold Regions Research and Engineering Laboratory, Hanover, N.H., Group under the leadership of Dr. Gordon Cox concerning our use of experimental data obtained by them. Under this agreement we can have immediate access to all their experimental data, although any publication by us of their data would in general be dated after they have had an opportunity to publish the results themselves.

4. BUDGET

The total expenditure as of September 30, 1985 is $ 52315.33. This reflects expenditures for the thirteen month period September 1, 1984 (the requested project starting date) through the end of September.

Professor S. Shyam Sunder charged 10% of his salary to the project and 20% to the SOHIO account through January 31, 1985. From February 1, 1985 he charged 20% of his salary to the MMS account, and an equal amount to the SOHIO account. He is charging 0.8 of a month's salary to the account in the Summer, and 1.2 months to the SOHIO account. Since September 1, 1985 he is charging 20% of his salary to the MMS and SOHIO accounts respectively. Professor Jerome J. Connor charged 10% of his salary to the MMS account and 10% to the SOHIO account through May 31, 1985, i.e., the academic year. During this academic year he is charging 10% to the Sohio account.

Mr. S-K Ting and Mr. F.S. Chehayeb were full-time Research Assistants on the project from September 1, 1984 through May 31, 1985. During the Fall Term their salary was charged to the SOHIO account, while during the Spring Term their salary was charged to the MMS account. In the Summer (6/1/85-8/31/85), Mr. S-K Ting and Mr. Jaideep Ganguly were full-time Research Assistants on the project. Their salary was being charged to the SOHIO account. This remains unchanged for the fall term.

SEA ICE INDENTATION ACCOUNTING FOR STRAIN-RATE VARIATION

Seng-Kiong Ting[1] and S. Shyam Sunder[2], A.M., A.S.C.E.

ABSTRACT: Global and local indentation pressures in the creeping mode of sea ice deformation are obtained, accounting for the spatial variation of strain-rates. Two approximate methods of analysis are considered; the upper bound and strain path methods. Theoretically postulated velocity fields required in the analysis are calibrated with field measurements. Sea ice behavior is described by a multi-axial power-law creep model and by the multi-axial extension of a new uniaxial model which accounts for both hardening and softening behavior. Results are compared with previously published indentation formulas.

INTRODUCTION

Two levels of ice loading are typically considered in the design of drilling and production platforms for the Arctic. Global ice pressures govern the overall structural geometry and dimensions as well as the foundation design, while local pressures are likely to dictate wall thicknesses and local framing, and may well govern structural cost. Most of the emphasis on ice force research has been on predicting global forces. Only during recent years, as the focus changed from overall feasibility to preliminary and detailed design, has the importance of local pressures emerged. Peak local pressures may be as high as three times the average global pressure. It is widely recognized that uncertainties exist in ice load prediction models in use today and that in some cases design loads may be overestimated by an order of magnitude.

Uncertainties in existing ice load models arise primarily from four sources: (i) incomplete modeling of the thermomechanical behavior of sea ice, (ii) use of semi-empirical formulations, calibrated without adequate regard for similitude modeling and scale effects, (iii) failure to realistically model the contact forces at the ice-structure interface and the presence of macrocracks, and (iv) not accounting for the finiteness of the environmental forces driving the ice features. Both approximate analytical methods and more rigorous numerical models based on the finite and boundary element methods of analysis can be used to study ice-structure interaction at full scale with realistic models for material and interface behavior.

This paper employs two approximate methods of analysis, the upper bound and strain path methods, to study the problem of sea ice indentation in the creeping mode of deformation, accounting for the spatial variation of strain-rates. This is a problem of concern for artificial islands in the Arctic nearshore region, where "break-out" and/or steady indentation conditions occurring in the winter form a basis for select-

[1]Research Assistant, Department of Civil Engineering, Massachusetts Institute of Technology, Cambridge, MA 02139
[2]Assistant Professor of Civil Engineering, Massachusetts Institute of Technology, Room 1-274, Cambridge, MA 02139

ing design ice loads. The key difference in the two analyses is that point stresses within the continuum can be obtained with the strain path method. As a result, local stresses at the ice-structure interface can be estimated, unlike the upper bound method which only yields the global pressure. However, both methods rely on an adequate specification of the velocity field in the ice sheet. This is obtained through a combination of theoretical modeling based on fluid mechanics and field ice movement survey data from an artificial island in the Beaufort Sea. In particular, two theoretical kinematic models are considered: one resulting from the superposition of a point source and a uniform flow (Kinematic Model A) that has been studied previously (3,9); and the other from the superposition of a doublet and a uniform flow (Kinematic Model B).

An important aspect of the analysis is the specification of the mechanical behavior of sea ice. In order to provide continuity with previous work, the isotropic, incompressible three-dimensional extension of the uniaxial power-law creep model is studied. The predicted global ice pressures are compared with those from previously published formulas (1,8). Finally, a new uniaxial law that models the stress-strain-strainrate behavior of sea ice, including its strain-softening behavior, is presented. The strength-strainrate relationship derived from this new model is used to predict global ice pressures during indentation.

BOUND METHOD VERSUS STRAIN PATH METHOD

An upper bound (conservative) solution to a continuum mechanics problem may be derived by relaxing the statical field equations and boundary conditions, and using velocity fields that satisfy the kinematic constraints for the problem. Applying the principle of virtual work and Drucker's convexity criterion, the upper bound estimate of the global load for incompressible materials may be obtained with (4):

$$\int_V S^*_{ij}\,\dot{\epsilon}^*_{ij}\,dV \geq \int_{S_T} T_i U^*_i\,dS + \int_{S_U} T_i U_i\,dS \qquad (1)$$

where S^*_{ij}, $\dot{\epsilon}^*_{ij}$ and U^*_i are the deviatoric stresses, strain-rates and velocities obtained from an assumed kinematically admissible velocity field. T_i and U_i are the actual surface tractions and velocities.

The upper bound method does not make use of the field equilibrium equations. As such, point stresses in the continuum are unknown. Hill (5) has suggested an approximate method by which octahedral (hydrostatic) stresses can be derived from deviatoric stress gradients using the equilibrium equation. This idea was developed and first applied to deep penetration problems in soil mechanics by Baligh (2), who called it the strain path method.

In applying the strain path method to the ice indentation problem, the major assumption is that the strain and strain-rate field can be obtained from the kinematic conditions with no reference to constitutive relations, equilibrium equations, or statical boundary conditions. This is an approximation and hence the derived stress field is approximate in general. However, the method is computationally very attractive when compared with a detailed finite element analysis. In addition, the method provides valuable insights to the indentation problem which is difficult to obtain from a purely numerical approach.

KINEMATIC MODELING OF ICE SHEET

Theoretical Kinematic Models.-- Kinematic Model A is shown in Fig. 1. The streamline passing through the stagnation point defines the bluff-body, i.e., the region where the oncoming sheet of ice cannot enter. The streamfunction, ψ, and flow velocities, U_r and U_θ, follow from the theory of fluid mechanics and are given by:

$$\psi = -U_o r \sin\theta - U_o a\,\theta \qquad (2)$$

$$U_r = \frac{-1}{r}\frac{\partial\psi}{\partial\theta} = U_o \cos\theta + U_o \frac{a}{r} \qquad (3)$$

$$U_\theta = \frac{\partial\psi}{\partial r} = -U_o \sin\theta \qquad (4)$$

where U_o is the uniform far field velocity. The bluff-body is described by $r=a(\pi-\theta)/\sin\theta$ with the half-width of the body at $r=\infty$ equal to πa. This model assumes that the normal velocity at the ice/bluff-body interface is zero. Even if this is valid, the tangential contact between the moving ice sheet and the half-body could in general be either friction-free or possess finite frictional forces. This imposes a statical boundary condition with which the chosen velocity field may or may not be consistent.

Kinematic Model B is shown in Fig. 2. The bluff-body in this case is a circle of radius, a. This represents flow past a cylindrical indenter with contact at all points on the circumference. The streamfunction and flow velocities are given by:

$$\psi = -U_o r \sin\theta + U_o \frac{a^2}{r}\sin\theta \qquad (5)$$

$$U_r = U_o\left[1 - \frac{a^2}{r^2}\right]\cos\theta \qquad (6)$$

$$U_\theta = -U_o\left[1 + \frac{a^2}{r^2}\right]\sin\theta \qquad (7)$$

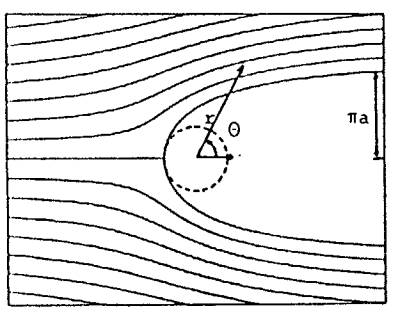

Fig. 1.--Kinematic Model A

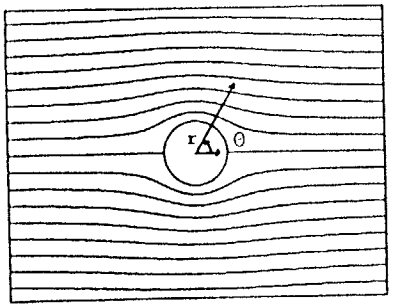

Fig. 2.--Kinematic Model B

Calibration with Field Ice Movement Data.-- The theoretical velocity fields are calibrated with field ice movement data from an artifical island in the Beaufort Sea, obtained over a period of seven weeks during peak winter ice formation. The surveys were carried out at the 39 stations at least once per day, although during high movement events the

surveys were made every 12 hours. The calibration is based on the following three criteria: (a) streamfunction values for a particle at the start and end of the observation period should be equal under steady flow conditions; (b) the average movement rate measured should be approximately equal to the average of the predicted velocities over the observation period; and (c) the measured direction of movement must equal the predicted bearing.

A careful analysis of the data shows that the ice movements downstream and directly at the back of the indenter are of the same order of magnitude as on the upstream side prior to macrocracking, which was observed to occur in a direction perpendicular to the flow on the downstream side. Thus Kinematic Model A which considers no flow within the bluff-body cannot model field conditions prior to macrocracking. Nevertheless, both kinematic models predict relatively accurate streamfunction values over their respective domains of applicability. For Model A the errors vary from less than 1% to as much as 25%, even when there is no macrocrack formation. For Model B, the errors are generally less than 1% in all cases except the case with macrocrack formation. The errors in velocity predictions are much higher for both models. Some stations near the rubble pile surrounding the structure are significantly in error due to an inadequate modeling of the structural geometry, e.g., choice of diameter D. In the cases affected by macrocracking: (a) separate and large regions of the continuum are adequately modeled by both velocity fields, (b) Model B is in general better than Model A. Typical errors in the velocity are on the order of 5% to 10% if the above exceptions are taken into account. The errors in bearing predictions are on the order of 5 to 10 degrees for Kinematic Model B and larger for Model A. The discrepancies, where they are larger, can be explained with arguments similar to that for velocities.

In summary: (a) Kinematic Model A does not adequately model the field data considered here; (b) Kinematic Model B provides a good description of the measured flow field and can be used to explain the observed macrocracking if tensile stresses develop on the downstream side; (c) even after macrocracking, Model B accurately models the upstream flow field; and (d) the transition from creeping behavior to macrocracking occurs for velocities less than 1 ft/hr (85×10^{-6} m s^{-1}).

ICE PRESSURES FOR POWER-LAW CREEP MODEL

The isotropic, incompressible three-dimensional extension of the uniaxial power-law creep leads to the following constitutive model:

$$S_{ij} = \frac{2}{3}\left(\frac{\sigma_o^N}{\dot{\varepsilon}_o}\right)^{\frac{1}{N}} \dot{\varepsilon}_e^{\frac{1}{N}-1} \dot{\varepsilon}_{ij} \qquad (8)$$

where S_{ij} and $\dot{\varepsilon}_{ij}$ are the deviatoric stress and strain-rate tensors, respectively. The effective strain-rate is defined as:

$$\dot{\varepsilon}_e = \left[\frac{2}{3}\dot{\varepsilon}_{ij}\dot{\varepsilon}_{ij}\right]^{1/2} \qquad (9)$$

N is the power-law exponent; σ_o and $\dot{\varepsilon}_o$ are material constants derivable from uniaxial testing of ice. The results presented in this paper are based on the sea ice data of Wang (10).

The basic steps for evaluating stresses using the strain path method are: (a) compute the strain-rate field by differentiating the velocities with respect to the spatial coordinates, (b) evaluate the deviatoric stress field using the constitutive equations, (c) obtain octahedral stresses by spatially integrating the equilibrium equations (the octahedral stresses will in general be path dependent), and (d) estimate the total stresses by summing the deviatoric and octahedral stresses. Then, the local stresses at the ice-structure interface can be obtained from the total stress field, while global pressures may be estimated with the bound method and/or by integration of the local stress field.

The degree of approximation in the estimated stress field can be assessed by comparing the octahedral stresses obtained by integration along different (i.e., orthogonal) paths and by noting the error in satisfying statical boundary conditions. Another way of making the former comparison is to integrate along one path and to compare the magnitude of fictitous body forces required for equilibrium in the orthogonal direction with the stress gradients in that direction.

Ice Pressure Prediction.-- Results from the application of the upper bound and strain path methods of analysis to the chosen kinematic models are presented below.

1. Kinematic Model A: The octahedral stress field for this kinematic model is path independent and as such equilibrium is exactly satisfied. In spite of this, the statical interface boundary conditions may not be satisfied by the model. In addition, the following comments can be made:

(i) the maximum strain-rate occurs at the ice/bluff-body interface at r=a, and is equal to U_o/a,
(ii) the stress field decays as $r^{-2/N}$, which for N=4 is $1/\sqrt{r}$,
(iii) the stress field is axisymmetric, and
(iv) the octahedral stress is zero for a viscoelastic material (N=1).

The global pressure can be estimated by the upper bound method, assuming a frictionless ice/bluff-body interface. This is similar to the case studied by Bruen and Vivatrat (3), and Eq. (1) reduces to:

$$\frac{p}{2at} \leq \frac{N}{\sqrt{3}} \int_0^{\pi} \left(\frac{\sin\theta}{\theta}\right)^{2/N} d\theta \left[\frac{2}{\sqrt{3}} \frac{\sigma_o^N}{\dot{\varepsilon}_o} \frac{U_o}{a}\right]^{\frac{1}{N}} \qquad (9)$$

A second approach to estimating the global pressure involves integration of the local stresses around the bluff-body, i.e.,

$$p = t \int (\sigma_{rr} \cos\theta \, r d\theta + \sigma_{\theta\theta} \sin\theta \, dr) \qquad (10)$$

Using the equation for the bluff-body, Eq. (10) shows that P=0, unlike the upper bound method. If the frictional forces predicted by the strain path method at the ice/bluff-body interface are included in the upper bound method, that method also predicts zero pressure. However, the bound theorems do not apply for the case of friction with relative motion. The implications of this finding are more fully discussed for Kinematic Model B.

2. Kinematic Model B: The octahedral stresses for this kinematic model are path dependent, although for N=1 and N=3 the fictitious body force is zero and equilibrium is satisfied exactly. However, the statical interface boundary conditions will in general not be satisfied. In addition, the following comments can be made:

(i) the maximum strain-rate occurs at the ice-structure interface, r=a, and is equal to $2U_o/a$ or $4U_o/D$,

(ii) the stress field decays as $r^{-3/N}$ (not $r^{-2/N}$ as predicted by Kinematic Model A), which for N=4 is $r^{-3/4}$,
(iii) the stress field is not axisymmetric, and
(iv) the octahedral stress is zero for a viscoelastic material.

The radial stresses downstream of the indenter are tensile and equal in magnitude to the upstream compressive stresses, consistent with the material law. The tangential stresses behave similarly for typical values of N, although their magnitudes could be less than half of the radial stresses. These are principal stresses at $\theta=0$. As such, it is reasonable to expect a macrocrack formation on the downstream side of the indenter. This is indeed borne out by the field ice movement data.

The global pressure can be estimated using the bound method, assuming either a frictionless interface or an interface with frictional stresses predicted by the strain path method. (The method does not strictly apply for the latter case.) The respective expressions, derived from Eq. (1) for D=2a, are:

No friction

$$\frac{P}{Dt} \leq \frac{4\pi}{\sqrt{3}} \frac{N}{N+3} \left[\frac{4}{\sqrt{3}} \frac{\sigma_o^N}{\dot{\epsilon}_o} \frac{2U_o}{D} \right]^{\frac{1}{N}} \qquad (11)$$

With friction

$$\frac{P}{Dt} \leq \sqrt{3}\pi \frac{N-1}{N+3} \left[\frac{4}{\sqrt{3}} \frac{\sigma_o^N}{\dot{\epsilon}_o} \frac{2U_o}{D} \right]^{\frac{1}{N}} \qquad (12)$$

The ratio of Eq. (11) to Eq. (12) is $4N/3(N-1)$, which varies between 1.8 and 2.2 for $2.5 \leq N \leq 4$. Intuitively, interface friction should increase indentation pressures. However, both kinematic models studied here predict a significant decrease in pressure. This is because they are derived from considerations for ideal, non-viscous fluids and as such do not correctly model interface conditions. Even if more exact velocity fields can be postulated theoretically, the available field data does not provide adequate resolution of the ice movements in the immediate vicinity of the structure to calibrate the kinematic models.

Integration of the local stresses around the bluff-body yields another estimate of global pressure accounting for the frictional stresses of the strain path method:

$$\frac{P}{Dt} = \frac{\pi}{2\sqrt{3}} (N-1) \left[\frac{4}{\sqrt{3}} \frac{\sigma_o^N}{\dot{\epsilon}_o} \frac{2U_o}{D} \right]^{\frac{1}{N}} \qquad (13)$$

Both Eqs. (12) and (13) predict zero pressure for a viscoelastic material. Furthermore, the ratio of the upper bound method to Eq. (13) is $6/(N+3)$, which varies between 0.86 and 1.09 for $2.5 \leq N \leq 4$.

For the artificial island considered in this paper the maximum strain-rate just prior to macrocracking is on the order of 10^{-6} s^{-1} or less. The peak local tangential stresses are on the order of 80 psi (0.55 MPa), the peak local radial stresses are on the order of 320 psi (2.2 MPa). The radial stresses are compressive upstream of the indenter and tensile on the downstream side, and are distributed in a cosinusoidal fashion. The typical order of magnitude value for the global pressure obtained with Eq. (13) is about 350 psi (2.4 MPa). A key inference here is that the local and global pressures are on the same order of magnitude. If instead Eq. (11) is used to estimate the global pressure, the peak local pressure becomes approximately half the global pressure.

Table 1.--Comparison of Average Global Pressures for Power-Law Creep with N=4 and Average Strain-Rate of $U_o/2D$

Model	Constraints	ϕ
API	Plane Strain	4.12
	Plane Stress	3.13
Ponter et al. (1983)	Plane Strain	3.64
	Plane Stress	1.85
Model A	D = 2πa	3.22
	D = 2a	7.60
Model B		7.22

Comparison with Other Ice Pressure Formulas.-- Average global pressures during sea ice indentation can be estimated using any one of the many predictive models available in the literature. In this study, the global pressures predicted by Kinematic Models A and B, neglecting interface frictional stresses, are compared with the models of API (1) and Ponter et al. (8). The general form of all these models is given by:

$$\frac{P}{Dt} = \phi \, \sigma(\dot{\epsilon}_a) \qquad (14)$$

where ϕ is a constant depending in general on N, and $\sigma(\dot{\epsilon}_a)$ is the uniaxial strength of ice evaluated at some average strain-rate, $\dot{\epsilon}_a = U_o/(\phi \Psi D)$ with Ψ being a second constant. In order to compare the various formulations, $\phi\Psi$ is assumed equal to two as suggested by API (1) and the comparison can therefore be based on the parameter ϕ.

The values of ϕ predicted by the four formulations for a power-law creep model with N=4 is given in Table 1. At first glance the numbers seem highly scattered, varying from 1.85 to 7.60. However, there are important differences among the models. The first two formulations apply for a flat indenter with ice pressures being allowed to develop only on the upstream side. For the API model, the sea ice is assumed columnar and the contact factor is set to one. In Ponter et al.'s model, a correction factor of 1.1 is applied to ϕ to make results consistent with N=4. In Kinematic Model A, the problem geometry (Fig. 1) is different from the other models and the choice of indenter diameter is subjective. If the indenter diameter is chosen as $2\pi a$, ϕ is about 42% of that for D=2a. In the former case the indenter is located far away ($r \to \infty$) from the tip of the bluff-body with the region in between consisting of inert ice, while in the latter case the indenter is located at the tip of the bluff-body with the inert region downstream of the indenter. Field data on deformation patterns considered here indicate that both assumptions may be unrealistic. The ϕ factor for Model B is based on a circular indenter with compressive and tensile stresses on the upstream and downstream sides respectively. This is more representative of actual field conditions prior to breakout.

If the API and Ponter et al. models are extended to account for downstream tensile stresses, the ϕ factors would probably be twice as much since for the problem and material model considered (a) tensile and compressive strengths are equal, and (b) stress levels are equal but opposite in sign on the upstream and downstream sides. Then, ϕ for the

API model would vary between 6.3 and 8.2 while for Ponter et al.'s it would vary between 3.7 and 7.3. For the artificial island considered earlier and other typical artificial islands with D/t>20, the behavior is closer to a plane stress condition. Both Model B and the API model tend to predict similar global pressures under this scenario.

ICE PRESSURES FOR NEW UNIAXIAL MODEL

The uniaxial behavior of sea ice has often been idealized with the power-law creep formulation. This model relates the strength of ice to the strain-rate, and as such is an incomplete description of the stress-strain-strainrate characteristics of the material. Several investigators have proposed more complete uniaxial models, some empirical in nature, that seem to be able to reproduce the post-peak decrease of stress in ice under constant strain-rate conditions. However, most of these models have not been fit to any specific data on sea ice. In addition, since they represent behavior only under constant strain-rate conditions, it is difficult to extend the models to other loading conditions such as constant stress (creep) and stress-rates.

A phenomenological approach based on simple thermorheological models is used here to develop a new uniaxial model, which is then calibrated with the sea ice data of Wang (10). This model applies equally well for constant stress-rate and creep conditions. In addition, under constant strain-rate conditions the strain at peak stress is a function of the strain-rate. The strength-strainrate relationship derived from the new uniaxial model is extended for multi-axial stress states and then applied to obtain indentation pressures.

New Uniaxial Constitutive Model.-- The new uniaxial constitutive model is based on the concept that the strength of an ice specimen is affected simultaneously by work or strain hardening and work softening or recovery. The latter phenomenon may occur due to recrystallization or micro-voids formation. This concept was used by Orowan (7) for examining steady state creep, and may be expressed as:

$$\frac{d\sigma}{dt} = \frac{\partial \sigma}{\partial \varepsilon} \dot{\varepsilon} + \frac{\partial \sigma}{\partial t} \qquad (15)$$

where $h=\partial\sigma/\partial\varepsilon$ is the coefficient of work hardening and $r=-\partial\sigma/\partial t$ is the rate of recovery. The parameter h is generally modelled as (6):

$$h = A \dot{\varepsilon}^{1/N} \exp(-M\varepsilon) \qquad (16)$$

where Q is the activation energy and R is the universal gas constant; A, N and M are the parameters of the equation. Due to a lack of general models for work softening, it is assumed here that the form is similar to that for work hardening:

$$r = B \dot{\varepsilon}^{1/K} \exp(-L\varepsilon) \qquad (17)$$

with B, K and L being the parameters of the equation. Substituting Eqs. (16) and (17) into Eq. (15) yields after integration (assuming $\dot{\varepsilon}$ and T are constant with $\varepsilon=\dot{\varepsilon}t$ and $\sigma=0$ at t=0):

$$\sigma = \left[\frac{A}{M} \dot{\varepsilon}^{1/N} \left[1-\exp(-M\varepsilon)\right] - \frac{B}{L} \dot{\varepsilon}^{1/K-1} \left[1-\exp(-L\varepsilon)\right] \right] \qquad (18)$$

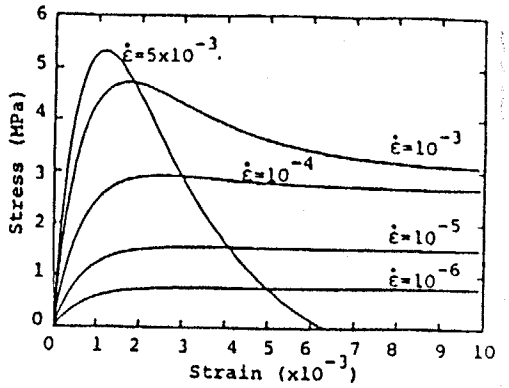

Fig. 3.--Stress-Strain Curves for Constant Strain-Rate Using New Model

The parameters of Eq. (18) obtained from Wang's (10) experimental data are: A=114025 MPa $s^{1/3}$, B=217408 MPa $s^{2/3}$, M=1411.2, L=430, N=3 and K=0.6. The stress-strain plots for the new model are shown in Fig. 3.

The two plots of the stress-strain behavior for $\dot{\varepsilon}=10^{-3}$ s^{-1} shown in Ref. 10 are vastly different, one shows strain softening behavior with resultant residual strength, while in the other the stress reduces to zero very sharply for strains exceeding the peak stress. The new model (Fig. 3) reflects this behavior for strain-rates of 10^{-2} - 10^{-3} s^{-1}, suggesting that the stress-strain behavior is very sensitive to strain-rate in this region.

Ice Pressure Prediction.-- The uniaxial model developed here relates the stress to strain and strain-rate. The strength-strainrate relationship derived from the model is extended for multi-axial stress states under the assumptions of isotropy and incompressibility made earlier for the power-law creep model. These assumptions are reasonable for the strain-rates of interest in this paper. Ice pressures obtained with this model can then be compared with the results for the power-law creep model. A general analysis strategy to incorporate the effect of strain and temperature is currently under development.

The strength-strainrate relationship for the new uniaxial model is plotted in Fig. 4 and compared with the power-law creep model. Notice that the new model predicts lower strength at strain-rates less than 10^{-5} s^{-1}, consistent with experimental data which suggests that the effective power-law exponent is an increasing function of strain-rate.

The new constitutive model can be viewed as the superposition of three power-law models of the type considered in the previous section and as such the local pressures will be distributed similarly. A typical order of magnitude global pressure for the artificial island considered here, based on Kinematic Model B and Eq. (13), is about 250 psi (1.7 MPa). This is only 70% of the pressure predicted by the power-law creep model. The 30% reduction in pressure is significant, although this reduces to approximately 10% when using Eq. (11). The pressure in the latter case is about 480 psi (3.3 MPa).

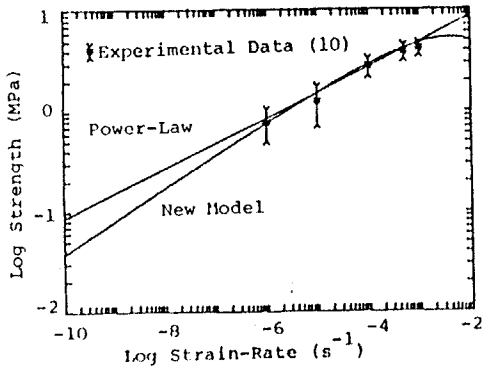

Fig. 4.--Comparison of Uniaxial Strength-Strainrate Relations

CONCLUSIONS

This study of global and local indentation pressures in the creeping mode of sea ice deformation, accounting for the spatial variation of strain-rates, leads to the following specific conclusions:

1. Kinematic Model B better models the ice movement survey data obtained from an artificial island in the Beaufort Sea than Kinematic Model A.
2. In the creeping mode of ice deformation, the local ice pressures are of the same order of magnitude as or lower than the global pressures. Even if the global pressures are reduced, e.g., by a factor of three, to account for scale (fracturing) effects, the local pressures based on the strain path method will only be 1.5 (and not three) times the upper bound global pressure neglecting interface friction.
3. Under essentially plane stress conditions, Kinematic Model B and the API model (1) predict similar global pressures. For a typical artificial island just prior to break-out with ice movements of less than 1 ft/hr (85×10^{-6} m s^{-1}), Model B predicts a pressure (neglecting interface friction) of approximately 530 psi (3.7 MPa).
4. The constitutive law based on the new uniaxial model predicts global pressures that are lower than that from the power-law creep model. For a typical artificial island, this reduction can be as much as 10-30 percent.

A key finding of this work is that for the rate-dependent material models describing sea ice behavior, interface adfreeze and friction stresses may significantly influence both local and global ice pressures. This has major economic consequences for platform design. Incorporation of these "non-conservative" stresses within the bound method may yield more accurate global ice pressures, but the solutions will not necessarily be upper bounds. More exact estimates of both local and global ice pressures using the strain path method may be

obtained by postulating kinematic models that more correctly model the interface conditions. However, currently available field data does not provide adequate resolution of the ice movements in the immediate vicinity of the structure to calibrate such models. In conclusion, it appears that the development of numerical models based on the finite and boundary element methods of analysis is necessary for more realistically studying ice-structure interaction problems where both global and local pressures are of interest.

ACKNOWLEDGEMENTS

The authors would like to thank Professors Jerome J. Connor and Mohsen M. Baligh for stimulating discussions during the course of this work. This research is funded by The Standard Oil Company (Ohio) through MIT's Center for Scientific Excellence in Offshore Engineering, and cosponsored by the U.S. Department of the Interior, Minerals Management Service.

APPENDIX.--REFERENCES

1. API Bulletin on Planning, Designing, and Constructing Fixed Offshore Structures in Ice Environments, Bul. 2N, First Edition, January, 1982.
2. Baligh, M.M., "The Strain Path Method in Geotechnical Engineering," Research Report R84-01, No. 761, Department of Civil Engineering, Massachusetts Institute of Technology, Cambridge, Massachusetts, 1984, 55p.
3. Bruen, F.J., and Vivatrat, V., "Ice Force Prediction Based on Strain-Rate Field," Third International Symposium on Offshore Mechanics and Arctic Engineering, New Orleans, LA, February 12-16, 1984, 7p.
4. Hill, R., "The Mathematical Theory of Plasticity," Oxford University Press, London, 1950, 355 p.
5. Hill, R., "A General Method of Analysis for Metal-Working Process," Journal of the Mechanics and Physics of Solids, Vol. 11, 1963, pp. 305-326.
6. Meyers, M.A. and Chawla, K.K., "Mechanical Metallurgy - Principles and Applications," Prentice-Hall Inc., Englewood Cliffs, New Jersey, 1984, 761 p.
7. Orowan, E. and Scott, J.W., "The Creep of Metals," Journal of Iron and Steel Institute, Vol. 54, 1946, p. 45.
8. Ponter, A.R.S. et al., "The Force Exerted by a Moving Ice Sheet on an Offshore Structure: Part I The Creep Mode," Cold Regions Science and Technology, Vol. 8, 1983, pp. 109-118.
9. Vivatrat, V., Chen, V., and Bruen, F.J., "Ice Load Prediction for Arctic Nearshore Zone," Brian Watt Associates, Inc., Texas, 1984, 26p.
10. Wang, Y.S., "Rate-Dependent Stress-Strain Relationship for Sea Ice," First International Symposium on Offshore Mechanics and Arctic Engineering, New Orleans, LA, 1982, pp. 243-248.

OTC 5056

Sea Ice Indentation in the Creeping Mode

by F.S. Chehayeb, S.K. Ting, S. Shyam Sunder, and J.J. Connor, *Massachusetts Inst. of Technology*

ABSTRACT

A finite element method of analysis is developed and applied to the study of global and local pressures generated on a cylindrical indenter during sea ice deformations in the creeping mode. Numerical simulations are performed under plane stress conditions to assess the influence of interface adfreeze and friction, material constants for a multi-axial power-law creep model, indenter diameter, and ice sheet velocity on predicted pressures. The results are compared with those based on approximate methods of analysis. Stress, strainrate and strain contours are obtained in addition to the distribution of interface pressures.

INTRODUCTION

Extraction of hydrocarbons from the Arctic offshore requires the design of drilling and production platforms to withstand loading generated by perennial ice features. Two levels of loading are typically considered; Global ice forces govern the overall structural geometry and dimensions as well as the foundation design while local pressures are likely to dictate wall thicknesses and local framing, and may well govern structural cost.

The interaction of an ice sheet with a vertically faced (and usually rigid) indenter is an important loading condition for cylindrical structures and for conical structures with grounded rubble pile or accreted ice foot. In general, this indentation phenomenon is characterized by the simultaneous occurrence of viscous (rate-dependent) and fracture behavior.

Several theoretical models based on approximate methods of analysis that idealize the ice sheet as a continuum have been proposed for predicting global ice forces. These include: (1) the upper and lower bound, plasticity type solutions of Michel and Toussaint[1], Croasdale et al.[2], and Ralston[3], (2) the reference stress, power law creep solution of Ponter et al.[4], and (3) the upper bound, power law creep solutions of Bruen, Vivatrat and Chen[5,6], and Ting and Shyam Sunder[7]. The plasticity type models require empirical definition of an average strain rate measure to account for the viscous behavior of ice, the reference stress approach accounts for the effect of variability in material constants in an approximate sense, and the upper bound, power law creep solutions require accurate specification of ice sheet kinematics. No equivalent theoretical models exist for the case where either pure (linear elastic) fracture or combined viscous and fracture effects dominate.

Theoretical predictions of interface pressures are not generally available. However, Ting and Shyam Sunder[7] have applied the (approximate) strain path method of analysis, originally developed for deep penetration problems in soil mechanics by Baligh[8], to study interface pressures during plane strain indentation. Their results for a power law creep model of ice showed that normal interface pressures may be 0.5-1 times the global pressure. They also found that interface adfreeze and friction stresses can significantly influence ice pressures.

The "continuum" predictions of ice pressures may in many cases be too high by a factor of 2-10. Four major factors can explain this uncertainty: (i) incomplete modeling of the mechanical behavior of ice, including temperature and fracture effects, (ii) empiricism in the theoretical models resulting from the use of approximate analysis methods, (iii) inadequate modeling of contact forces at the ice-structure interface, and (iv) ignoring the effects of size on material strength.

A study of ice indentation in the creeping mode is important for two reasons: (a) creep is the predominant mode of deformation for artificial islands in the Arctic nearshore region during "breakout" and/or steady indentation conditions occurring in the winter, and (b) stresses, strains, and strainrates within the continuum resulting from creep are necessary to predict the initiation and possibly even the propagation of cracks when viscous effects influence fracture behavior. In a recent paper, Shyam Sunder and Ting[9] have shown that a limiting tensile strain criterion dependent on the instantaneous strainrate can explain crack initiation in ice. Furthermore, for load transmitting systems such as ice features (as opposed to load bearing structural systems) the use of this criterion for fracture propagation is likely to be

References and illustrations at end of paper.

conservative when compared to a classical fracture mechanics approach. This is because the latter considers only the propagation of pre-existing cracks with a given distribution of sizes, while the former may be used to predict both the initiation and propagation of cracks in a material originally in virgin (flawless) form.

This paper is concerned with the development and application of a finite element method of analysis for studying global and local pressures generated on a rigid, cylindrical indenter during sea ice deformations in the creeping mode. Numerical simulations are performed under plane stress conditions to assess the influence of interface adfreeze and friction, material constants for a multi-axial power law creep model, indenter diameter, and ice sheet velocity on predicted pressures. The results are compared with those based on approximate methods of analysis. Stress, strainrate, and strain contours are obtained in addition to the distribution of interface pressures.

FINITE ELEMENT FORMULATION

Governing Equations.-- For general viscoplastic behavior, which includes creep, it is convenient to work with time derivatives of the governing equations for a solid. The weighted equilibrium-rate equation which forms the basis for the finite element displacement method is then given by:

$$\int \underline{B}^T \dot{\underline{\sigma}}\, dV = \dot{\underline{P}} \qquad (1)$$

where $\underline{B}$ is the strainrate - nodal velocity transformation matrix derived from the chosen displacement expansion for the finite element, i.e.,

$$\dot{\underline{\varepsilon}} = \underline{B}\, \dot{\underline{U}} \qquad (2)$$

The strainrate vector consists of two components, one due to elastic strains, characterized by the compliance matrix $\underline{C}$ and its inverse the rigidity matrix $\underline{D}$, and the other due to inelastic (irrecoverable) strains.

$$\dot{\underline{\varepsilon}} = \underline{C}\, \dot{\underline{\sigma}} + \dot{\underline{\varepsilon}}_I \qquad (3)$$

where I refers to the inelastic strains. For linearly elastic behavior, the compliance and rigidity matrices do not vary in time. The inelastic component may consist of rate-independent plastic strains, permanent creep (nonlinear viscoelastic) strains, and/or viscoplastic strains. In general, this may be expressed as:

$$\dot{\underline{\varepsilon}}_I = f(\underline{\sigma}, \dot{\underline{\sigma}}, \underline{\varepsilon}_I, T) \qquad (4)$$

where T allows for temperature dependence.

Combining Eqs. (1)-(3) and defining $\underline{K}$ as the elastic stiffness matrix of the element leads to the element equilibrium equation:

$$\underline{K}\, \dot{\underline{U}} = \dot{\underline{P}} + \int \underline{B}^T \underline{D}\, \dot{\underline{\varepsilon}}_I\, dV \qquad (5)$$

and the element stressrate - nodal velocity relations:

$$\dot{\underline{\sigma}} = \underline{D}\, \underline{B}\, \dot{\underline{U}} - \underline{D}\, \dot{\underline{\varepsilon}}_I \qquad (6)$$

The global stiffness matrix, $\underline{K}_G$, is obtained from Eq. (5) using conventional procedures.

Material Modeling.-- In this paper, sea ice is treated as a linearly elastic plus creeping material. Thus, $\underline{K}$ is the element stiffness matrix usually employed in linear elastic analyses. Under uniaxial (compressive) loading conditions, creep in ice is generally expressed in terms of a power law[10], i.e.,

$$\dot{\varepsilon}_c = a\, \sigma^N \qquad (7)$$

where a and N are constants with the temperature dependence being included in the parameter a following an Arrhenius activation energy law.

The multi-axial generalization of the creep law as proposed by Palmer[11] is based on assuming incompressibility, which is valid for ice as long as the hydrostatic stress is not too high such as under plane stress conditions. It suffices then to relate the creep strainrate tensor to the deviatoric stress tensor. This is accomplished by assuming that the two tensors are directly proportional to one another as given by the associative flow rule:

$$\dot{\underline{\varepsilon}}_c = \lambda\, \underline{S} \qquad (8)$$

where λ is a scalar parameter and $\underline{S}$ is a vector containing the deviatoric stresses. For a von Mises (isotropic) yielding surface, λ is the ratio of the octahedral shear strainrate to the octahedral shear stress. For the uniaxial power law given in Eq. (7), it follows that:

$$\lambda = 3/2\, a\, \sigma_e^{N-1} \qquad (9)$$

with the effective stress measure σ_e defined as:

$$\sigma_e = (3/2\, S_{ij} S_{ij})^{1/2} \qquad (10)$$

Given the stress vector, the deviatoric stresses may be obtained by subtracting the hydrostatic stress, i.e., $\underline{S} = \underline{G}\underline{\sigma}$ in matrix form. Then applying Eqs. (10), (9), and (8) in succession leads to the creep strainrate vector.

Solution Algorithm.-- An iterative solution algorithm is developed to solve a pseudo-force form of the nonlinear governing equations given in Eqs. (5) and (6). Although the algorithm has been applied to the specific material model presented above, it can be easily generalized to account for material anisotropy and for cracking based on the limiting tensile strain criterion. For purposes of discussion, attention is focussed at the element rather than the global level. At first the governing equations are integrated in time between t_i and t_{i+1} to yield:

$$\underline{K}(\underline{U}_{i+1} - \underline{U}_i) = \underline{P}_{i+1} - \underline{P}_i + \int \underline{B}^T \underline{D}(\underline{\varepsilon}_{c,i+1} - \underline{\varepsilon}_{c,i})\, dV \qquad (11)$$

$$\underline{\sigma}_{i+1} - \underline{\sigma}_i = \underline{D}\, \underline{B}(\underline{U}_{i+1} - \underline{U}_i) - \underline{D}(\underline{\varepsilon}_{c,i+1} - \underline{\varepsilon}_{c,i}) \qquad (12)$$

Creep strains which appear in both the equations are nonlinear functions of stress since λ in Eq. (8) is not a constant. A two-level interative algorithm is used to solve these equations for each new time step t_{i+1}. The key steps in the solution algorithm are as follows:

1. Compute the displacement increments from (the global form of) Eq. (11) for the given loading vector. In the first iteration on the equation, the incremental creep strains are assumed to be zero.

2. Compute the incremental stresses and incremental creep strains from Eq. (12) for the displacement increments obtained in step 1 using the iterative algorithm (lower-level iteration in k) discussed below. In the first iteration on this equation assume the incremental creep strains to be zero.

3. Return to step 1 and iterate on Eq. (11) (higher-level iteration in j) using the incremental creep strains obtained in step 2 until convergence is achieved. Two convergence criteria are used: (a) ratio of norm of displacement increment vector to norm of displacement vector at given time step is less-than-or-equal-to 0.001; and (b) absolute value of energy norm is less-than-or-equal-to 0.001, i.e.,

$$\left| \frac{\Delta \underline{P}^j \cdot \Delta \underline{U}^j}{\Delta \underline{P}^o \cdot \Delta \underline{U}^o} \right| \leq 0.001 \qquad (13)$$

where $\Delta \underline{P}$ refers to the entire right hand side of Eq. (11). The evaluation of the integral defining the inelastic load vector is based on a Gaussian quadrature formula (for a four-noded quadrilateral element, four integration points are used). Typically, 4-6 iterations are required for convergence at the higher-level.

The evaluation of the incremental stresses and incremental creep strains in step 2 requires the simultaneous consideration of Eqs. (12) and (8). In addition to a nonlinear equation solver, a numerical time integrator is needed to obtain results. Previous investigators[12,13,14] have used a simple successive substitution type algorithm to decouple the two equations. This involves the use of incremental creep strains from iteration k to evaluate the incremental stresses for iteration k+1 using Eq. (12). The incremental creep strains for iteration k+1 are then evaluated with the α-method of numerical time integration which expresses Eq. (8) as:

$$(\underline{\varepsilon}_{c,i+1} - \underline{\varepsilon}_{c,i}) = \lambda_\alpha \, \underline{S}_\alpha \, (t_{i+1} - t_i) \qquad (14)$$

where $\underline{S}_\alpha$ is a weighted average of the deviatoric stress vector in the time interval $(t_{i+1} - t_i)$ and λ_α is derived from a similar weighting on the effective stress, i.e.,

$$\underline{S}_\alpha = (1-\alpha) \, \underline{S}_i + \alpha \, \underline{S}_{i+1} \qquad (15)$$

Typical values of α lie in the range 0-1. A value of α equal to zero yields the forward (explicit) Euler method, while α equal to one yields the backward (implicit) Euler method. Both these formulas are first-order accurate (for linear problems in which λ is a constant, and not dependent on the effective stress), although the actual error of the backward formula is considerably less than that of the forward formula assuming that the former is iterated up to convergence. A value of α equal to 0.5 yields the well-known trapezoidal rule, also called the improved Euler's method since it is second-order accurate. A linear stability analysis of the α-method shows that it is unconditionally stable only for $\alpha \geq 0.5$.

For quasi-elastic problems in which creep deformations are not dominant, experience has shown that for small time increments $\alpha=0.5$ is more accurate, and that for large time increments $\alpha=1$ is to be preferred. However for creep dominant problems of concern here, the convergence rate slows down considerably for highly stressed elements when $\alpha=1$ is used, and more than 10-12 iterations may be needed for convergence at the lower-level. This is computationally unattractive since iteration is necessary at each integration point within an element (four in the case of a quadrilateral element) and highly stressed elements may occur often in a large finite element grid, e.g., consisting 250 elements.

Convergence is accelerated here by developing a lower-level algorithm that combines a Newton-Raphson or tangent type iteration with the α-method. The resulting equations are listed below:

$$\left[\underline{I} + \underline{D} \left[\frac{\partial \Delta \underline{\varepsilon}_c}{\partial \underline{\sigma}}\right]^k_{i+1}\right] \underline{\sigma}^{k+1}_{i+1} = \underline{\sigma}_i + \underline{D}\left[\underline{B}\Delta \underline{U} - \Delta \underline{\varepsilon}^k_c\right] + \underline{D}\left[\frac{\partial \Delta \underline{\varepsilon}_c}{\partial \underline{\sigma}}\right]^k_{i+1} \underline{\sigma}^k_{i+1} \qquad (16)$$

where $\Delta \underline{\varepsilon}_c{}^k$ is obtained by applying Eq. (14) after obtaining the stress quantities at iteration k, and similiarly:

$$\left[\frac{\partial \Delta \underline{\varepsilon}_c}{\partial \underline{\sigma}}\right]^k_{i+1} = \Delta t \; \alpha \left[\lambda \underline{I} + \frac{3}{2} \sigma_e^{-1} \frac{\partial \lambda}{\partial \sigma_e} \underline{S} \, \underline{S}^T\right]^k_\alpha \underline{G} \qquad (17)$$

For the given material model, $\partial\lambda/\partial\sigma_e$ can be obtained from Eq. (9). Notice that the algorithm becomes explicit for $\alpha=0$ as it should and no iteration is required. Convergence is defined to occur when the maximum absolute value of the relative change in point stresses between iteration k and k+1 is less-than-or-equal-to 0.001. Iteration is also stopped if the actual point stresses are zero at k and their maximum absolute value is less-than-or-equal-to 0.001 at k+1. Application of this iterative scheme with $\alpha=1$ shows that convergence is typically obtained in 4 iterations instead of more than 10-12, thereby cutting down the computational effort by approximately 50% if the increased computational effort per iteration is accounted for.

Computer Implementation.-- The finite element analysis algorithm has been implemented in a computer code called DECNEC (Discrete Element Computational NEtwork Controller). Data input is simplified by the use of a pre-processor specially written for the program. A post-processor called ORION, originally developed at the Lawrence Livermore Laboratory, can produce graphical display of stress, strain, and strainrate contours as well as interface pressure distributions.

The current implementation is a two-dimensional version for plane stress problems, while the development of a plane strain version is underway. A four-noded quadrilateral element is currently available. Although an eight-noded quadratic element is often preferred (and will be included in the future), accurate results can and have been obtained with the four-noded element using a finer finite element mesh. The program has the ability to simulate a free or frictional contact between two deformable bodies, i.e., no contact stresses due to adfreeze bond, by defining the interface as a "slideline".

Code Verification.-- The accuracy of the computer code has been verified in two ways; through the solution of simple test problems, and by comparing (see subsequent section) the variability in predicted global pressures due to indenter diameter, material model parameters, and ice sheet velocity with that predicted by approximate methods of analysis. In both cases, the numerical solutions are accurate to within specified tolerances typically achievable in finite element analyses.

One of the test problems, for example, considers a two-dimensional rectangular element subjected to a uniform compressive stress ($\sigma_z = -\sigma$) normal to one of its sides and with normal movement constrained on the other three sides (Fig. 1). A simple analysis shows that for the given material model, the lateral stress (σ_y) is given by:

$$\sigma_y = -\sigma_z/2 \left[(1-2\nu)e^{-2/3E\lambda t} - 1\right] \qquad (18)$$

where ν is the Poisson's ratio and E is the Young's modulus. This solution is valid for a constant value of λ, which in an average sense may be defined as its value at steady state. Under steady state conditions, i.e., large t, Eq. (18) shows that the lateral stress is compressive and equal to half the z-stress. Furthermore, the z-strainrate is the creep strainrate and equals $-1/2\ \lambda\sigma$ while the lateral strainrate is zero as it should be for the given boundary conditions. Application of DECNEC using two finite elements verified this analysis.

NUMERICAL SIMULATIONS

Description of Case Studies.-- Numerical simulations are performed for the seven cases identified in Table 1. The objectives of the first three simulations are to quantify the effect of interface adfreeze and friction on predicted indentation pressures. The fixed condition provides an upper bound solution since the ice-structure interface is considered to be infinitely strong. The free condition corresponds to no adfreeze bond and interface friction, while the roller condition provides an intermediate solution. The next two simulations study the influence of ice sheet velocity on pressures. The chosen base velocity of 0.195 m/hr corresponds to the recorded maximum average velocity over a twelve-hour period just prior to "breakout" (macrocracking) for an artificial island in the Beaufort Sea. The sixth simulation attempts to quantify the effect of a grounded rubble pile or an accreted ice foot on ice pressures by defining a larger effective indenter diameter (2.85 times the structural diameter). The final simulation studies the effect of variability in constants defining the material model on ice pressures. Two sets of parameters for sea ice based on the work of Sanderson[15] and Wang[16], respectively, are considered: N=3, $a=2.125\times10^{-6}$ (MPa)$^{-3}s^{-1}$; and N=4, $a=1.848\times10^{-6}$ (MPa)$^{-4}s^{-1}$. The elastic constants, which have negligible influence on the steady state solutions, are taken to be E=9.5 GPa and ν=0.3.

Numerical Implementation.-- Prior to carrying out the above studies, it is necessary to set up the finite element mesh, specify a time increment for the analysis, and define the excitation.

The finite element mesh is defined such that (i) the aspect ratio of each element is as close to one as possible, (ii) the scatter in stresses predicted by adjacent elements at their commmon boundary is less than 10%, and (iii) the boundary of the ice sheet is a circle whose extent is sufficient to simulate the infinite medium. The first criterion is maintained by the pre-processor which makes the radial length of each element equal to its arc length nearer the indenter. The second criterion is controlled by specifying the number of radial segments into which a quarter-plane may be divided. A value of nine is considered here (for an eight-noded element five or six may suffice). The last criterion is also implemented by the pre-processor which makes the radius of the circular boundary equal to 9.5 times the indenter radius. Accounting for symmetry about the z-axis, the above discretization leads to a finite element mesh with 252 elements and 285 nodal points (Fig. 2). The number of degrees-of-freedom is 476 for the fixed condition, 538 for the roller condition, and 540 for the free condition.

The choice of time increment is made to satisfy the conflicting requirements of accuracy and computational effort. Accuracy, in turn, is achieved by allowing sufficient time for the solution to reach steady state and by specifying a time increment that captures the variability in response prior to reaching steady state. Experience with the simulations has shown that it is appropriate to consider a time increment which makes the exponent in Eq. (18) equal to 40 in 20 time steps. For typical values of λ and E, the time increment is approximately 100 s.

The chosen uniform far-field velocity listed in Table 1 defines the excitation here, although other types of excitation such as environmental traction on the ice sheet can be handled equally well. For a given time step, the excitation is defined in terms of an imposed displacement in the z-direction at the far-field boundary nodes. This displacement value is made to increase linearly in time, consistent with the chosen uniform velocity.

DISCUSSION OF RESULTS

Global Forces.-- Table 2 lists the global pressures predicted by the finite element analysis for the seven cases of interest. Pressure values are the global forces divided by the indenter diameter D, and ice sheet thickness t.

Comparing the first three values of global pressure it is seen that the fixed condition does provide an upper bound solution. The global pressure for the fixed case is about 28% higher than that for the roller case. In turn, the global pressure for the roller case is 1.93 or almost twice that for the free case. This spread in global pressures is indicative of the influence of interface friction and adfreeze bond. The hundred percent reduction in pressure between the roller and free case can be explained by examining the stresses within the ice sheet. For the roller case, the upstream and downstream stresses are equal in magnitude and their resultants act together in the z-direction. In the free case, the downstream stresses are almost zero since the lack of contact at the interface on this side tends to eliminate any influence of the indenter on the ice sheet. As a result, the downstream part of the ice sheet acts predominantly like a rigid body. This tends to reduce global pressures by almost a half.

The fourth and fifth values of global pressure indicate that reducing the ice sheet velocity by a factor of 6.4 leads to a 46% reduction in pressures

while increasing the velocity by a factor of 1.6 leads to a 17% increase in pressures. Thus even a factor of two uncertainty in velocity will affect the pressures only by about 20-30%.

Cases 2 and 6 provide some idea of the effect of a grounded rubble pile or an accreted ice foot. By defining an effective indenter diameter equal to 2.85 times the structural diameter, the global pressure has reduced by 31%. However, the global force has actually increased by 97% from 211 MN/(unit ice thickness) for case 2. Two extreme scenarios can be considered to estimate the global force felt by the structure when there is a grounded rubble pile: (i) the entire global force is transmitted to the structure which in turn transmits it to the foundation, and (ii) both the structure and the grounded rubble pile resist the global force, each transmitting to the foundation a force proportional to its contact area with the foundation. Under the first scenario, which is probably overconservative, the global force on the structure is 414 MN/(unit ice thickness) an increase of 97% from case 2. Under the second scenario, which may be reasonable only if the rubble pile is consolidated and grounded firmly in the foundation soil such as in the case of constructed ice packs, the global force on the structure is 51 MN/(unit ice thickness) a reduction of 76% from case 2. Further research is necessary to quantify the level of force that can be directly transmitted to the foundation by a grounded rubble pile.

The last case shows that the two sets of material constants considered in this paper lead to ice pressures which differ by about 19%. Combining this information with earlier experience indicates that uncertainties in material constants for an isotropic power law creep model may yield ice pressures that vary by about 15-30%. However, improved material models that include fracture and temperature effects in addition to the transversely isotropic behavior of sheet ice can have a major influence on ice pressure predictions.

Calibration with Approximate Solutions.-- The global pressures for cases 4 through 7 indicate the influence of ice sheet velocity V, indenter diameter D, and material constants a and N on the results. In order to provide perspective and calibration with solutions based on approximate methods of analysis, the upper bound solution of Ting and Shyam Sunder[7] corresponding to a two-dimensional velocity field obtained by superposing a uniform flow and a doublet, is considered. The resulting kinematic model resembles the flow of an infinite ice sheet past a circular indenter with the interface matching most the roller condition. According to the solution, the global pressure is proportional to $(V/D)^{1/N}$. If this variation is valid, the ratio of global pressures in cases 4 through 6 to case 2 should be 0.54, 1.16 and 0.70, respectively. The finite element analysis predicts the ratios to be 0.54, 1.17 and 0.69. For the two sets of material constants in cases 7 and 2, the approximate solution predicts a ratio of 1.17 while the finite element analysis predicts a ratio of 1.19. In all cases, the effect of changes in V, D, a and N on the finite element solutions is almost identical to that predicted by the upper bound, creep law solution.

In order to compare the actual (as opposed to ratios of) global pressures, it is necessary to recognize that the two-dimensional nature of the chosen kinematic field makes the approximate analysis strictly correspond to a plane strain condition and not a plane stress condition. Ponter et al.'s[4] analysis for both plane strain and plane stress based on the reference stress method can be used to derive a correction factor by which to divide the approximate solution for applying it under plane stress conditions. For the material model with N=3 the correction factor is 1.8 and for the N=4 model it is 1.96. The approximate formula corrected by a rounded factor of 2 is given below:

$$\frac{P}{Dt} = \frac{2\pi}{\sqrt{3}} \frac{N}{N+3} \left[\frac{4}{\sqrt{3}} \frac{1}{a} \frac{2V}{D}\right]^{1/N} \qquad (19)$$

where the quantity in brackets raised to the power of 1/N may be interpreted as the uniaxial strength of ice evaluated at an average effective strainrate of $8/\sqrt{3}$ V/D using Eq. (7). Table 2 shows that the predictions based on Eq. (19) differ from the finite element solutions by less than 10%. The fixed condition is obtained by multiplying the above equation by 1.3, while the free condition uses a multiplying factor of 0.5 (Table 3). Note that (i) the uncorrected upper bound solutions are overconservative by almost hundred percent or more, and (ii) the approximate solutions need no longer be upper bounds once the correction factor is applied.

Local Pressures.-- The maximum (peak) interface normal stress for each of the seven simulations is listed in Table 2. The table also lists a maximum interface shear stress of 0.73 MPa for the fixed condition. There are no interface shear stresses for the roller and free conditions. Notice that in all cases the maximum normal pressure is approximately 0.35-1.10 times the global pressure, and not several (e.g., three) times the global pressure.

The maximum normal stress for the fixed condition is lower than that for the roller condition by 17%, although a reverse trend is observed for global pressures. This occurs because part of the force in the fixed condition is carried by interface shear stress. On the other hand, the maximum normal stress for the free condition is about 4% higher than that for the roller condition. There are no interface stresses on the downstream side for the free condition due to lack of contact between the ice sheet and the indenter. The small level of stresses that exist in the predominantly rigid continuum on the downstream side are transmitted to the structure from the upstream side, thereby increasing the normal stresses on that side by the 4% mentioned above.

Comparison of the local and global pressures shows that the ratio of the maximum normal interface stress to the global pressure is approximately 0.35 for the fixed condition, 0.55 for the roller condition, and 1.10 for the free condition. Furthermore, the variation of local pressures with V, D, a and N is similar to that for global pressures. Thus multiplication of Eq. (19) by 0.46, 0.55, and 0.55 can be used to estimate the respective maximum normal pressures (Table 3). In a similar fashion, the maximum interface shear stress for the fixed condition may be estimated from the equation with a multiplication factor of 0.37.

For purposes of design it is necessary to consider not only the maximum values of normal stress but also its distribution on the structure. The design of

individual structural components is typically based on a tributary loaded area. It is possible that the average integrated stress on this area due to contact with the ice sheet is significantly less than the point maxima of stress. Further, the average stress may reduce for structural components which have larger tributary areas. Figures 3 and 4 present the normal stress distributions on the interface. Note that the normal stresses are always zero where the indenter is tangential to the direction of ice sheet movement (i.e., angle equal to zero degrees). At the end of the first time step where the solution is predominantly elastic, the distributions are cosinusoidal as one may expect. However as steady state is reached, there is a tendency for the distributions to become rectangular or uniform. The distribution is more rectangular for the free and roller conditions than for the fixed condition which appears to be predominantly consinusoidal due to lower stress levels, as well as for the N=4 case than for the N=3 case since an increasing value of N makes the ice behave more like a rigid-plastic material. The figures also show that downstream interface stresses are zero for the free condition. The distributions are not affected, at least visually, as V and D are varied, although they have to be scaled according to the maximum normal stresses in Table 2. A conservative design approach may be to assume a uniform distribution of stresses based on the maximum normal interface stress.

A careful consideration of the interface stress levels sheds some light on which of the three conditions, fixed, roller or free, is realistic. Figure 5 shows the distribution of interface shear stresses for the fixed condition. At steady state, the distribution is predominantly sinusoidal with the maximum value of 0.73 MPa occurring at the tangent point. The shear strength of adfreeze bond and sea ice as reported in the literature[17,18] varies over a wide range 0.02-1.38 MPa. It is very likely that either the adfreeze bond will give way or the ice will fracture in shear over a significant fraction of the indenter perimeter. In addition, for the typical range of effective strainrates close to the downstream tip of the indenter, the tensile strength of ice is less than the downstream normal interface stresses for the fixed and roller conditions, both of which are tensile. Once again, if the adfreeze bond does not give way, a tensile fracture may occur in the ice over the perimeter close to the interface on the downstream side. Thus, for local pressures the use of the free condition should be preferred. The choice will be conservative over the fixed condition and, marginally so, over the roller condition. However, the free condition may be unconservative for global pressures if the indentation problem is one in which the structure is surrounded by an infinite ice sheet and it is possible for frictional stresses or adfreeze bond to develop at the interface.

Comparison with Pressure-Area Curves.-- Pressure-area curves are often constructed to help designers obtain the average pressures over tributary loaded areas for structural components[19]. A typical curve developed by Sanderson[20] is shown in Fig. 6. The darkly shaded areas on the figure correspond to actual measurements of ice pressure under widely varying conditions, while the lightly shaded areas represent the author's extrapolation of the measurements. The dark regions in the extreme left are from laboratory indentation tests such as those of Frederking and Gold[21], and Michel and Toussaint[1]. The central region reflects measurements from ice breakers traveling in the Arctic, while the two smaller regions on the right correspond to global forces on artificial islands estimated from pressure sensor measurements in the ice sheet. The contact area is defined as the indenter area of contact for the laboratory and artificial island data. For the ice breaker data, the contact area is the local area over which the pressure measurement is made and not the form area of the ice breaker. This figure shows that for an artificial island with a contact area of 200 m^2, the indentation pressure may be around 1 MPa. However for a local area of 10 m^2 on the same structure, the indentation pressure may be around 3 MPa.

The local to global pressure ratio of three obtained from the pressure-area curve seems to contradict the findings in the previous subsection. Fortunately, this is not so. If the contact area in Fig. 6 is interpreted as Dt, then a smaller contact area implies a smaller indenter diameter if the ice thickness remains unchanged. The effect of indenter diameter is well modelled by Eq. (19). A plot of the maximum normal interface pressure estimate from the equation leads to the solid line in the figure. Eq. (19) is appropriately modified to account for transition from plane stress to plane strain using Ponter et al.'s reference stress method[4]. This affects the curve, in an insignificant manner, over the region 1-10 m^2. When the effective strainrate, i.e., $8/\sqrt{3}\ V/D$, exceeds $5\times10^{-4}\ s^{-1}$, ice is assumed to have fractured (crushed) and the uniaxial strength is capped, leading to the flat portion of the curve on the extreme left. The predicted behavior provides an excellent match to Fig. 6. Thus, a more appealing interpretation of the figure is to consider the contact area as the indenter area (Dt in our case) and not the tributary loaded area for a structural component, and the indenter pressure corresponding to a given contact area as the maximum normal interface pressure for that indenter. The distribution of the interface stresses may be assumed uniform over the indenter area of contact as concluded earlier. However, a different boundary value problem involving a smaller contact area, as opposed to contact over half the perimeter in the free condition, will lead to higher interface pressures.

The key assumption in generating the analytical curve in Fig. 6 concerns the choice of V. The value of 0.195 m/hr considered here is based on data for an artificial island just prior to "breakout" or macro-cracking, which leads to an excellent match between predicted and measured indentation pressures for the structure. However, significantly higher velocities do occur in the field for which the current predictive models based purely on an isotropic creep law will lead to increasing pressures. Fracture in ice will be the key mechanism that limits pressures generated under higher velocities.

Multiaxial Behavior of Ice Sheet.-- A study of the multiaxial behavior of an ice sheet during indentation in the creeping mode provides clues to likely failure modes, particularly fracture. All forms of fracture (crushing, spalling, splitting) initiate as a result of tensile strains perpendicular to the crack direction. Even if the applied loads at the element level are not tensile, it is possible for tensile conditions to occur in a rotated frame of reference, e.g., a 45° rotation in the case of pure shear.

Table 4 lists the principal stresses at the point of maximum interface pressure at two time instants: at the end of the first time step (around 100 s) where

the solution is predominantly elastic, and at the twentieth time step (around 2000 s or 30 minutes) where the solution has reached steady state and is predominantly creep. The biaxial stress state at the first time step is compression-tension for all the cases except for a fixed condition where it is compression-compression. As creep starts to dominate, all the cases tend to compression-compression. Figures 7 and 8 shows how this compression-compression region grows in time for the fixed and free cases. The region is much larger for the fixed condition than for the free condition. The roller condition is somewhere in between although it resembles more the free condition. The most striking observation that can be made from these figures is that tensile stresses occur almost all over the ice sheet. Biaxial tension tends to occur on the downstream side, while compression-tension states of stress are present on both sides. Experimental evidence under compression-tension states of stress[22] shows that the occurrence of even small tensile stresses weakens ice considerably, leading to premature fracture when compared with uniaxial tensile loading.

Figure 9 shows the strain fields, which are more relevant to explaining fracture initiation. Since the algebraically maximum principal strains are positive (or almost so) over the entire ice sheet for the fixed and roller conditions at steady state, there is no compression-compression (and by symmetry no tension-tension) region of strain. A tension-compression state of strain dominates the ice sheet, with tensile strains exceeding 0.001 at steady state. As the tensile failure strain is about 0.001 or less for strainrates greater than 10^{-7} s^{-1} under just uniaxial loading, it seems likely that cracking will occur even before steady state creep is reached. Similar conclusions apply for the free condition, the only difference being that downstream strains are negligible.

The maximum effective strainrates for the seven simulations are listed in Table 2. For the kinematic model considered by Ting and Shyam Sunder[7] which is closest to the roller condition, the maximum effective strainrate equals $8/\sqrt{3}$ V/D. The prediction of 2.3×10^{-6} s^{-1} for case 2 compares well with the finite element analysis value of 3.4×10^{-6} s^{-1}. Further, cases 4 through 6 are consistent with the predicted proportionality to V/D. Contours of effective strainrate are plotted in Fig. 10. The strainrates tend to zero at the tangent points for the roller and free conditions as one may expect and is a maximum close to but not at the tips. On the other hand, the tangent point has the maximum value for the fixed condition. In the immediate vicinity of the indenter, these plots are different from the circular contours predicted by the kinematic model in the approximate analysis. This finding reinforces Ting and Shyam Sunder's[7] observation that the approximate upper bound analysis is quite accurate for global pressures, although the use of the strain path method with a kinematic model that does not capture interface conditions may be inadequate for local pressure predictions.

CONCLUSIONS

This paper has presented a finite element method of analysis for studying the problem of sea ice indentation in the creeping mode of deformation. The analysis strategy, applicable to general viscoplastic behavior including creep (nonlinear viscoelasticity), is based on a secant type iteration involving 4-6 cycles per time step on the global equations of motion and a Newton-Raphson or tangent type iteration, combined with the α-method of time integration and typically not exceeding 4 cycles per time step, on the rate-dependent constitutive relations at each integration point within an element. The resulting computer code, called DECNEC, is capable of simulating a free or frictional contact between two deformable bodies, i.e., no contact stresses due to adfreeze bond, by defining the interface as a "slideline".

Numerical simulations of ice-structure interaction for a rigid cylindrical indenter under plane stress conditions, a problem of general interest for structural concepts in the Arctic, and an isotropic (von Mises) multi-axial power law creep model for sea ice showed that:

1. Global forces vary by a factor of 2.5 depending upon whether the interface condition is fixed (infinite adfreeze bond strength), roller, or free (no adfreeze bond strength or interface friction). The fixed condition is about 1.3 times and the free condition about 0.5 times the roller condition.

2. Finite element analysis predictions of global pressure differ from a (approximate) modified upper bound solution of Ting and Shyam Sunder[7] by less than 10% for varying velocity, indenter diameter, and material constants.

3. The ratio of maximum normal interface pressure to global pressure approximately varies in the range 0.35-1.10 depending upon the interface condition. It is 0.35 for the fixed condition, 0.55 for the roller condition, and 1.10 for the free condition.

4. The maximum (peak) normal interface pressures vary by a factor of 1.26 depending upon the interface condition. The fixed condition is about 0.83 times and the free condition about 1.04 times the roller condition. The maximum interface shear stress for the fixed condition is about 0.81 times the corresponding maximum normal pressure. However, a different boundary value problem involving a smaller contact area, as opposed to contact over half the perimeter in the free condition, will lead to higher interface pressures.

5. Pressure-area curves should be considered as providing the maximum normal interface pressure for a given indenter area of contact (form area), rather than the average integrated normal pressure over a tributary loaded area for a structural component. It is conservative to assume a uniform or rectangular distribution of the local pressure over the indenter area of contact for purposes of design.

6. Tensile stresses, strains and strainrates occur almost all over the ice sheet, and may be the key to explaining fracture behavior during indentation. While biaxial compression and tension states tend to occur for stress on the upstream and downstream sides, respectively, the state of strain is almost always compression-tension. The levels of

tensile strain are often sufficient to cause cracking even before steady state creep is reached.

The possible effect of a grounded rubble pile or accreted ice foot on ice pressures was assessed by defining an effective indenter equal to a multiple (2.85) of the structural diameter. This resulted in a factor of 1.97 increase in global force. In the case of a grounded rubble pile, it would be overconservative to consider that all this force is transmitted to the foundation by the structure. On the other hand, the force transmitted to the foundation by the structure would decrease by a factor of 4.14 if both the structure and the grounded rubble pile could transmit a force proportional to the contact area of each with the foundation. This may be reasonable only if the rubble pile is consolidated and grounded firmly in the foundation soil such as in the case of constructed ice packs. Further research is necessary to quantify the level of force that can be directly transmitted to the foundation by a grounded rubble pile.

The numerical simulations also showed that (i) even a factor of two uncertainty in velocity will affect ice pressures only by about 20-30%, and (ii) uncertainties in material constants for an isotropic power law creep model may yield ice pressures that vary by about 15-30%. However, improved material models that include fracture and temperature effects in addition to the transversely isotropic behavior of sheet ice can have a major influence on ice pressure predictions. In particular, fracture in ice will be the key mechanism that limits ice pressures generated under the significantly higher velocities that occur in the field when compared with the value just prior to "breakout" or macrocracking considered here. This is an area for further research.

NOMENCLATURE

a	constant parameter in power law
$\underline{B}$	transformation matrix
$\underline{C}$	finite element material compliance matrix
D	diameter of structure
$\underline{D}$	elastic rigidity matrix
E	Young's modulus
$\underline{G}$	transformation matrix for relating $\underline{S}$ to $\underline{\sigma}$
$\underline{K}$	elastic stiffness matrix of finite element
$\underline{K}_G$	global stiffness matrix
N	power law exponent
P	global force acting on structure
$\underline{P}$	applied load vector
$\underline{S}$	deviatoric stress vector
T	temperature
t	time or ice thickness
$\underline{U}$	nodal displacement vector
V	approach velocity of ice sheet
α	parameter in time integrator
$\underline{\varepsilon}$	total strain vector
$\underline{\varepsilon}_I$	inelastic strain vector
$\underline{\varepsilon}_c$	creep strain vector
λ	associative flow rule constant
ν	Poisson's ratio
σ_e	effective stress meassure
$\underline{\sigma}$	stress vector
$\dot{}$	rate form is represented by a dot above the symbol

ACKNOWLEDGEMENTS

This research is funded by the Standard Oil Company (Ohio) through MIT's Center for Scientific Excellence in Offshore Engineering, and cosponsored by the U.S. Department of the Interior, Minerals Management Service. The authors thank Jaideep Ganguly, graduate student, for computational assistance.

REFERENCES

1. Michel, S. and Toussaint, N., "Mechanisms and Theory of Indentation of Ice Plates," Journal of Glaciology, Vol. 19, No. 81, 1977, pp.285-300.

2. Croasdale, K.R., Morgenstern, M.R. and Nuttall, J.B., "Indentation Tests to Investigate Ice Pressures on Vertical Piers," Journal of Glaciology, Vol. 19, No. 81, 1977, pp.310-312.

3. Ralston, T.D., "An Analysis of Ice Sheet Indentation," IAHR Ice Symposium, Lulea, Sweden, 1978, pp.13-31.

4. Ponter, A.R.S. et al, "The Force Exerted by a Moving Ice Sheet on an Offshore Structure: Part I The Creep Mode," Cold Regions Science and Technology, Vol. 8, 1983, pp. 109-118.

5. Bruen, F.J. and Vivatrat, V., "Ice Force Prediction Based on Strain-Rate Field," Third International Symposium on Offshore Mechanics and Artic Engineering, New Orleans, LA, 1984, 7 p.

6. Vivatrat, V. and Chen, V.L., "Ice Load Prediction with the Use of a Rate-Dependent Anisotropic Constitutive Law," Proc. of the ASCE Specialty Conference: Arctic '85 - Civil Engineering in the Arctic Offshore, San Francisco, California, March 1985, 11p.

7. Ting, S-K. and Shyam Sunder, S., "Sea Ice Indentation Accounting for Strain-Rate Variation," Proc. of the ASCE Specialty Conference: Arctic '85 - Civil Engineering in the Arctic Offshore, San Francisco, California, March 1985, 11p.

8. Baligh, M.M., "The Strain Path Method," Research Report R84-01, No. 761, Department of Civil Engineering, Massachusetts Institute of Technology, Cambridge, Massachusetts, Jan. 1984, 47 p.

9. Shyam Sunder, S. and Ting, S-K., "Ductile to Brittle Transition in Sea Ice under Uniaxial Loading," Proc. of the 8th International Conference on Port and Ocean Engineering under Arctic Conditions, Narssarssuaq, Greenland, Sept. 1985, 12 p.

10. Glen, J.W., "The Creep of Polycrystalline Ice," Proc. of the Royal Society of London, Ser. A, Vol. 228, No. 1175, 1955, pp.519-538.

11. Palmer, A.C., "Creep-Velocity Bounds and Glacier-Flow Problems," Journal of Glaciology, Vol. 6, No. 46, 1967, pp.479-488.

12. Snyder, M.D. and Bathe, K.J., "A Solution Procedure for Thermo-Elastic-Plastic and Creep Problems," Nuclear Engineering and Design, Vol. 64, 1981, pp. 49-80.

13. Hughes, T.J.R. and Taylor, R.L., "Unconditionally Stable Algorithms for Quasi-Static Elasto/Visco-Plastic Finite Element Analysis," Computer and Structures, Vol. 8, 1978, pp. 169-173.

14. Krieg, R.D., "Numerical Integration of Some New Unified Plasticity-Creep Formulations," SMIRT-4, M6/4, 1977.

15. Sanderson, T.J.O., "Theoretical and Measured Ice Forces on Wide Structures," Proc. 7th International Symposium on Ice, IAHR, Hamburg, August 1984, 32p.

16. Wang, Y.S., "A Rate-Dependent Stress-Strain Relationship for Sea Ice," First International Symposium on Offshore Mechanics and Artic Engineering, New Orleans, 1982, pp. 243-248.

17. Gershunov, E.M., "Shear Strength of Adfreeze Bond and its Effect on Global Ice Load Applied to Mobile Offshore Drilling Units Under Artic Conditions," Offshore Technology Conference, Paper OTC 4687, 1984, pp. 357-362.

18. Oksanen, P., "Friction and Adhesion of Ice," IAHR Ice Symposium, Quebec, Canada, 1981, pp.628-640.

19. Bruen, F.J., Byrd, R.C., Vivatrat, V. and Watt, B.J., "Selection of Local Design Ice Pressures for Arctic Systems," Offshore Technology Conference, Paper OTC 4334, 1982, pp. 417-435.

20. Sanderson, T.J.O., Personal Communications, 1984.

21. Frederking, R. and Gold, L.W., "Experimental Study of Edge Loading of Ice Plates," Canadian Geotechnical Journal, Vol. 12, No. 4, 1975, pp. 456-463.

22. Haynes, F.D., "Tensile Strength of Ice under Triaxial Stresses," USA CRREL Research Report 312, 1973, 21 p.

TABLE 1 - SUMMARY OF CASES

Case	Velocity (ft/hr)	Diameter (ft)	N	Interface Condition
1	0.64	350	3	Fixed
2	0.64	350	3	Roller
3	0.64	350	3	Free
4	0.10	350	3	Roller
5	1.00	350	3	Roller
6	0.64	1000	3	Roller
7	0.64	350	4	Roller

Note: 1 ft = 0.3048 m

TABLE 2 - SUMMARY OF RESULTS

Case	P/Dt (MPa)		Maximun Interface Normal Stress (MPa)	Maximum Effective Strainrate (s^{-1})
	Finite Element Analysis	Modified Upper Bound		
1	2.54	2.44	0.90	4.0×10^{-6}
2	1.98	1.87	1.08	3.4×10^{-6}
3	1.02	0.94	1.13	4.0×10^{-6}
4	1.07	1.01	0.59	5.5×10^{-7}
5	2.31	2.18	1.28	5.5×10^{-6}
6	1.36	1.32	0.76	1.1×10^{-6}
7	2.34	2.20	1.27	4.5×10^{-6}

Note: Maximum Interface Shear Stress for Fixed Condition is 0.732 MPa
1 MPa = 145 psi

TABLE 3 - MULTIPLYING FACTORS FOR APPROXIMATE MODEL (Eq. 19)

Condition	Global Pressure	Maximum Interface Normal Stress
Roller	1.0	0.55
Fixed	1.3	0.46
Free	0.5	0.55

Note: Factor for Maximum Interface Shear Stress in Fixed Condition = 0.37

TABLE 4 - PRINCIPAL STRESSES AT UPSTREAM TIP OF INDENTER

Case	Elastic (Time Step 1)		Steady State Creep (Time Step 20)	
	σ_z(MPa)	σ_y (MPa)	σ_z(MPa)	σ_y(MPa)
1	-0.19	-0.07	-0.90	-0.39
2	-0.30	+0.07	-1.08	-0.16
3	-0.36	+0.10	-1.13	-0.16
4	-0.18	+0.04	-0.59	-0.09
5	-0.35	+0.08	-1.28	-0.20
6	-0.11	+0.03	-0.76	-0.10
7	-0.31	+0.08	-1.27	-0.26

Note: Tension is Positive
1 MPa = 145 psi

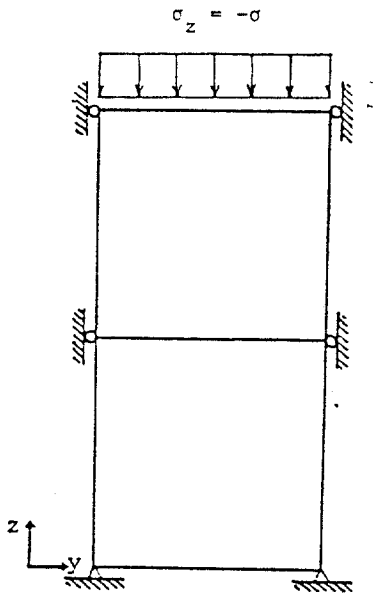

Fig. 1 - Test Problem

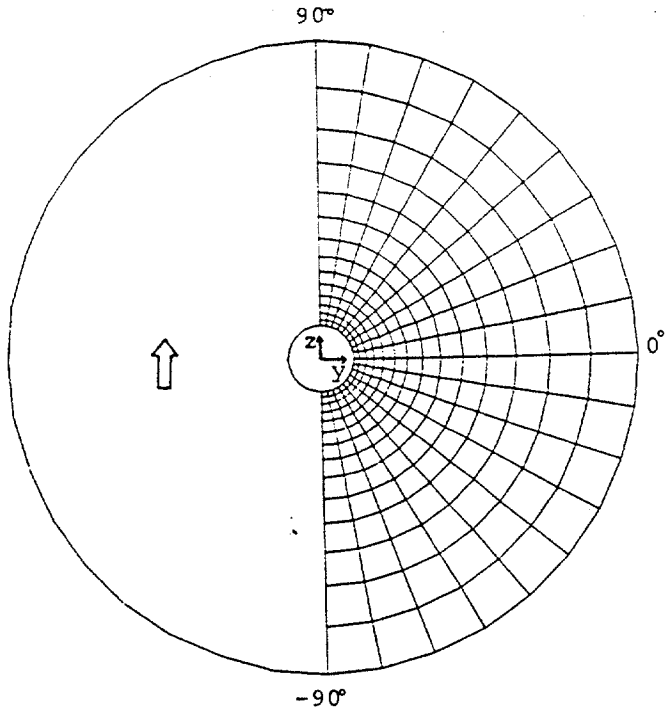

Fig. 2 - Finite Element Grid

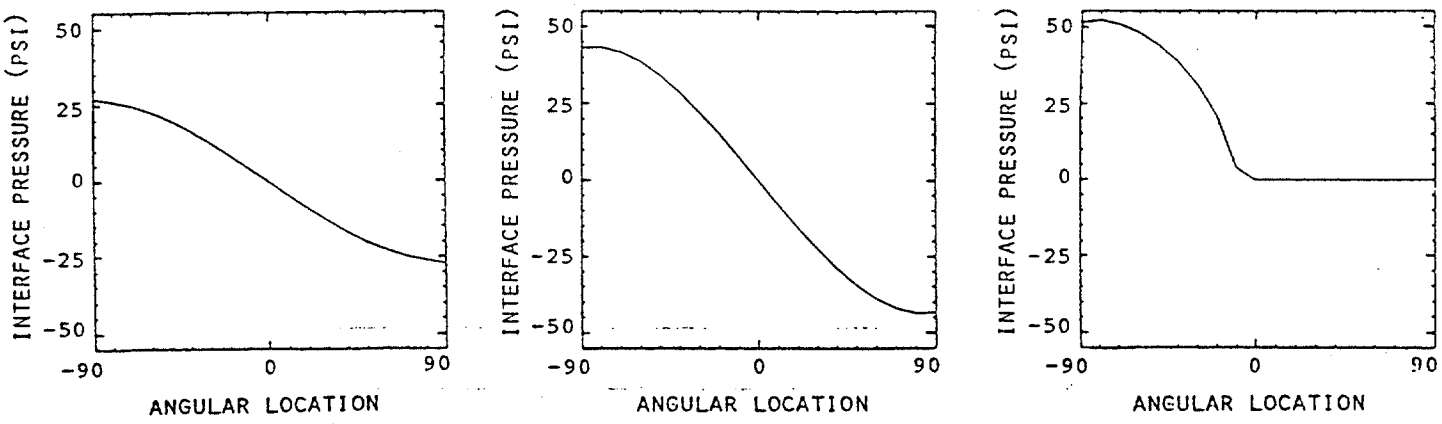

(a) Fixed Condition (b) Roller Condition (c) Free Condition

Fig. 3 - Normal Stress Distribution on Interface (Time Step 1)

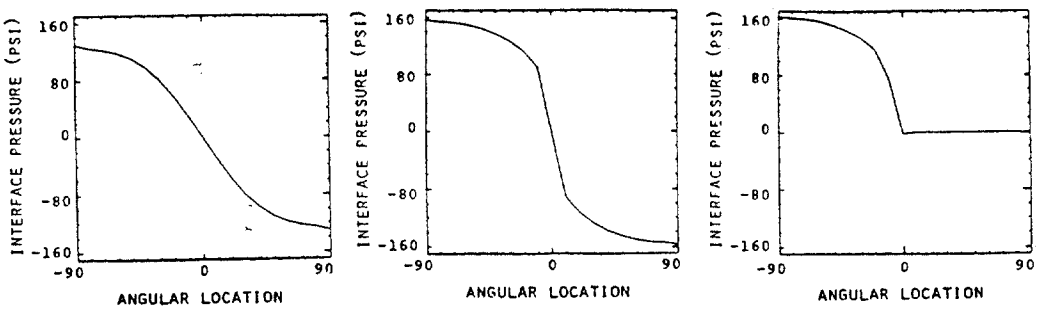

(a) Fixed Condition (b) Roller Condition (c) Free Condition

Fig. 4 - Normal Stress Distribution on Interface (Time Step 20)

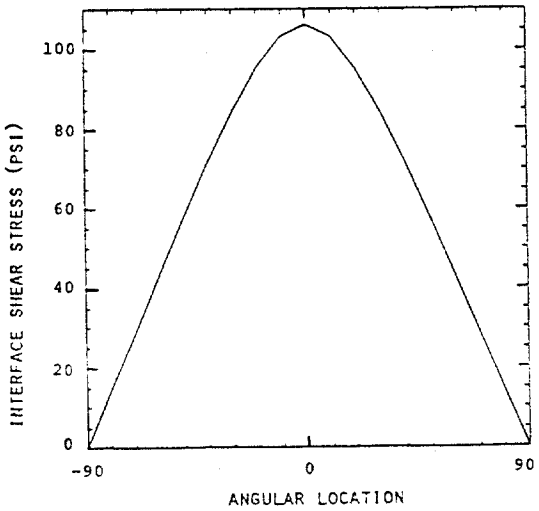

Fig. 5 - Shear Distribution on Interface for Fixed Condition (Time Step 20)

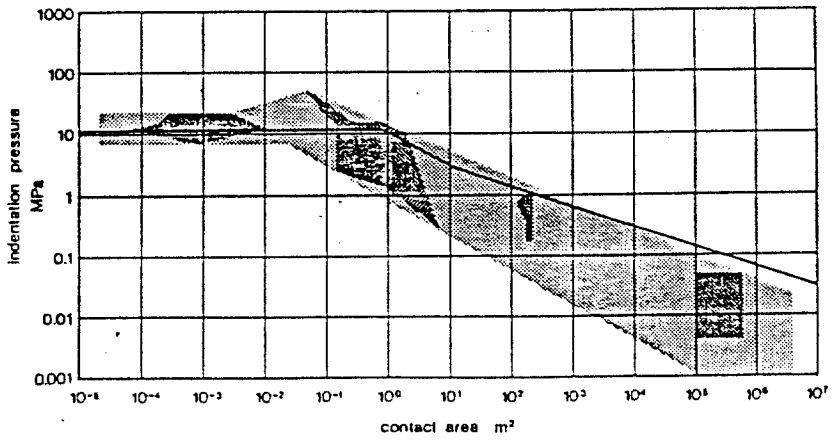

Fig. 6 - Pressure-Area Curve

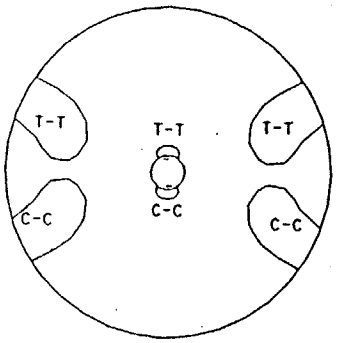

(a) Time Step 1

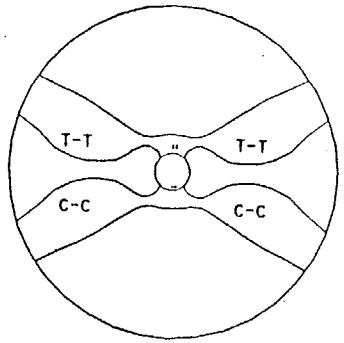

(b) Time Step 20

Fig. 7 - Biaxial Stress Regions for Fixed Condition

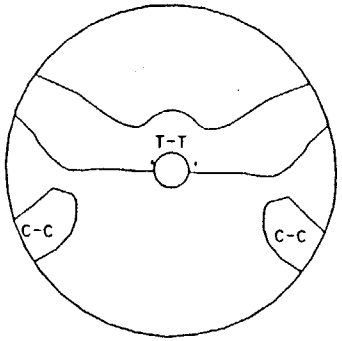

(a) Time Step 1

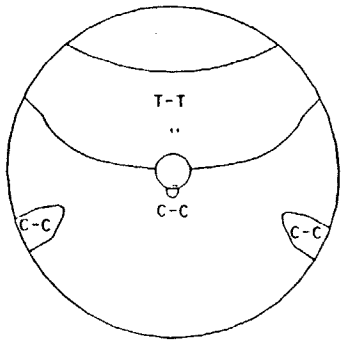

(b) Time Step 20

Fig. 8 - Biaxial Stress Regions for Free Condition

Maximum Principal Strain
Contour Levels
A = 0.0
B = 0.0005
C = 0.0010
D = 0.0015
E = 0.0020
F = 0.0025

Minimum Principal Strain
Contour Levels
A = -0.0030
B = -0.0025
C = -0.0020
D = -0.0015
E = -0.0010
F = -0.0005
G = 1.2×10^{-10}

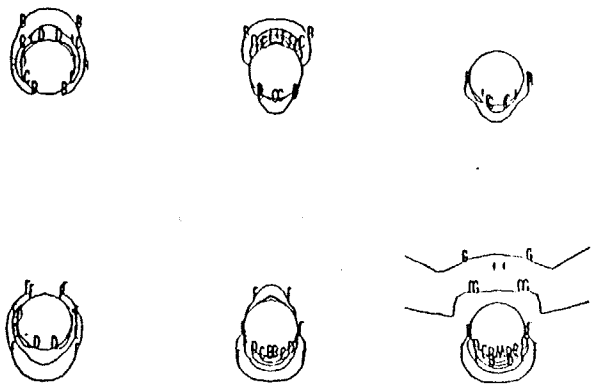

(a) Fixed (b) Roller (c) Free

Fig. 9 - Principal Strain Contours (Time Step 20)

Contour Levels
A = 0.5×10^{-6}
B = 1.5×10^{-6}
C = 2.5×10^{-6}
D = 3.5×10^{-6}

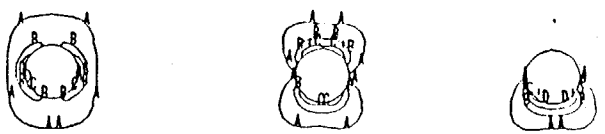

(a) Fixed (b) Roller (c) Free

Fig. 10 - Effective Strainrate Contours (Time Step 20)

ANISOTROPIC SEA ICE INDENTATION IN THE CREEPING MODE

S. Shyam Sunder
Associate Professor of Civil Engineering
and
Jaideep Ganguly and Seng-Kiong Ting
Research Assistants, Department of Civil Engineering
Massachusetts Institute of Technology
Cambridge, Massachusetts 02139

ABSTRACT

A general orthotropic elastic - power law creep model for sea ice is presented and then a finite element method of analysis is developed and applied to study the effect of sea ice anisotropy on indentation in the creeping mode. Numerical simulations are performed under plane stress conditions to predict the influence of interface adfreeze and friction, material constants for a transversely isotropic elastic - power law creep model, rubble pile or grounded ice foot, and ice sheet velocity on global forces and local pressures generated on a rigid cylindrical indenter. The results are compared with those based on approximate methods of analysis. Interface pressure distributions are obtained in addition to contours of stress and strain.

INTRODUCTION

The interaction of an ice sheet with a vertically faced indenter is an important loading condition for cylindrical structures and conical structure with grounded rubble pile or accreted ice foot in the Arctic. In general, this indentation phenomenon is characterized by the simultaneous occurrence viscous (rate-dependent) and fracture behavior.

Several theoretical models based on approximate methods of analysis tha idealize the ice sheet as an isotropic continuum have been proposed for

predicting global ice forces. These include: (1) the upper and lower bound, plasticity solutions of Michel and Toussaint (1), and Croasdale et al. (2), (2) the reference stress, power law creep solution of Ponter et al. (3), and (3) the upper bound, power law creep solutions of Bruen, Vivatrat and Chen (4,5), and Ting and Shyam Sunder (6). Theoretical predictions of interface pressures are not generally available. However, Ting and Shyam Sunder (6) have applied the (approximate) strain path method of analysis to study interface pressures during plane strain indentation. In a recent paper (7), two of the authors and their colleagues have developed and applied a finite element ("exact") method of analysis to predict both global forces and local pressures assuming an isotropic elastic - power law creep model for sea ice.

Sea ice, however, is not an isotropic material. Field observations have shown that this type of ice, which is predominantly columnar, has two sources of anisotropy: (a) the c-axis is oriented perpendicular to the axis of crystal growth, and (b) the c-axes of different crystals may show preferred azimuthal orientation in the plane on which they lie. There is strong evidence suggesting that the preferred azimuthal orientation is correlated with the instantaneous current direction just underneath a growing ice sheet (8,9,10). While such alignments are common in landfast ice, observations suggest that strong alignments can develop in pack ice when there is little rotation of the floes relative to the current direction (11,12).

The anisotropy of sea ice strongly influences the macromechanical behavior of first year sheet ice, while its influence on the behavior of multi-year floes, though less well studied, may be less. In first year sheet ice, the first source of anisotropy leads to a ratio of vertical to horizontal stress at constant strainrate varying from 2-5 (13-17), while the second

source of anisotropy leads to stress ratios of 0.25-0.60 at a 45 degree azimuthal angle to the c-axis and 0.50-0.95 at a 90 degree angle (18-21).

Two theoretical models have been developed for predicting indentation pressures assuming the ice sheet to be transversely isotropic. They are: (1) the upper and lower bound, plasticity solution of Ralston (22), and (2) the upper bound, power-law creep solution of Vivatrat and Chen (23). The former model has been incorporated in the API Bulletin 2N guidelines (24).

A study of sea ice indentation in the creeping mode is important for two reasons: (a) creep is the predominant mode of deformation for artificial islands in the Arctic nearshore region during "breakout" and/or steady indentation conditions occuring during the winter, and (b) stresses, strains, and strainrates resulting from creep are necessary to predict the nucleation, growth initiation and propagation of cracks when viscous effects influence fracture behavior.

This paper is concerned with (i) the development of a general orthotropic elastic - power law creep model for sea ice, and (ii) the development and application of a finite element method of analysis to study the influence of sea ice anisotropy on indentation in the creeping mode. Numerical simulations are performend under plane stress conditions to predict the influence of interface adfreeze and friction, material constants for a transversely isotropic elastic - power law creep model, rubble pile or accreted ice foot, and ice sheet velocity on predicted pressures. The results are compared with those based on approximate methods of analysis. Interface pressure distributions are obtained in addition to contours of stress and strain.

MATERIAL MODELING

Theoretical Formulation

The rate-dependent material model for sea ice assumes that the total strainrate is the sum of the elastic strainrate and the creep or viscous strainrate, i.e.,

$$\dot{\underline{\varepsilon}} = \underline{C}\,\dot{\underline{\sigma}} + \dot{\underline{\varepsilon}}_c \tag{1}$$

where $\underline{C}$ is the linear elastic compliance matrix for an orthotropic material.

To derive the relationship between the creep strainrate and stress vectors, first an effective stress measure generalized for orthotropic materials with identical behavior in compression and tension is defined.

$$\sigma_e^2 = 3/A \left[\frac{a_1}{3}(\sigma_{xx}-\sigma_{yy})^2 + \frac{a_2}{3}(\sigma_{yy}-\sigma_{zz})^2 + \frac{a_3}{3}(\sigma_{zz}-\sigma_{xx})^2 + 2a_4\,\sigma_{xy}^2 + 2a_5\,\sigma_{yz}^2 + 2a_6\,\sigma_{zx}^2\right] \tag{2}$$

with $A=a_1+a_2$. This may be expressed in compact form using matrix notation as:

$$\sigma_e^2 = 3/A\ \underline{\sigma}^T\,\underline{G}\,\underline{\sigma} \tag{3}$$

Under uniaxial (compressive) loading conditions, creep in ice is usually expressed in terms of a power law (25). Then, the effective strainrate and effective stress are related by:

$$\dot{\varepsilon}_e = a\,\sigma_e^N \tag{4}$$

where a and N are constants with the temperature dependence being included in the parameter a following an Arrhenius activation energy law which is valid for temperatures less than -10°C.

The strainrate vector can be related to the effective stress vector by defining a scalar potential function ϕ which obeys the associated flow rule, i.e.,

$$\dot{\underline{\varepsilon}}_c = \frac{\partial \phi}{\partial \underline{\sigma}} \tag{5}$$

with

$$\phi = a \frac{\sigma_e^{N+1}}{N+1} \tag{6}$$

Combining Eqs. (5), (6) and (3) yields the desired relationship:

$$\dot{\underline{\varepsilon}}_c = \lambda \, \underline{S}^* \tag{7}$$

where

$$\lambda = 3/A \; a \; \sigma_e^{N-1} \tag{8}$$

and

$$\underline{S}^* = \underline{G} \; \underline{\sigma} \tag{9}$$

Note that $\underline{S}^*$ is not the conventional deviatoric stress vector. It may be thought of as a pseudo deviatoric stress vector for an anisotropic material.

Given the stress vector, the pseudo deviatoric stresses may be obtained from Eq. (9). Then applying Eqs. (3), (8), and (7) in succession leads to the creep strainrate vector. Note that under isotropic conditions, i.e., $a_1 - a_6 = 1$, all these equations reduce to the formulation proposed by Palmer (26) and described in Ref. (7).

Estimation of Model Parameters

Six uniaxial (compression) tests at constant strainrate are necessary to obtain the seven orthotropic model parameters: a, N, a_2-a_6. Note that (i) a_1 can be set equal to one without loss of generality, and (ii) there is experimental evidence which shows that the power law exponent N can be considered independent of the direction of loading. For purposes of the current derivation, it is assumed that the c-axes of the sea ice crystals lie on the y-z plane and that they are aligned in the y-direction. This implies that the x-axis represents the crystal growth direction.

Let the tests be conducted in the three orthogonal directions y, x and z respectively, and along the three 45° axes on the y-z, x-y and z-x planes respectively. Furthermore, let β_1-β_5 represent the experimentally determined ratios of the maximum stresses for the last five tests, respectively, to the maximum stress in the reference y-direction at the same strainrate. According to the theoretical formulation, the parameters a and N refer directly to the uniaxial test along the c-axis, i.e., the y-direction. The remaining parameters may be determined from the following equations:

$$a_2 = -\frac{\beta_1^n - \beta_2^n(1-\beta_1^n)}{\beta_1^n - \beta_2^n(1+\beta_1^n)} \tag{10}$$

$$a_3 = -\frac{\beta_1^n + \beta_2^n(1-\beta_1^n)}{\beta_1^n - \beta_2^n(1+\beta_1^n)} \tag{11}$$

$$a_4 = \frac{A}{6}\left[4\beta_4^{-n} - \beta_2^{-n}\right] \tag{12}$$

$$a_5 = \frac{A}{6}\left[4\beta_3^{-n} - \beta_1^{-n}\right] \tag{13}$$

$$a_6 = \frac{A}{6}\left[4\beta_5^{-n} - 1\right] \tag{14}$$

where $n=2N/(N+1)$. Typical ranges for the βi's (previously referred to in the introduction) are 2-5 for β_1, 0.50-0.95 for β_2, and 0.25-0.60 for β_3. Values for β_4 and β_5 are not generally available in the literature. Since these two parameters determine only the out of plane shear strains and stresses in sheet ice, they have no influence on plane strain and plane stress indentation problems. However, the parameters will have to be obtained in the case of three-dimensional indentation problems.

For a tranversely isotropic material, i.e., isotropy in the y-z plane, $\beta_2=\beta_3=1$ and $\beta_4=\beta_5$. As a result $a_1=a_3=1$, $a_4=a_6$, the parameters a_2 and a_5 are functions of only β_1, while a_4 depends on both β_1 and β_4. Only three uniaxial tests are required to obtain a, N, β_1 and β_4; one each in the y and x directions and one along the 45° axis on the x-y or z-x planes.

Frederking (27) has conducted plane strain uniaxial compression tests on columnar-grained transversely isotropic freshwater ice. For his type A tests, strains in the z-direction are constrained to zero and stresses are applied in the y-direction. The ratio Γ_z of the plane strain stress to the unconfined stress at the same strainrate is directly related to β_1 by the following equation:

$$\Gamma_z = \left[\frac{4\beta_1^{2n}}{4\beta_1^{n} - 1}\right]^{1/n} \tag{15}$$

The equation predicts Γ_z to vary between 2.1-5.1 for experimentally observed values of β_1 ranging from 2 to 5, and N between 3 and 4. This is consistent with Frederking's experimental observations of Γ_z which were close to 2 at high strainrates and to 5 at low strainrates. In the type B tests, strains in

the x-direction are constrained to zero while stresses are again applied in the y-direction. In this case, the stress ratio Γ_x is given by:

$$\Gamma_x = [1 + \frac{1}{4\beta_1^n - 1}]^{1/n} \tag{16}$$

Since β_1 is generally greater than one, Γ_x will be less than approximately 1.2 for N between 3 and 4. For typical values of β_1, the predicted values of Γ_x range from 1.01 to 1.06. This is consistent with Frederking's experiments which showed negligible influence of x-direction confinement on stresses.

Triaxial tests of first-year sea ice have been conducted by Richter-Menge, Cox et al. (20) on samples obtained from horizontal cores in the plane of the ice sheet at angles of 0°, 90°, and 45° to the preferred c-axis orientation. According to the orthotropic material model, the ratio Γ_t of the maximum axial stress with a confining pressure equal to τ times the axial stress to the maximum axial stress in the unconfined state at the same strainrate should be given by:

$$\Gamma_t = \frac{1}{1-\tau} \tag{17}$$

The deviatoric stress (i.e., axial stress minus radial stress) normalized by the unconfined stress is independent of τ or confining pressure for the model and equal to one. Experimental data for this quantity is plotted versus confining pressure in Fig. 1, which shows that sea ice is moderately pressure sensitive .

FINITE ELEMENT FORMULATION

Governing Equations

For general viscoplastic behavior, which includes creep, it is convenient to work with time derivatives of the governing equations for a solid. The weighted equilibrium-rate equation which forms the basis of the finite element displacement method is then given by:

$$\int \underline{B}^T \dot{\underline{\sigma}} \, dV = \dot{\underline{P}} \tag{18}$$

where $\underline{B}$ is the strainrate - nodal velocity transformation matrix derived from the chosen displacement expansion for the finite element, i.e.,

$$\dot{\underline{\varepsilon}} = \underline{B} \, \dot{\underline{U}} \tag{19}$$

Combining Eqs. (18) and (19) with Eq. (1) and defining $\underline{K}$ as the elastic stiffness matrix of the element leads to the element equilibrium equation:

$$\underline{K} \, \dot{\underline{U}} = \dot{\underline{P}} + \int \underline{B}^T \underline{D} \, \dot{\underline{\varepsilon}}_c \, dV \tag{20}$$

and the element stressrate - nodal velocity relations:

$$\dot{\underline{\sigma}} = \underline{D} \, \underline{B} \, \dot{\underline{U}} - \underline{D} \, \dot{\underline{\varepsilon}}_c \tag{21}$$

where $\underline{D}$ is the linear elastic rigidity matrix for an orthotropic material. The global stiffness matrix $\underline{K}_G$ is obtained from Eq. (20) using conventional procedures.

Solution Algorithm

An iterative solution algorithm is developed to solve the pseudo-force form of the nonlinear governing equations given in Eqs. (20) and (21). This is a generalization of the algorithm for isotropic materials presented in an earlier paper (7). For purposes of discussion, attention is focussed at the element level rather than the global level. At first the governing equations are integrated in time between t_i and t_{i+1} to yield:

$$\underline{K}\ (\underline{U}_{i+1}-\underline{U}_i) = \underline{P}_{i+1}-\underline{P}_i + \int \underline{B}^T\ \underline{D}\ (\underline{\varepsilon}_{c,i+1}-\underline{\varepsilon}_{c,i})\ dV \tag{22}$$

$$\underline{\sigma}_{i+1}-\underline{\sigma}_i = \underline{D}\ \underline{B}\ (\underline{U}_{i+1}-\underline{U}_i) - \underline{D}\ (\underline{\varepsilon}_{c,i+1}-\underline{\varepsilon}_{c,i}) \tag{23}$$

Creep strains which appear in both equations are nonlinear functions of stress since λ in Eq. (7) is not a constant. A two-level iterative algorithm is used to solve these equations for each new time step t_{i+1}. The key steps in the solution algorithm are as follows:

1. Compute the displacement increments from (the global form of) Eq. (22) for the given loading vector. In the first iteration on the equation, the incremental creep strains are assumed to be zero.
2. Compute the incremental stresses and incremental creep strains from Eq. (23) for the displacement increments obtained in step 1 using the iterative algorithm (lower-level iteration in k) discussed below. In the first iteration on this equation assume the incremental creep strains to be zero.
3. Return to step 1 and iterate on Eq. (22) (higher-level iteration in j) using the incremental creep strains obtained in step 2 until convergence is achieved. Two convergence criteria are used: (a) ratio of norm of displacement increment vector to norm of displacement vector at given time step is less-than-or-equal-to 10^{-3}; and (b) absolute value of energy norm is less-than-or-equal-to 10^{-5}, i.e.,

$$\left| \frac{\underline{\Delta P}^j \cdot \underline{\Delta U}^j}{\underline{\Delta P}^o \cdot \underline{\Delta U}^o} \right| < 10^{-5} \tag{24}$$

where $\underline{\Delta P}$ refers to the entire right hand side of Eq. (22). The evaluation of the integral defining the inelastic load vector is based on a Gaussian quadrature formula. Typically, 4-6 iterations are required for convergence at the higher level.

The evaluation of the incremental stresses and incremental creep strains in step 2 requires the simultaneous consideration of Eq. (23) and Eq. (7). In addition to a nonlinear equation solver, a numerical time integrator is needed to obtain results.

The incremental creep strains for iteration k+1 are evaluated with the α-method of numerical time integration which expresses Eq. (7) as:

$$(\underline{\varepsilon}_{c,i+1} - \underline{\varepsilon}_{c,i}) = \lambda_\alpha \, \underline{S}^*_\alpha \, (t_{i+1} - t_i) \tag{25}$$

where $\underline{S}^*_\alpha$ is a weighted average of the pseudo deviatoric stress vector in the time interval $(t_{i+1} - t_i)$ and λ_α is derived from a similar weighting on the effective stress. Since $\underline{G}$ in Eq. (9) is independent of time, $\underline{S}^*_\alpha$ is equal to the product of $\underline{G}$ with the weighted average of the total stress vector over the same time interval given by:

$$\underline{\sigma}_\alpha = (1-\alpha) \, \underline{\sigma}_i + \alpha \, \underline{\sigma}_{i+1} \tag{26}$$

A value of α greater than or equal to 0.5 results in an unconditionally stable, implicit algorithm. The well-known trapezoidal rule and backward Euler method are obtained with α=0.5 and α=1, respectively.

For accelerating solution convergence in creep dominant problems of concern here, a lower-level algorithm is developed which combines a Newton-Raphson or tangent type nonlinear equation solver with the α-method. The resulting equations are listed below:

$$\left[\underline{I} + \underline{D} \left[\frac{\partial \Delta \underline{\varepsilon}_c}{\partial \underline{\sigma}_{i+1}^T}\right]^k\right] \underline{\sigma}_{i+1}^{k+1} = \underline{\sigma}_i + \underline{D} \, [\underline{B} \, \underline{\Delta U} - \underline{\Delta \varepsilon}_c^k] + \underline{D} \left[\frac{\partial \Delta \underline{\varepsilon}_c}{\partial \underline{\sigma}_{i+1}^T}\right]^k \underline{\sigma}_{i+1}^k \tag{27}$$

where $\underline{\Delta\varepsilon_c}^k$ is obtained by applying Eq. (25) after obtaining the stress quantities at iteration k, and similarly:

$$\left[\frac{\partial \underline{\Delta\varepsilon_c}}{\partial \underline{\sigma}_{i+1}^T}\right]^k = \Delta t\ \alpha \left[\lambda \underline{G} + 3/A\ \ \sigma_e^{-1}\ \frac{\partial \lambda}{\partial \sigma_e}\ \underline{S}^*\ \underline{S}^{*T}\right]_\alpha^k \tag{28}$$

For the given material model, $\partial\lambda/\partial\sigma_e$ can be obtained from Eq. (8). Convergence is defined to occur when the maximum absolute value of the relative change in point stresses between iteration k and k+1 is less than 0.01. Iteration is also stopped if the actual point stresses are zero at k and their maximum absolute value is less than 0.01 at k+1. Application of this iterative scheme with α=1 shows that convergence is typically obtained in 4 iterations.

Computer Implementation and Code Verification

The generalization of the finite element analysis algorithm for material anisotropy has been implemented in the computer code called DECNEC (7). The current implementation is a two-dimensional version for plane stress problems.

The accuracy of the computer code for the anisotropic material model has been verified for the case of transverse isotropy through the following test problems:

(a) Constant strainrate unconfined compression tests in and transverse to the plane of isotropy.

(b) Constant stress and constant strainrate tests with boundary conditions similar to Frederking's (27) type A tests.

(c) Pure shear test with stresses applied in the plane of isotropy.

The first test in (a) checks on the parameters a and N of the material model, while the second is a check on β_1 when it is conducted at the same strainrate. The two tests in (b) are further checks on a, N, and β_1. For an applied

constant y-direction stress σ_y, a simple analysis shows that the lateral stress (σ_z) is given by:

$$\sigma_z = - \sigma_y [(a_2/A - \nu) e^{-(A/3)E\lambda t} - a_2/A] \quad (29)$$

where ν is the Poisson's ratio in the plane of isotropy and E is the corresponding Young's modulus. This solution is valid for a constant value of λ, which in an average sense may be defined as its value at steady state. Under steady state conditions, i.e., large t, Eq. (29) shows that the lateral stress is equal to a_2/A or $1-0.5\beta_1^{-n}$ times the y-stress. Application of DECNEC verified this analysis. If the strainrate in the plane of isotropy for the second test is kept the same as that in (a), then the stress in the direction of the applied strainrate must be greater than the corresponding stress in (a) by the factor Γ_z of Eq. (15). Note that Γ_z is a function of only β_1. The pure shear test in (c) is a check on Eq. (13) for a_5 which is a function of only β_1 in the case of transverse isotropy. The test conditions are illustrated in Fig. 2. Verification is achieved by comparing the theoretical predictions for shear strains with the numerical results. No checks are needed for parameters β_4 and β_6 or a_4 and a_6 since they do not influence plane stress indentation behavior.

NUMERICAL SIMULATIONS

Description of Case Studies

Numerical simulations are performed for the 14 cases identified in Table 1 based on transversely isotropic behavior of sea ice. The objectives of simulations 1-3 and 10-14 are to quantify the effect of interface adfreeze and friction on predicted indentation pressures. For global forces, the fixed condition provides an upper bound solution since the ice-structure interface is considered to be infinitely strong. The free condition corresponds to no

adfreeze and friction, while the roller condition provides an intermediate solution. Simulations 4 and 5 study the influence of ice sheet velocity on pressures. The chosen base velocity of 0.195 m/hr corresponds to the recorded maximum average velocity over a twelve-hour period just prior to "breakout" (macrocracking) for an artificial island in the Beaufort Sea. The sixth simulation attempts to quantify the effect of a grounded rubble pile or an accreted ice foot on ice pressures by defining a larger effective indenter diameter (2.85 times the structural diameter). Simulations 9-14 study the effect of variability in constants a, N, and β_1 defining the material model on ice pressures. Two sets of the parameters a and N for sea ice based on the work of Sanderson (28) and Wang (29), respectively, are considered: N=3, $a=2.125\times10^{-6}$ $(MPa)^{-3}s^{-1}$; and N=4, $a=1.848\times10^{-6}$ $(MPa)^{-4}s^{-1}$. Three values of β_1 equal to 2,3 and 5 are studied. The elastic constants in the plane of isotropy, which have negligible influence on the steady state solutions, are taken to be E=9.5 GPa and ν=0.3. Finally, simulations 7 and 8 are used to predict pressure area curves under plane stress conditions.

The criteria governing the choice of finite element mesh and time increments for the simulations are described in an earlier paper (7). The chosen uniform far-field velocity listed in Table 1 defines the excitation here. For a given time step, the exication is specified in terms of an imposed displacement in the z-direction at the far-field boundary nodes (Fig. 3). This displacement value is made to increase linearly in time, consistent with the chosen uniform velocity.

Discussion of Results

Global forces. Table 2 lists the global pressures predicted by the finite element analysis for the 14 cases of interest. Pressure values are the global forces divided by the indenter diameter D, and ice sheet thickness t.

The table also lists the factor by which the global pressure increases as a result of anisotropy.

Comparing the global pressures for cases 1-3 and 10-14, it is seen that the fixed condition does provide an upper bound solution. The global pressure for the fixed condition is greater than that for the roller condition by a factor of about 1.22 to 1.27. In turn, the global pressure for the roller condition is 1.97 to 2.00 times that for the free condition. The hundred percent reduction in pressure between the roller and free cases occurs because the lack of downstream interface contact in the latter case tends to release the downstream stresses in the ice sheet.

The fourth and fifth values of global pressure indicate that reducing the ice sheet velocity by a factor of 6.4 leads to a 47-48% reduction in pressures while increasing the velocity by a factor of 1.6 leads to a 15-18% increase in pressures. Thus even a factor of two uncertainty in velocity will affect the pressures by only about 20-30%.

Cases 2 and 6 provide some idea of the effect of a grounded rubble pile or an accreted ice foot. The global force increases by a factor of 1.92 when the effective indenter diameter is taken to be a multiple (2.85) of the structural diameter. In the case of a grounded rubble pile, it would be overconservative to consider that all this force is transmitted to the foundation by the structure. On the other hand, the force transmitted to the foundation by the structure would decrease by a factor of 4.25 if both the structure and the grounded rubble pile could transmit a force proportional to the contact area of each with the foundation. These results for a transversely isotropic material are identical to that from the isotropic analysis in Ref. (7), although the absolute value of the global force for the

anisotropic case is greater than that for the isotropic case by a factor of 1.12.

Case 9 shows that for β_1 equal to 1 (isotropic) and 3, the two sets of values for the material constants a and N lead to ice pressures for the roller condition which differ by a factor of 1.19 and 1.30, respectively. However for N=3 and the corresponding a, and β_1 varying between 1 and 5 (cases 1-3 and 10-14), global ice pressures vary by a factor of 1.10, 1.12, and 1.13 for the fixed, roller and free conditions, respectively. This indicates that the degree of anisotropy β_1 is approximately two to three times less important than the actual values of a and N.

Calibration with approximate solutions. In order to provide perspective and calibration with solutions based on approximate methods of analysis, an upper bound solution corresponding to the two-dimensional velocity field postulated in Ref. (6) is obtained for a transversely isotropic power law material. The kinematic model, obtained by superposing a uniform flow and a doublet, resembles the flow of an infinite ice sheet past a circular indenter with the interface matching most the roller condition. The approximate formula may be expressed as given below:

$$\frac{P}{Dt} = \Theta(\beta_1)\ \Gamma_p(\beta_1)\ \frac{4\pi}{\sqrt{3}}\ \frac{N}{N+3}\ \left[\frac{4}{\sqrt{3}}\ \frac{1}{a}\ \frac{2V}{D}\right]^{1/N} \tag{30}$$

where P is the global force, V is the ice sheet velocity, and Γ_p is the theoretically obtained ratio of global pressures for the anisotropic and isotropic cases which is a function of only β_1, i.e.,

$$\Gamma_p = \frac{\beta_1}{[(4\beta_1^n - 1)/3]^{1/n}} \tag{31}$$

Note that $\Gamma_p=1$ under isotropic conditions, i.e., $\beta_1=1$, and that $\Gamma_p=(3/4)^{1/n}$ as $\beta_1 \to \infty$. For $2.5<N<4$, this asymptotic value varies between 0.818-0.835. A fraction equal to 98.5% of the asymptotic value is reached at $\beta_1=5$. The factor Θ is used to modify the upper bound solution, which corresponds to a plane strain condition as a result of the two-dimensional kinematic field selected, in order to be able to apply it under plane stress conditions. As discussed in Ref. (7), Ponter et al.'s (3) analysis for both plane strain and plane stress yields $\Theta=0.5$ for the isotropic case. On the other hand as $\beta_1 \to \infty$, i.e., the material becomes infinitely strong transverse to the plane of isotropy, the difference between the plane strain and plane stress conditions disappears. Thus, the ratio of the global pressures at these two extremes of anisotropy is equal to $\Theta_\infty(3/4)^{1/n}/0.5$, which for N=3 is $1.65\Theta_\infty$ and for N=4 is $1.67\Theta_\infty$. Table 2 shows that case 11 with N=3 and $\beta_1=5$ predicts the ratio of global pressures to be 1.124 which suggests that $\Theta_\infty \approx 0.69$. The variation of Θ with β_1 may be expressed as:

$$\Theta = 0.69 - 0.19\exp[-0.7(\beta_1-1)] \tag{32}$$

Table 2 shows that the predictions based on Eqs. (30)-(32) differ from the finite element solutions by less than 10%. The fixed condition is obtained by multiplying Eq. (30) by 1.27, while the free condition uses a multiplying factor of 0.5 (Table 3).

Local pressures. The maximum (peak) interface normal stress for each of the 14 simulations is listed in Table 2. The table also lists the maximum interface shear stress for the fixed cases. Notice that in all cases the maximum normal pressure is approximately 0.36-1.16 times the global pressure.

The maximum normal stress for the fixed condition is lower than that for the roller condition by 16-23%, although a reverse trend is observed for global pressures. This occurs because part of the force in the fixed condition is carried by interface shear stress. On the other hand, the maximum normal stress for the free condition is about 0-3% higher than that for the roller condition. This negligible increase occurs since the small level of stresses that exist in the predominantly rigid continuum on the downstream side for the free condition is transmitted to the structure from the upstream side. These results confirm the conclusion reached in Ref. (7) that for local pressures the use of the free condition is conservative while for global forces the fixed condition is conservative.

Comparison of the local and global pressures shows that the ratio of the maximum normal interface stress to the global pressure is approximately 0.36 for the fixed condition, 0.56 for the roller condition, and 1.14 for the free condition. Furthermore, the variation of local pressures with V, D, a and N is similar to that for global pressures. Thus multiplication of Eq. (30) by 0.46, 0.56 and 0.57 can be used to estimate the respective maximum normal pressures (Table 3). In a similar fashion, the maximum interface shear stress for the fixed condition may be estimated from the equation with a multiplication factor of 0.33.

For purposes of design it is necessary to consider not only the maximum values of normal stress but also its distribution on the structure. Figure 4 presents typical normal stress distributions corresponding to $\beta_1=5$, which are very similar to the stress distributions for the isotropic case given in Ref. (7). The distributions are not affected, at least visually, as V, D, N and β_1 are varied, although they have to be scaled according to the maximum normal stresses in Table 2. A conservative design approach may be to assume a uniform or rectangular distribution of stress based on the maximum normal interface stress.

Comparison with pressure-area curves. Pressure-area curves are often constructed to help designers obtain the average pressures over tributary loaded areas for structural components (see for example Ref. (30)). A typical curve developed by Sanderson (31) and discussed in Ref. (7) is shown in Fig. 5. The darkly shaded areas represent field and laboratory experimental data, while the lightly shaded areas represent his extrapolation of the measurements. The lower solid line is the local pressure under free interface conditions predicted by Eq. (30) assuming isotropy and N=3. The upper solid line corresponds to an extreme level of anisotropy, i.e., $\beta_1=5$. For contact areas greater than 10 m^2 where plane stress conditions exist, the two lines differ by only a factor of 1.2. These predictions represent an excellent match to measured local pressures. The theoretical predictions made here assume knowledge of the ice sheet velocity just prior to "breakout" or macrocracking. At higher velocities, fracture in ice will be the key mechanism that limits the pressures.

Multiaxial behavior of ice sheet. Stress contours identifying the compression-compression, compression-tension, and tension-tension regions in the ice sheet are generally similar for both the isotropic and anisotropic material models, i.e., (a) tensile stresses occur almost all over the ice sheet, (b) the compression-compression region on the upstream side, is much smaller for the free condition than for the fixed condition, and (c) under free interface conditions the relatively small downstream stresses are predominantly tension-tension. Figures 6 and 7 show that increasing anisotropy, i.e., β_1, leads to increasing compression-compression and tension-tension regions. Experimental evidence for compression-tension states of stress (32) shows that the occurrence of even small tensile stresses weakens ice considerably, leading to premature fracture when compared with uniaxial tensile loading.

The strain fields also are very similar for isotropic and anisotropic material behavior (Fig. 8). The strains are smaller as β_1 increases for the roller and free conditions but remain almost unchanged for the fixed condition. The reduction in strains is associated with the increase in lateral confinement near the upstream and downstream tips of the indenter which in turn significantly affects the behavior of transversely isotropic sea ice. Lateral confinement effects are smaller for the fixed condition since the influence of anisotropy is more evenly distributed over the interface due to the presence of interface shear stresses. The peak values of these stresses occur not at the tips but at points tangential to the direction of the ice movement. The strains are compression-tension almost everywhere on the ice sheet with tensile strains exceeding 0.001 at steady state. Since tensile failure strain for sea ice is about 0.001 or less for strainrates greater than 10^{-7} s^{-1} under just uniaxial loading, it seems likely that cracking will occur even before steady state is reached.

CONCLUSIONS

This paper has (i) presented a general orthotropic elastic - power law creep model for sea ice, and (ii) developed and applied a finite element method of analysis to study the effect of sea ice anisotropy on indentation in the creeping mode. Numerical simulations of ice-structure interaction for a rigid cylindrical indenter under plane stress conditions, a problem of general interest for structural concepts in the Arctic, and a transversely isotropic elastic - power law creep model for sea ice showed that:

1. Anisotropy, as represented by the stress ratio β_1 varying between 1 and 5, can cause global forces to increase by almost 15 percent depending upon whether the interface condition is fixed (infinite adfreeze bond strength), roller, or free (no adfreeze bond strength or interface friction). The factor is 1.10 for the fixed condition, 1.12 for the roller condition, and 1.13 for the free condition.

2. Anisotropy can cause maximum (peak) normal interface pressures to increase by almost 20 percent depending upon the interface condition. The factor is 1.07 for the fixed condition, 1.16 for the roller condition, and 1.19 for the free condition. The interface shear stress for the fixed condition essentially remains unchanged.
3. Finite element predictions of global forces and local pressures differ from a (approximate) modified upper bound solution by less than about 10% for varying velocity, indenter diameter, and material constants.
4. Theoretical predictions of pressure-area curves provide an excellent match to measured local pressures.
5. Anisotropy leads to an increase in the size of the compression-compression and tension-tension states of stress on the upstream and downstream sides, respectively, of the indenter.
6. Anisotropy leads to decreasing strains for the roller and free conditions but to almost no change for the fixed condition. This is associated with the increase in lateral confinement near the upstream and downstream tips of the indenter which in turn significantly affects the behavior of transversely isotropic sea ice. Lateral confinement effects are smaller for the fixed condition since the influence of anisotropy is more evenly distributed over the interface due to the presence of interface shear stresses.

The numerical simulations also showed that (i) even a factor of two uncertainty in velocity will affect ice pressures only by about 20-30%, and (ii) the uncertainties in pressures resulting from variability in the degree of anisotropy is approximately two to three times less important than the variability in the reference power law constants a and N.

Further research is required to (a) predict the level of force that can be directly transmitted to the foundation by a rubble pile, and (b) study the influence of high confining pressures, temperature gradients, and fracture in problems of ice-structure interaction.

ACKNOWLEDGEMENTS

The authors would like to thank Professor Jerome J. Connor and Mr. Fadi S. Chehayeb, graduate student, for their technical contributions during the course of this work. This research is funded by the Standard Oil Company (Ohio) through MIT's Center for Scientific Excellence in Offshore Engineering, and cosponsored by the U.S. Department of the Interior, Minerals Management Service.

The anisotropy of sea ice strongly influences the macromechanical behavior of first year sheet ice, while its influence on the behavior of multi-year floes, though less well studied, may be less. In first year sheet ice, the first source of anisotropy leads to a ratio of vertical to horizontal stress at constant strainrate varying from 2-5 (Butkovich, 1959, Peyton, 1966, Vaudrey, 1977, Sinha, 1983a, and Frederking, 1983), while the second source of anisotropy leads to stress ratios of 0.25-0.60 at a 45 degree azimuthal angle to the c-axis and 0.50-0.95 at a 90 degree angle (Wang, 1979, Vittoratos, 1979, Richter-Menge, et al., 1985, Peyton, 1968).

Theoretical formulations which account for anisotropy in ice with a transversely isotropic model have been developed by Reinicke and Ralston (1977) and by Vivatrat and Chen (1985). The former model is based on plasticity theory and considers ice to be a pressure sensitive material as well. On the other hand, the latter is a pressure insensitive, elastic - power law creep formulation.

The development presented here is based on an orthotropic generalization of the uniaxial, rate-sensitive damage model. Only the continuum (i.e., yielding) behavior of ice is sought to be modelled; not the fracture (bounding) surface. This is unlike some models for ice that fail to distinguish the phenomena of yielding and fracture. The fracture model for ice is described in a separate paper (Ting and Shyam Sunder, in preparation). As a result of this separation, a pressure insensitive model which predicts similar behavior in compression and tension is studied in detail. Such a model appears to be reasonable for sea ice as justified by experimental data.

Theoretical Formulation.-- The multiaxial generalization of Eq. (11) may be expressed in matrix notation as:

$$\dot{\underline{\varepsilon}} = \underline{C}\,\dot{\underline{\sigma}} + \dot{\underline{\varepsilon}}_{cr} \qquad (23)$$

REFERENCES

1. Michel, S. and Toussaint, N., "Mechanisms and Theory of Indentation of Ice Plates," Journal of Glaciology, 19(81), 1977, 285-300.

2. Croasdale, K.R., Morgenstern, M.R. and Nuttall, J.B., "Indentation Tests to Investigate Ice Pressures on Vertical Piers," Journal of Glaciology, 19(81), 1977, 310-312.

3. Ponter, A.R.S. et al., "The Force Exerted by a Moving Ice Sheet on an Offshore Structure: Part I - The Creep Mode," Cold Regions Science and Technology, 8, 1983, 109-118.

4. Bruen, F.J. and Vivatrat, V., "Ice Force Prediction Based on Strain-Rate Field," Proceedings, Third International Symposium on Offshore Mechanics and Arctic Engineering, New Orleans, LA, 3, February 1984, 275-281.

5. Vivatrat, V., Chen, V. and Bruen, F.J., "Ice Load Prediction for Arctic Nearshore Zone," Brian Watt Associates Inc., Houston, TX, 1984, 26p.

6. Ting, S-K, and Shyam Sunder, S., "Sea Ice Indentation Accounting for Strain-Rate Variation," Proceedings, ASCE Specialty Conference: ARCTIC '85 - Civil Engineering in the Arctic Offshore, San Francisco, CA, March 1985, 931-941.

7. Chehayeb, F.S., Ting, S-K., Shyam Sunder, S. and Connor, J.J., "Sea Ice Indentation in the Creeping Mode," Proceedings, 17th Annual Offshore Technology Conference, OTC 5056, May 1985, 329-341.

8. Weeks, W.F. and Gow, A.J., "Preferred Crystal Orientations Along the Margins of the Arctic Ocean," Journal of Geophysical Research, 84(C10), 1978, 5105-5121.

9. Langhorne, P.J., "Crystal Alignment in Sea Ice," Ph.D. Thesis, University of Cambridge, U.K., 1982.

10. Langhorne, P.J., "Laboratory Experiments on Crystal Orientation in NaCl Ice," Annals of Glaciology, 4, 1983, 163-169.

11. Cherepanov, N.V., "Spatial Arrangement of Sea Ice Crystal Structure," Prob. Arkt. i Antarki, 38, 1971, 171-181.

12. Kovacs, A. and Morey, R.M., "Investigations of Sea Ice Anisotropy, Electromagnetic Properties, Strength, and Under-Ice Current Orientation," Research Report No. 80-20, U.S. Army Cold Regions Research and Engineering Laboratory, Hanover, NH, 1980, 18p.

13. Butkovich, T.R., "On the Mechanical Properties of Sea-Ice," Research Report RR54, U.S. Snow, Ice and Permafrost Research Establishment, Thule, Greenland, 1959.

14. Peyton, H.R., "Sea-Ice Strength," Research Report No. UAG R-182, University of Alaska, Geophysical Institute, 1966.

15. Vaudrey, K.D., "Ice Engineering - Study of Related Properties of Floating Sea-Ice Sheets and Summary of Elastic and Viscoelastic Analyses," Technical Report R860, Naval Civil Engineering Laboratory, Port Hueneme, CA, 1977.

16. Sinha, N.K., "Field Tests on Rate Sensitivity of Vertical Strength and Deformation of First-Year Columnar-Grained Sea Ice," Proceedings, 7th International Conference on Port and Ocean Engineering Under Arctic Conditions, Helsinki, 1, April 1983, 909-919.

17. Frederking, R., "Ice Engineering I," Lecture Notes, 1983.

18. Wang, Y.S., "Crystallographic Studies and Strength Tests of Field Ice in the Alaskan Beaufort Sea," Proceedings, 5th International Conference on Port and Ocean Engineering Under Arctic Conditions, Trondheim, Norway, 1979, 651-665.

19. Vittoratos, E.S., "Existence of Oriented Sea Ice by the Mackenzie Delta," Proceedings, 5th International Conference on Port and Ocean Engineering Under Arctic Conditions, Trondheim, Norway, 1979, 643-650.

20. Richter-Menge, J.A. et al., "Triaxial Testing of First-Year Sea Ice," Internal Research Report 877, U.S. Army Cold Regions Research and Engineering Laboratory, Hanover, NH, 1985.

21. Peyton, H.R., "Ice and Marine Structures," Ocean Industry, 3(3), March 1968, 40-41; 3(9), September 1968, 59-65; 3(12), December 1968, 51-58.

22. Ralston, T.D., "An Analysis of Ice Sheet Indentation," Proceedings, IAHR Ice Symposium, Lulea, Sweden, 1978, 13-31.

23. Vivatrat, V. and Chen, V., "Ice Load Prediction with the Use of a Rate-Dependent Anisotropic Constitutive Law," Proceedings, ASCE Specialty Conference: ARCTIC '85 -Civil Engineering in the Arctic Offshore, San Francisco, CA, March 1985, 942-952.

24. American Petroleum Institute, "Bulletin on Planning, Designing, and Constructing Fixed Offshore Structures in Ice Environments," Bul. 2N, First Edition, January 1982.

25. Glen, J.W., "The Creep of Polycrystalline Ice," Proceedings, Royal Society of London, Series A, 228(1175), 1955, 519-538.

26. Palmer, A.C., "Creep-Velocity Bounds and Glacier Flow Problems," Journal of Glaciology, 6(46), 1967, 479-488.

27. Frederking, R., "Plane Strain Compressive Strength of Columnar-Grained and Granular-Snow Ice," Journal of Glaciology, 18(80), 1977, 505-516.

28. Sanderson, T.J.O., "Theoretical and Measured Ice Forces on Wide Structures," Proceedings, IAHR Ice Symposium, Hamburg, August 1984, 32p.

29. Wang, Y.S., "A Rate-Dependent Stress-Strain Relationship for Sea Ice," Proceedings, First International Symposium on Offshore Mechanics and Artic Engineering, New Orleans, LA, 1982, 243-248.

30. Bruen, F.J., Byrd, R.C., Vivatrat, V. and Watt, B.J., "Selection of Local Design Ice Pressures for Arctic Systems," Proceedings, 14th Annual Offshore Technology Conference, OTC 4334, May 1982, 417-435.

31. Sanderson, T.J.O., Personal Communications, 1984.

32. Haynes, F.D., "Tensile Strength of Ice Under Triaxial Stresses," Research Report 312, U.S. Army Cold Regions Research and Engineering Laboratory, Hanover, NH, 1973, 21p.

NOMENCLATURE

a	parameter of power law model in reference direction
a_i	six parameters of orthotropic material model
A	constant equal to a_1+a_2
$\underline{B}$	finite element transformation matrix
$\underline{C}$	linear elastic orthotropic compliance matrix
D	indenter diameter
$\underline{D}$	linear elastic orthotropic rigidity matrix
E	Young's modulus for transversely isotropic sea ice
$\underline{G}$	transformation matrix relating $\underline{S}^*$ to σ
$\underline{K}$	linear elastic stiffness matrix of finite element
$\underline{K}_G$	linear elastic global stiffness matrix
n	constant equal to $2N/(N+1)$
N	power law exponent
P	global force on indenter
$\underline{P}$	applied load vector
$\underline{S}^*$	pseudo deviatoric stress vector for orthotropic material
t	thickness of ice sheet
t_i	time at instant i
$\underline{U}$	nodal displacement vector
V	approach velocity of ice sheet
α	parameter in time integrator
β_i	five ratios of maximum stress along x, z and the 45° axes on the y-z, x-y and z-x planes, respectively, to the stress in the reference y-direction
Γ	ratios of stresses or pressures under different conditions
$\underline{\varepsilon}$	total strain vector
$\underline{\varepsilon}_c$	creep strain vector
ε_e	effective strainrate measure
θ	plane strain to plane stress conversion factor
λ	associative flow rule constant
ν	Poisson's ratio for transversely isotropic sea ice
$\underline{\sigma}$	stress vector
σ_e	effective stress measure
τ	ratio of confining pressure to axial stress
ϕ	scalar potential function
$\dot{\ }$	rate form is represented by a dot above the symbol

TABLE 1 - SUMMARY OF CASES

Case	Velocity (ft/hr)	Diameter (ft)	N	β_1	Interface Condition
1	0.64	350	3	3	Fixed
2	0.64	350	3	3	Roller
3	0.64	350	3	3	Free
4	0.10	350	3	3	Roller
5	1.00	350	3	3	Roller
6	0.64	1000	3	3	Roller
7	0.64	16.4	3	5	Free
8	0.64	328000	3	5	Free
9	0.64	350	4	3	Roller
10	0.64	350	3	5	Fixed
11	0.64	350	3	5	Roller
12	0.64	350	3	5	Free
13	0.64	350	3	2	Fixed
14	0.64	350	3	2	Free

Note: 1 ft = 0.3048 m

TABLE 2 - SUMMARY OF RESULTS

Case	P/Dt (MPa)		Maximum Interface Normal Stress (MPa)		Anisotropy/Isotropy	
	Finite Element Analysis	Modified Upper Bound	Finite Element Analysis	Modified Upper Bound	Global Pressure	Maximum Interface Normal Stress
1	2.41	2.62	0.87	0.95	1.08	1.06
2	1.98	2.06	1.10	1.15	1.12	1.12
3	0.99	1.03	1.13	1.17	1.11	1.15
4	1.03	1.11	0.58	0.62	1.10	1.12
5	2.33	2.39	1.29	1.34	1.15	1.15
6	1.33	1.45	0.74	0.81	1.08	1.09
7		2.96		3.37	-	-
8	0.10	0.11	0.11	0.12	-	-
9	2.57	2.43	1.43	1.36	1.22	1.25
10	2.46	2.71	0.88	0.98	1.10	1.07
11	1.99	2.13	1.14	1.19	1.12	1.16
12	1.01	1.07	1.17	1.22	1.13	1.19
13	2.35	2.49	0.85	0.90	1.05	1.04
14	0.96	0.98	1.12	1.12	1.08	1.12

Note: The maximum interface shear stress for the fixed condition is 0.61 MPa for β_1=3, 0.63 MPa for β_1=5, and 0.60 MPa for β_1=2.
1 MPa = 145 psi

TABLE 3 - MULTIPLYING FACTORS FOR APPROXIMATE MODEL (Eq. 30)

Condition	Global Pressures	Maximum Interface Normal Stress
Roller	1.00	0.56
Fixed	1.27	0.46
Free	0.50	0.57

Note: Factor for Maximum Interface Shear Stress in Fixed Condition = 0.33

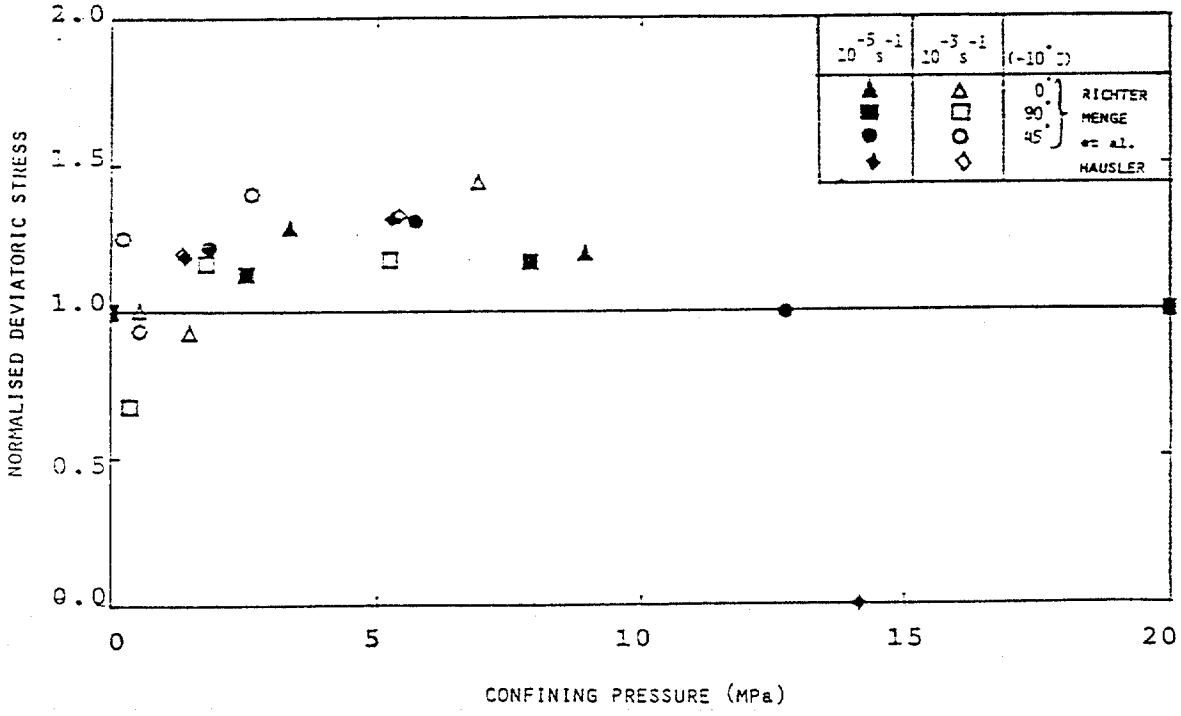

Fig. 1 - Normalised Deviatoric Stress Versus Confining Pressure

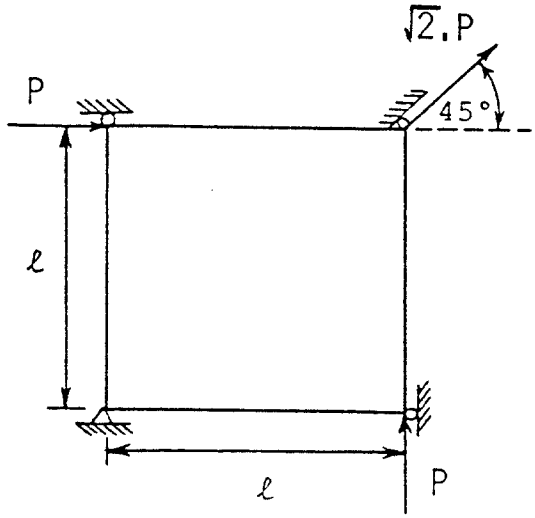

Fig. 2 - Test Problem

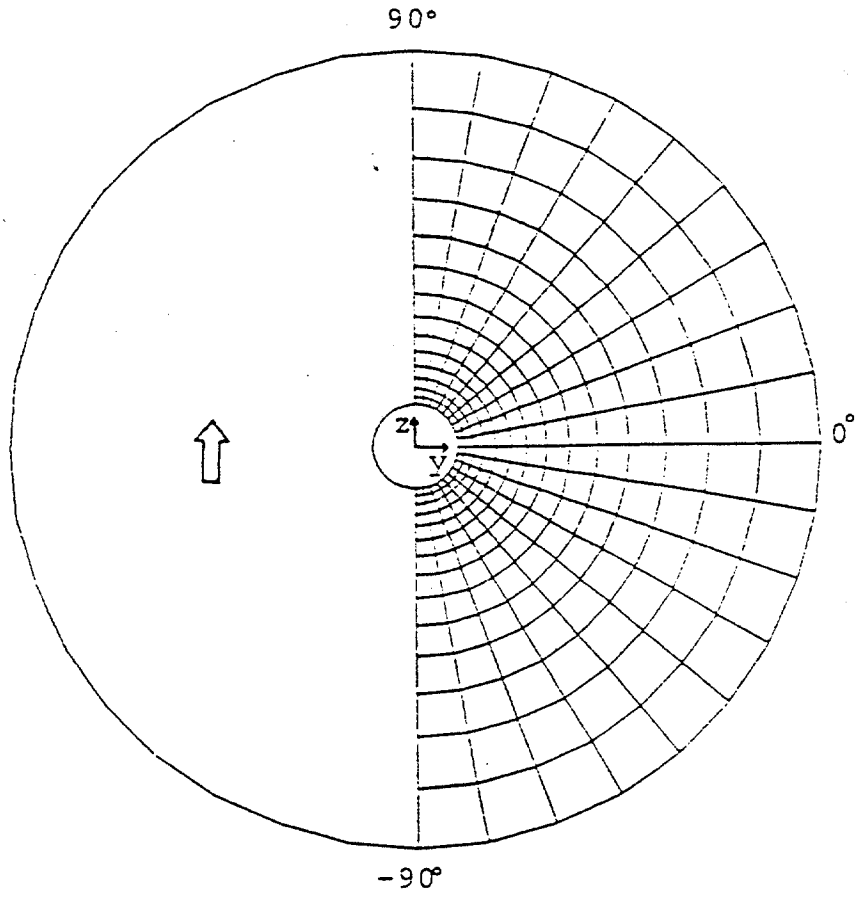

Fig. 3 - Finite Element Grid

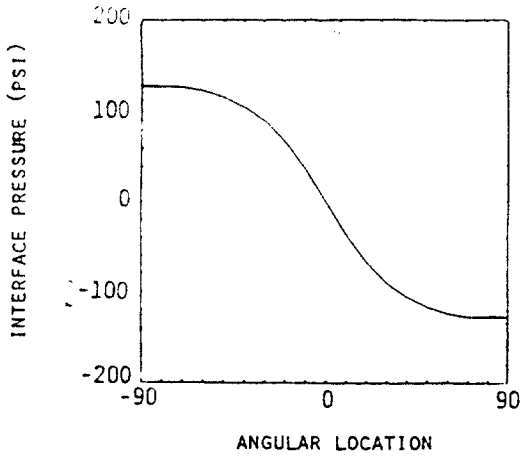

(a) Fixed Case

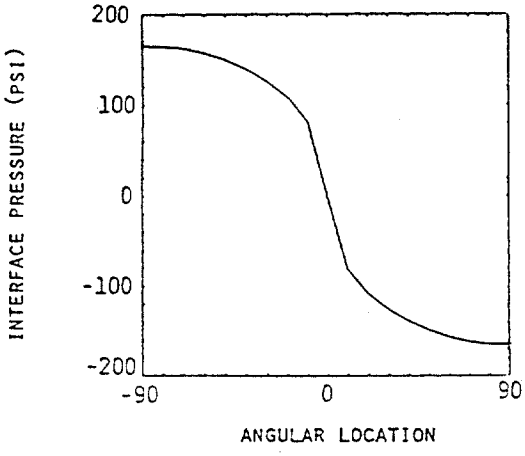

(b) Roller Case

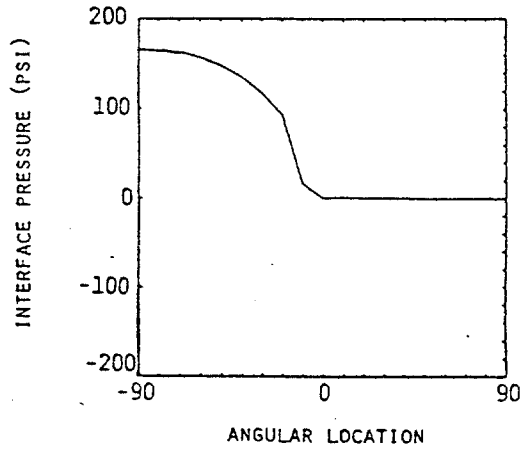

(c) Free Case

Fig. 4 - Normal Stress Distribution on Interface at Steady State for $\beta_1 = 5$

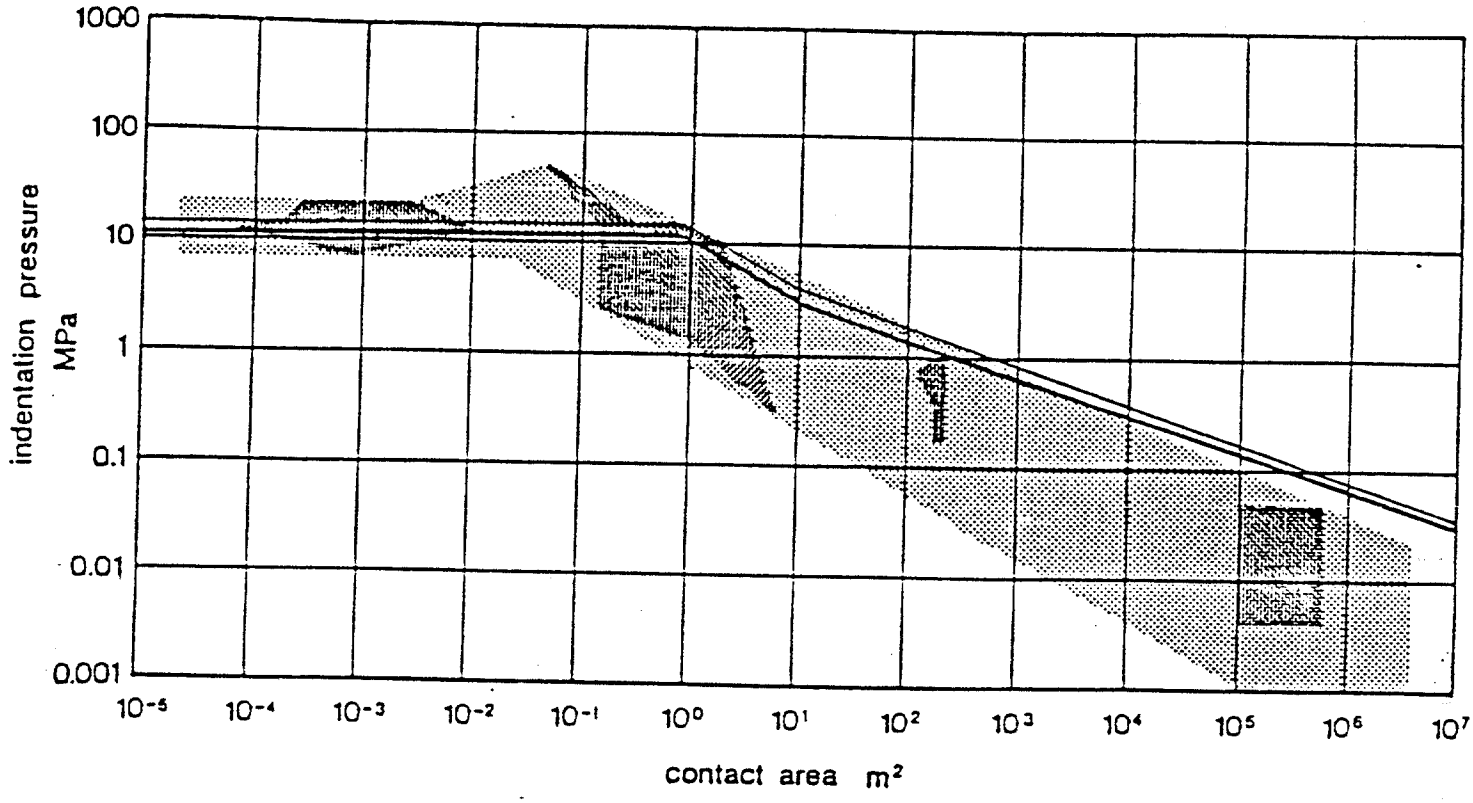

Fig. 5 - Pressure-Area Curve

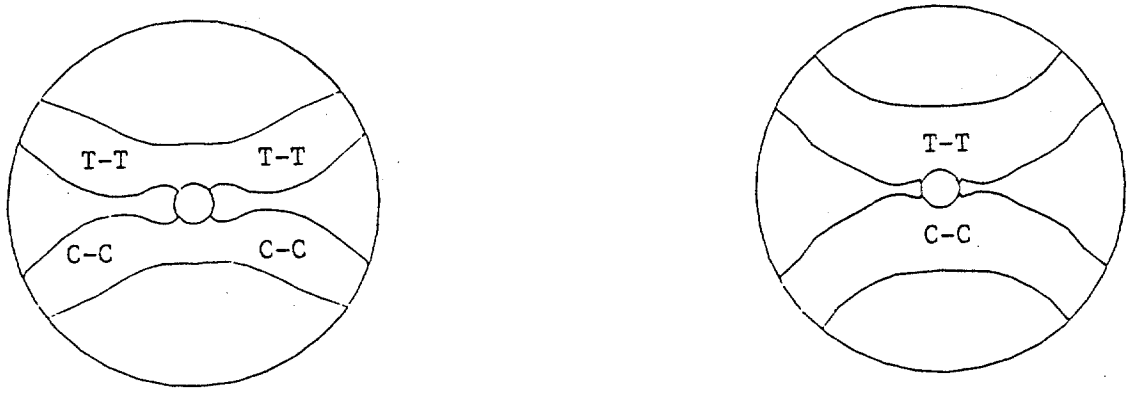

(a) Isotropic Case ($\beta_1=1$)

(b) Anisotropic Case ($\beta_1=5$)

Fig. 6 - Biaxial Stress States at Steady State for Fixed Condition

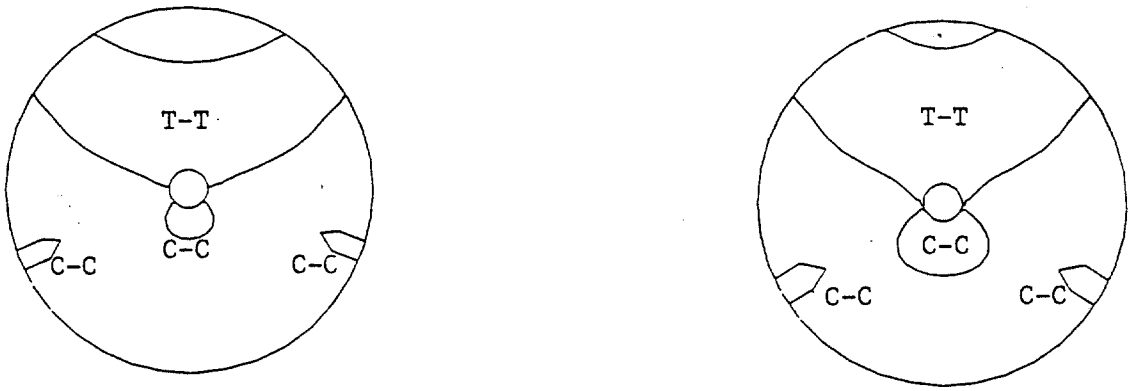

(a) Isotropic Case (β_1=1)

(b) Anisotropic Case (β_1=5)

Fig. 7 - Biaxial Stress States at Steady State for Free Condition

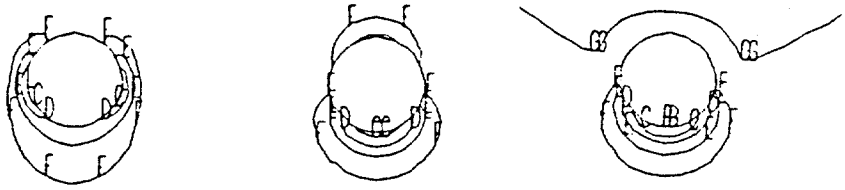

Minimum Principal Strain

Contour Levels

A = -0.0030
B = -0.0025
C = -0.0020
D = -0.0015
E = -0.0010
F = -0.0005
G = 1.2×10^{-10}

(i) Isotropic Case ($\beta_2=1$)

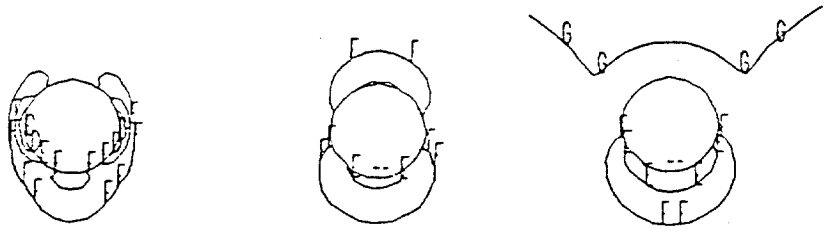

(ii) Anisotropic Case ($\beta_2=5$)

(a) Fixed Case (b) Roller Case (c) Free Case

Fig. 8 - Minimum Principal Strain Rate Contours (Time Step 20)

S. Shyam Sunder and Seng-Kiong Ting
Department of Civil Engineering
Massachusetts Institute of Technology
Room 1-274, Cambridge, MA 02139 USA

DUCTILE TO BRITTLE TRANSITION IN SEA ICE UNDER UNIAXIAL LOADING

Abstract

A new constitutive model for sea ice, applicable to monotonic uniaxial loading in both compression and tension, is proposed. The stress-strain-strainrate behavior of sea ice is modelled accounting for strain softening and for fracture which manifests itself in terms of tensile cracking and crushing in compression. The model is used to predict first cracking in ice under uniaxial compressive loading based on a limiting tensile strain criterion and the results are calibrated with experimental data available in the literature.

1 INTRODUCTION

Field observations of sea ice indentation on offshore structures in the Arctic show that fracture processes are a major factor in ice-structure interaction.

The occurrence of first cracks in ice under compressive creep conditions in the laboratory has been studied by Gold /2/. Based on the assumption that grain boundary shear or sliding can be associated with a delayed elastic effect, Sinha /10/ postulated that

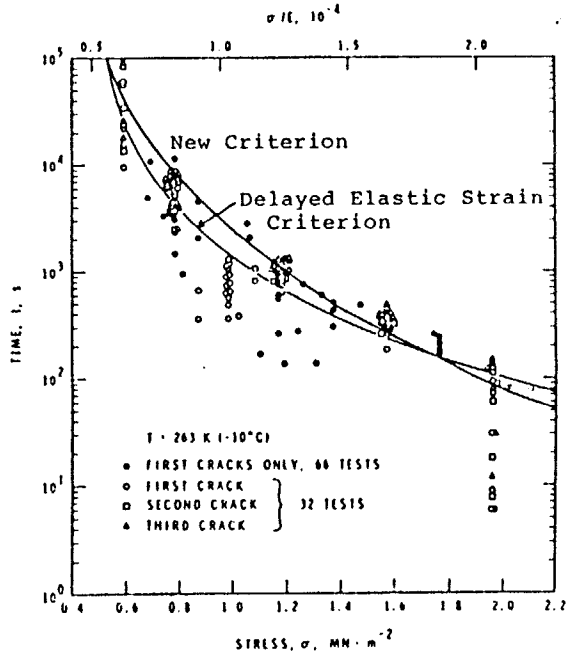

Fig. 1 Formation of first cracks during uniaxial compressive creep tests.

delayed elasticity can be linked to crack nucleation. With the help of his mathematical model for delayed elasticity and the experimental data of Gold, he showed that for S-2 ice of grain size 4.5 mm cracks begin to form if the delayed elastic strain exceeds 1.04×10^{-4}. The time to formation of first crack based on Gold's laboratory experiments and Sinha's delayed elastic strain criterion is plotted in Fig. 1.

A suddenly applied constant load case, i.e., creep, is not representative of loading conditions on offshore structures. A constant strainrate or stress-rate condition may be more realistic. Sanderson and Child /8/ consider typical stress-rates of 0.010-0.035 kPa s^{-1} and extreme stress-rates of 1-5 kPa s^{-1}. Using the principle of superposition, which Sinha /11/

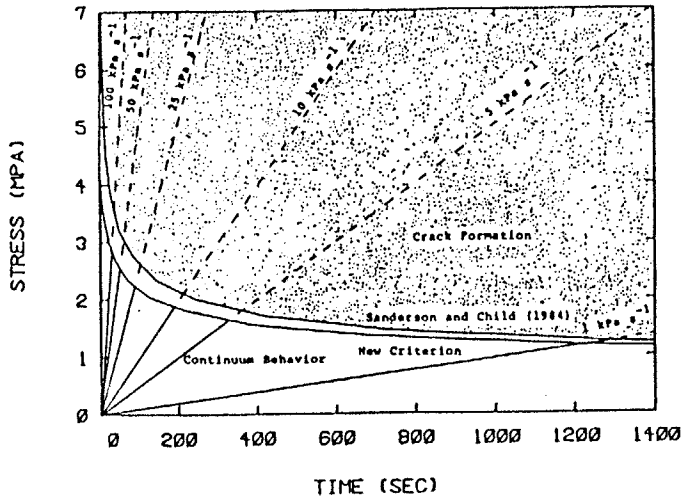

Fig. 2 Formation of first cracks during tests at constant stress-rate.

has shown to be valid for "icelike" materials under monotonically increasing stress, and the delayed elastic strain criterion they predict that first cracks in pure S-2 ice should typically occur at a stress of 0.6-0.7 MPa and in extreme conditions may occur at 1.3-1.8 MPa (Figs. 2 and 3). For sea ice, the stress levels are corrected by altering the net section stress due to brine volume as described by Sanderson /7/. The corresponding stresses are 0.4 MPa and 0.8-1.1 MPa (Fig. 4).

In order to explain the well-known discrepancy in ice forces between predictive models which use mechanical properties obtained in the laboratory and actual field measurements, Sanderson and Child /8/ propose that formation of first cracks in the field is synonymous with failure of the ice. As such, the stress levels identified in the previous paragraph are considered to limit ice forces. Although intuitively appealing, it is not clear how this failure criterion

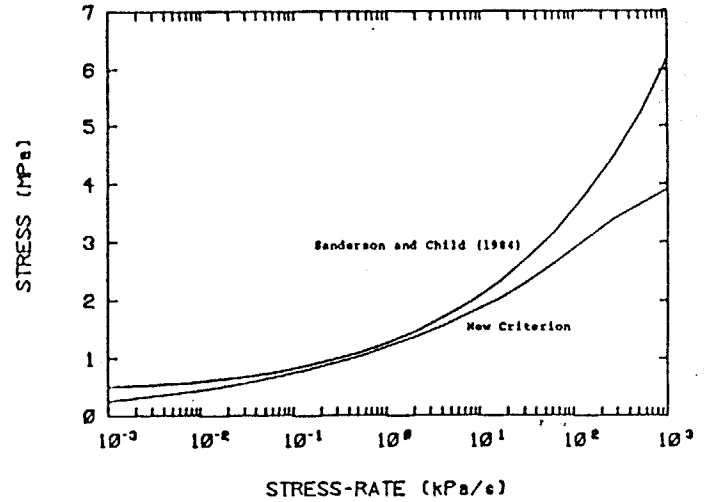

Fig. 3 Stress at which first cracks appear for pure ice at constant stress-rates.

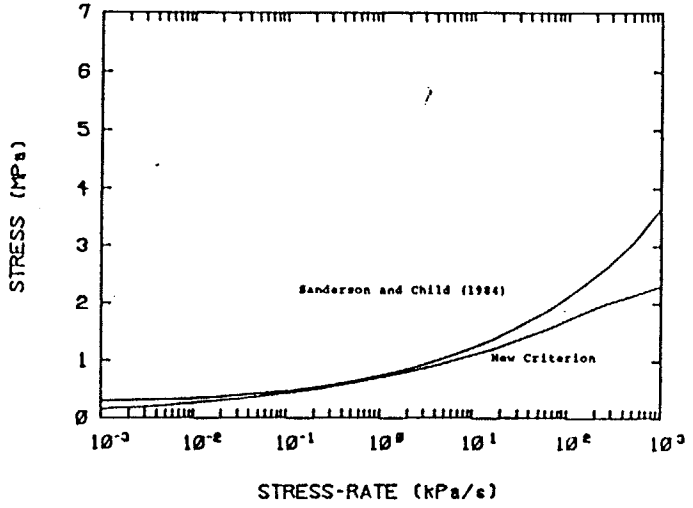

Fig. 4 Stress at which first cracks appear for sea ice at constant stress-rates.

can be incorporated in a finite element analysis framework for ice force prediction.

Fracture manifests itself in terms of tensile cracking and crushing in compression. Numerical analysis of ice-structure interaction processes in the creeping mode of deformation /1/ indicates that tensile stresses occupy a large fraction of the area of an ice sheet. Since ice is weaker in tension than in compression once cracks occur, accounting for the differing behavior of ice in tension may help to reduce ice force predictions significantly.

This paper presents a new constitutive model for sea ice, applicable to monotonic uniaxial loading in both compression and tension. The stress-strain-strainrate behavior of ice is modelled accounting for strain softening and fracture. The model is used to predict the occurrence of first cracks in ice under uniaxial compressive loading. Tensile strains occur under this loading condition as a result of the Poisson effect or incompressibility condition. Once cracks occur, the material continues to sustain compressive load but loses its ability to carry tensile loads in the transverse direction if applied. This is a realistic assumption and is often used in modeling concrete behavior /12/. A limiting tensile strain criterion dependent on the instantaneous strainrate in tension is developed to predict crack nucleation. The results for compressive creep compare very well with the experimental data of Gold /2/.

2 NEW UNIAXIAL CONSTITUTIVE MODEL

A phenomelogical approach based on simple thermo-rheological models has been used in developing the new

uniaxial constitutive model /13/. The model is based on Orowan's concept /5/ that material strength is affected simultaneously by work hardening or strain hardening and work softening or recovery. Fracture in pure ice is modelled using the 'strength'-strainrate data of Ashby and Cooksley contained in Palmer et al. /6/. The resulting model is consistent with Michel's /4/ schematic idealization of ice behavior.

For constant strainrates of up to 5×10^{-4} s^{-1} under compressive loading, the stress-strain-strainrate behavior of ice is given by:

$$\sigma = \frac{A}{M}\,\dot{\varepsilon}^{\frac{1}{N}}\,[1-\exp(-M\varepsilon)] - \frac{B}{L}\,\dot{\varepsilon}^{\frac{1}{K}-1}\,[1-\exp(-L\varepsilon)] \qquad (1)$$

where A=114025 MPa $s^{1/3}$, B=217408 MPa $s^{2/3}$, M=1411.2, L=430, N=3 and K=0.6 based on Wang's /14/ experimental data for sea ice. At strainrates greater than 10^{-2} s^{-1}, pure ice is assumed to fracture (crush) at a stress of 5.1 MPa and to behave as a linear elastic material with Young's modulus, E, equal to 9.5 GPa. The intermediate strainrates define the ductile-to-brittle transition in compression. For strainrates between 5×10^{-4} and 10^{-3} s^{-1}, the fracture strength is assumed to be 7.14 MPa and the stress-strain behavior up to fracture is given by Eq. (1). For strainrates in the range 10^{-3}-10^{-2} s^{-1}, a linear interpolation between 7.14 and 5.1 MPa on log-log scale is used to define the fracture strength, while the stress-strain behavior up to fracture is defined by Eq. (1) for a strainrate of 10^{-3} s^{-1} (the initial tangent modulus of Eq. (1) reaches a value of 9.5 GPa, the linear elastic modulus, at this strainrate).

Constant stress-rate and creep curves in compression generated with this model agree with Wang's

/14/ theoretical model and the experimental data used by him for calibration purposes. Moreover, the adopted modeling strategy avoids the numerical problems encountered by Wang.

The stress-strain-strainrate behavior in uniaxial tension prior to fracture is considered to be identical to that under uniaxial compression as given by Eq. (1). Hawkes and Mellor /3/ justify this assumption for creep data. For strainrates less than 3×10^{-8} s^{-1} (i.e., tension 'strength' of 0.42 MPa for pure ice and 0.25 MPa for sea ice), ice does not fracture in tension. For strainrates greater than 5×10^{-5} s^{-1}, tensile cracking occurs at a stress of 2.04 MPa. A linear interpolation on log-log scale is used for intermediate strainrates, defining the ductile-to-brittle transition in tension.

3 PREDICTION OF FIRST CRACK OCCURRENCE

The prediction of first crack occurrence under uniaxial compressive creep and constant stress-rate conditions is considered here. In order to make this prediction, it is necessary to monitor the tensile strains resulting from the Poisson effect or incompressibility condition and to compare them with the strain for tensile fracture at the instantaneous strainrate. When the actual instantaneous tensile strain becomes equal to the instantaneous fracture strain the first crack is assumed to occur. This is the limiting tensile strain criterion for crack nucleation. A numerical procedure is developed to make the crack prediction. A time increment not exceeding 10^{-5} divided by the instantaneous strainrate is necessary to obtain accurate results.

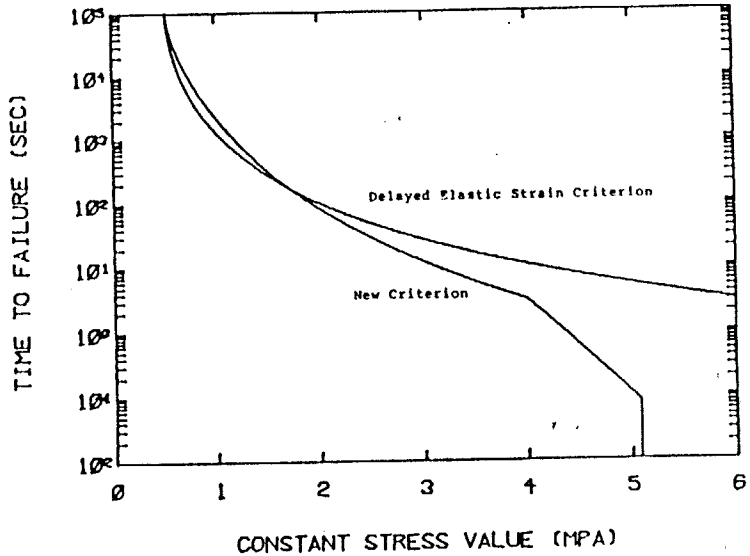

Fig. 5 Formation of first cracks in uniaxial creep up to the fracture stress in compression.

Figure 1 contains the prediction of first cracks using the limiting tensile strain criterion under creep conditions. Comparison with the experimental data of Gold shows that the proposed criterion is in excellent agreement with data. In particular, the time to first crack asymptotically approaches infinity as the compressive stress reduces to 0.52 MPa. The choice of stress-strainrate at which ice transits from ductile to fracture behavior in tension , i.e., 0.42 MPa and 3×10^{-8} s^{-1},defines this asymptote. The large scatter in the experimental results at σ=2 MPa is possibly due to the finite rise time of two seconds for the applied load to reach the constant stress state for ideal creep. The limiting tensile strain criterion compares well with the delayed elastic strain criterion of Sinha for the range of stresses considered in the figure. However, at higher stresses the two criteria are in significant disagreement (Fig. 5). At

the compressive fracture stress of 5.1 MPa, the proposed model predicts a zero time to first crack since no creep can occur under this loading. At stresses greater than about 4 MPa which corresponds to the leveling-off of the tensile fracture stress to 2.04 MPa, the tensile strain to fracture reduces faster than at lower stresses. This leads to a faster reduction in time to first crack. The sharp kink at the 4 MPa transition point can be eliminated by a smoother transition in the cracking criterion around the strainrate of 5×10^{-5} s^{-1}.

Figure 2 contains the prediction of first cracks under constant stress-rate conditions. The agreement between Sanderson and Child's analysis based on the delayed elastic strain criterion and the present criterion is very good in general. At infinite stress-rate, the stress at first crack is limited by the compressive fracture stress of 5.1 MPa. This is predicted by the proposed fracture criterion. Figures 3 and 4 show that for typical stress-rates the stress at first crack is 0.45-0.60 MPa for pure ice and 0.26-0.35 MPa for sea ice. For extreme stress-rates the corresponding numbers are 1.2-1.6 MPa and 0.7-0.9 MPa.

4 CONCLUSIONS

This paper has proposed a new uniaxial constitutive model for sea ice that accounts for strain softening and fracture (cracking and crushing). The adequacy of the model has been demonstrated by comparison with experimental data obtained under constant strainrate, creep, and constant stress-rate conditions. A limiting tensile strain criterion has been postulated to predict first cracks in ice and its

validity has been established by comparison with available experimental data.

The constitutive model is being extended to account for unloading and reloading conditions and for multiaxial stress states. The resulting model will be incorporated in a finite element analysis framework to predict indentation pressures and forces using the limiting tensile strain criterion for crack initiation and propagation. For load transmitting systems such as ice features (as opposed to load bearing structural systems) a limiting tensile strain criterion for fracture propagation is likely to be conservative when compared to a classical fracture mechanics approach. This is because the latter considers only the propagation of pre-existing cracks with a given distribution of sizes, while the former may be used to predict both the initiation and propagation of cracks in a material originally in virgin (flawless) form.

5 ACKNOWLEDGEMENTS

This research is funded by The Standard Oil Company (Ohio) through MIT's Center for Scientific Excellence in Offshore Engineering, and cosponsored by the U.S. Department of the Interior, Minerals Management Service.

6 REFERENCES

1. Chehayeb, F.S., Ting, S-K., Shyam Sunder, S. and Connor, J.J., Sea ice indentation in the creeping mode. Proc. of the 17th Annual Offshore Technology Conference, Paper OTC 5056, Houston, Texas, May 1985.

2. Gold, L.W., The process of failure of columnar-grained ice. Philosophical Magazine, Vol. 26, No. 2, 1972, pp. 310-328.

3. Hawkes, I. and Mellor, M., Deformation and

fracture of ice under uniaxial stress. Journal of Glaciology, Vol. 11, No. 61, 1972, pp. 103-131.

4. Michel, B., Advances in ice mechanics. The 6th int. conf. on Port and Ocean Engineering under Arctic Conditions (POAC). Quebec 1981. Universite Laval, Quebec 1981, pp.189-204.

5. Orowan, E. and Scott, J.W., The creep of metals. Journal of Iron and Steel Institute, Vol. 54, 1946, 45 p.

6. Palmer, A.C., Goodman, D.J., Ashby, M.F., Evans, A.G., Hutchinson, J.W., and Ponter, A.R.S., Fracture and its role in determining ice forces on offshore structures. Annals of Glaciology, Vol. 4, 1983, pp. 216-221.

7. Sanderson, T.J.O., Theoretical and measured ice forces on wide structures. Proc. 7th International Symposium on Ice, IAHR, Hamburg, August 1984, 32 p.

8. Sanderson, T.J.O. and Child, A.J., Ice loads on offshore structures: the transition from creep to fracture. 1984, 8 p.

9. Sinha, N.K., Rheology of columnar-grained ice. Experimental Mechanics, Vol. 18, No. 12, December 1978, pp. 464-470.

10. Sinha, N.K., Delayed elastic strain criterion for first cracks in ice. Proc. IUTAM Symposium on the Deformation and Failure of Granular Materials. Delft 1982, A.A. Balkema, Rotterdam, pp. 323-330.

11. Sinha, N.K., Creep model of ice for monotonically increasing stress. Cold Regions Science and Technology, Vol. 8, 1983, pp.25-33.

12. Task Committee on Finite Element Analysis of Reinforced Concrete Structures, Finite element analysis of reinforced concrete. ASCE, New York, NY 1982, 545 p.

13. Ting, S.K. and Shyam Sunder, S., Sea ice indentation accounting for strain-rate variation. Proc. of the ASCE Specialty Conference: Arctic '85 - Civil Engineering in the Arctic Offshore, San Francisco, California, March 1985, 11 p.

14. Wang, Y.S., A rate-dependent stress-strain relationship for sea ice. First International Symposium on Offshore Mechanics and Arctic Engineering, New Orleans, 1982, pp. 243-248.

A RATE-SENSITIVE DAMAGE MODEL FOR THE CONTINUUM BEHAVIOR OF SEA ICE

Seng-Kiong Ting and S. Shyam Sunder
Massachusetts Institute of Technology Department of Civil Engineering, Rm 1-274, Cambridge, MA 02139 (U.S.A.)

ABSTRACT

A rate-sensitive damage model is developed for describing the macroscale continuum behavior of sea ice under variable loading conditions. This model, based on a nonlinear generalization of the Maxwell differential model, is characterized by its ability to (a) decompose the various recoverable and irrecoverable components of strain, (b) represent continuously damaging or strain-softening material behavior in the ductile to brittle transition region, (c) capture the rate-dependent behavior of sea ice with rate-independent model parameters, and (d) describe materially anisotropic mechanical behavior. Further, the model shows strong dependency of the creep and constant strainrate behavior. Calibration of the model is achieved with several independent sets of data, particularly those for first-year sea ice.

1. INTRODUCTION

Ice in general, and columnar sea ice in particular, is a very complex material which exhibits a wide range of behaviors often at the same time. As a consequence of its occurrence at thermorheologically high temperatures, the macroscale mechanical behavior of ice is strongly influenced by temperature and rate of loading, in addition to elasticity, plasticity, damage, and fracture. In many applications ice behaves predominantly as a continuum undergoing deformation and a constitutive model which captures that behavior is necessary to simulate the deformation process.

Shapiro (1978) has presented a four element nonlinear viscoelastic model for sea ice which can be applied under general loading conditions. Under

constant strainrate tests, this model predicts an approximately linear increase of strength with the logarithm of strainrate which appears to differ from available test data. Furthermore, this model cannot simulate the post-peak decrease of stress due to material damage.

Sinha (1978, 1979, 1983b) has proposed a simple thermorheological model to describe the uniaxial stress-strain-strainrate-temperature relationship for columnar-grained ice. The model, consisting of eight parameters, accounts for the instantaneous elastic, delayed elastic, and secondary creep components of strain. According to the model, the delayed elastic strain under creep loading conditions is directly proportional to the applied stress and grain size while its value reaches a maximum asymptotically with time. Calibration has been achieved with the extensive creep and constant stressrate tests conducted on columnar-grained ice by him and the creep data of Brill and Camp (1961).

Michel (1981) has proposed a similar model for ice based on dislocation theory. The model, consisting of a network of linear springs and nonlinear dashpots with ten parameters, has been applied under constant stress (creep) and strainrate conditions. Unlike Sinha's model, this formulation shows a peak followed by a stage of permanent creep at a lower stress. Calibration with limited data from Brill and Camp (1961) and his own tests suggests the need for adjustment of model parameters for each test case.

Wang (1982) has proposed a four parameter semi-empirical uniaxial model for sea ice in compression. Under constant strainrate conditions, the model displays a peak followed by a stage of permanent creep at a lower stress. The model has not been extended to allow decomposition of the various strain components. Furthermore, numerical problems associated with the mathematical formulation can arise under certain conditions during constant stressrate and

creep loading. Calibration of the model has been performed with his constant strainrate and stressrate tests and with the creep data contained in Mellor (1980).

Spring and Morland (1981, 1982, 1983) have investigated viscoelastic fluid and solid relations of differential type as well as single integral representations for the nonlinear viscoelastic deformation of ice. In the fluid relation the constant stress and constant strainrate responses are neither completely independent nor completely dependent, so reflect some common and some distinct properties. In the solid relation these two responses are completely independent and, in fact, are insufficient to determine the model without further reductions. Mellor (1980) conjectured that the two types of response should be dependent, which is the familiar linear result. While the differential fluid relation is closer to this conjecture, it cannot model anisotropy and strain jumps. In both types it is necessary to incorporate dependence of one or more response coefficients on both stress and strainrate or strain respectively, and covering adequate stress-strainrate or stress-strain domains by practical test programs is non-trivial. On the other hand, the single integral representation is sensitive to kernel detail, which in turn is dependent on strainrate histroy. Calibration of the formulations with experimental data has been very limited.

More recently, Karr (1984, 1985a, 1985b) has been investigating the use of continuous damage models for describing the uniaxial behavior of ice. His four parameter model for sea ice displays a peak followed by a stage of permanent creep at a lower stress and has been derived for constant strainrate loading conditions. For creep loading, an empirical approach is used in conjunction with the damage mechanics based stress-strain law for constant strainrate loading. The constant stressrate case has not been studied, and

the methodology for strain decomposition under general loading conditions is unclear.

This paper presents a rate-sensitive damage model for describing the macroscale continuum behavior of sea ice under variable loading conditions. The model, based on a nonlinear generalization of the Maxwell differential model, is characterized by its ability to (a) decompose the various recoverable and irrecoverable components of strain, (b) represent continuously damaging or strain-softening material behavior in the ductile to brittle transition region, (c) capture the rate-dependent behavior of sea ice with rate-independent model parameters, and (d) describe materially anisotropic mechanical behavior. Further, the model shows strong dependency of the creep and constant strainrate behavior. Calibration of the model is achieved with several independent sets of data, particularly those for first-year sea ice.

2. UNIAXIAL MODEL FORMULATION

The nonlinear generalization of the two element Maxwell fluid model consists of an elastic spring in series with a viscous dashpot (Fig. 1). The rate-sensitive spring represents recoverable strains and accounts for both instantaneous elasticity and delayed elasticity or primary creep. The viscous dashpot represents irrecoverable strains associated with nonlinear viscosity or secondary creep. Both the rate-sensitive spring and the nonlinear viscous dashpot are affected by material damage and as a result account for strain-softening or tertiary creep. The mathematical formulation of the two Maxwell elements is discussed in what follows.

Rate-Sensitive Elastic Spring.-- Most conventional materials are used at thermorheologically low temperatures where their elastic properties are relatively insensitive to rate of loading. The modulus of elasticity or

Young's modulus for such materials is obtained from tests conducted at commonly encountered rates of loading and taken to be a constant. However, in certain high loading rate applications, e.g., blast and impact, it is known that the modulus of elasticity increases with rate. As a consequence of its occurrence at thermorheologically high temperatures, the elastic modulus of ice is sensitive to even "slight" variations in rate of loading (Mellor, 1983) and cannot be taken as a constant. If the Young's modulus for ice, E, is defined to be the modulus value at very high rates of loading, then the variation of effective elastic modulus, E_{eff}, with rate may be expressed as:

$$E_{eff} = E\,[1 - r \exp\,(-A/E\,\dot{\varepsilon}^{\,1/N})] \qquad (1)$$

where $\dot{\varepsilon}$ is the strainrate, r and A are constants, and N is the power law index for ice. Equation (1) shows that the effective modulus tends to the Young's modulus as the strainrate approaches infinity. As the strainrate tends to zero, the effective modulus tends to (1-r)E. If r is one the effective modulus tends to zero, and if r is zero the effective modulus is rate-insensitive and equal to the Young's modulus. A value of r less than one is necessary to model stress relaxation, as explained later in this paper.

The rate-sensitive elastic spring represents recoverable strains contributed both by instantaneous elasticity and by delayed elasticity. By defining the total elastic strain to be the sum of the strains due to these two components it is possible to model the rate-sensitive spring as the series combination of two springs, one with modulus equal to E, i.e., the Young's modulus, and the other with a modulus equal to E_d. It then follows that:

$$1/E_{eff} = 1/E + 1/E_d \qquad (2)$$

with:

$$E_d = E\,[1/r \exp(A/E\,\dot{\varepsilon}^{1/N}) - 1] \qquad (3)$$

Equation (3) shows that the modulus of delayed elasticity tends to infinity at infinite strainrate and to $[(1-r)/r]E$ at zero strainrate. In the latter case, the modulus tends to zero if r is one and to infinity if r is zero. Use of Eq. (2) shows that when the modulus of delayed elasticity is infinity, the effective modulus equals the Young's modulus. When the modulus of delayed elasticity is very small with respect to the Young's modulus, the effective modulus equals the modulus of delayed elasticity. This occurs at low strainrates. Research on the mechanical behavior of materials at thermorheologically high temperatures (Grant, 1971) has shown that delayed elasticity associated with grain boundary sliding does lead to the behavior predicted by this model.

Nonlinear Viscous Dashpot.-- The secondary creep strain, ε_{sc}, in most materials including ice is assumed to follow the well known Glen's power law (Glen, 1955). A generalization of that formulation adopted here is mathematically expressed as:

$$\sigma = [(A/M)\ \dot{\varepsilon}^{1/N-1}]\ \dot{\varepsilon}_{sc} \qquad (4)$$

where A and N are the constants in Eq. (1), and M is a third constant. Normally (A/M) is taken to be a single constant and $\dot{\varepsilon}$ equals $\dot{\varepsilon}_{sc}$ when modeling steady state secondary creep, i.e., where primary and tertiary components of creep are absent. Since A is used to describe the primary creep strains, an additional degree of freedom in the form of the constant M is necessary to model secondary creep strains. The nonlinearity is associated with the dashpot constant $\sigma/\dot{\varepsilon}_{sc}$ which is a function of the total strainrate.

Continuous Damage Model.--In the transition from pure ductile to pure brittle behavior under compressive loading ice behaves as continuum undergoing damage. Under tensile loading the transition region is much smaller and a continuum description of damage is of limited value. Damage in ice leads to tertiary creep under constant stress loading and to strain-softening under

constant strainrate loading. Damage is almost nonexistant at very small strain and strainrate but increases as both strain and strainrate increase. Further, unloading a damaged material generally shows a reduction in the effective modulus of elasticity. Thus the phenomenon affects both the rate-sensitive spring and the nonlinear viscous dashpot. The development here is based on the hypothesis that this effect influences the constant A, which appears in both the elements of the generalized Maxwell model. Defining D as a one-dimensional damage parameter and A_D as the damaged value of the constant A, it is possible to state that:

$$A_D = (1-D)A \tag{5}$$

where D=0 in the case of no damage, and the A's in Eqs. (1), (3), and (4) are replaced with A_D. In general, D varies between zero and one. For the case of total damage, i.e., D=1, the stress reduces to zero. This formulation is unlike some others which model damage with "negative" springs that have little physical appeal and can cause numerical problems, for example, in the form of stresses with wrong sign. The following mathematical form describes the dependence of the damage parameter on strain and strainrate, and satisfies the physical constraints identified above.

$$D = 1 - [\exp(-c_1\dot{\varepsilon}\varepsilon) + \exp(-c_2\dot{\varepsilon}) \{1 - \exp(-c_1\dot{\varepsilon}\varepsilon)\}] \tag{6}$$

where c_1 and c_2 are constants. This equation shows that as strainrate approaches infinity D tends to one, i.e., the material is completely damaged. Further, as strain approaches infinity D tends to $[1 - \exp(-c_2\dot{\varepsilon})]$, i.e., there is a limiting value of damage at any given strainrate. The repeated use of c_1 in Eq. (6) is to ensure that D does not have a negative value.

Damage in a material is directly related to microcracking activity during deformation. Gold (1960) cites a paper by E. Brown (1926) who noted the presence of audible "crackling" of ice samples subject to compressive loads. Brown associated the audible crackling with the development of cracks in ice. He also noted that the crackling of the ice was related to the level of the

stress applied and the temperature at which the test was conducted. In his own early research, Gold (1960) used a piezoelectric crystal frozen to the ice sample to acoustically monitor the fractures which took place in the ice. In his seminal paper more than a decade later, Gold (1972) reported the results of an extensive study on the process of failure of columnar grained ice. He developed statistics on cracking activity based on visual observations during creep tests. His distribution of cracking activity followed an expression similar to Eq. (6) with strain as the variable. Stress and temperature were identified as additional variables that could affect cracking activity, but they were found to have limited effect on his test results. More recently, Zaretsky et al. (1979) and St. Lawrence and Cole (1982) have studied in detail the acoustic emissions from columnar-grained and fine-grained polycrystalline ice, respectively. Observations from the above test programs lend additional credibility to the general functional form of the proposed damage model.

The formulation of the damage parameter in Eq. (6) is appropriate under a given monotonic loading condition. For a variable loading history the evolution of the damage parameter is assumed to follow Miner's rule, i.e., the incremental damage accumulation depends only on the current state of damage and can be defined in terms of an equivalent strain at the instantaneous strainrate.

Temperature Effects.-- At rates of loading where no material damage is present in sea ice, the effect of temperature on the stress versus secondary creep strain relationship is characterized by an Arrhenius activation energy law. Mellor (1983) states that for temperatures greater than -10°C the law is not valid and that the complete empirical relation derived from experiments should be used to model the temperature dependence in such cases. Sinha (1978) has concluded that the variation of the delayed elastic or primary creep strain with temperature also follows an Arrhenius law. He found the

activation energy for both the viscous flow and the delayed elastic deformation to be equal. Noting that the Young's modulus is relatively independent of temperature, Sinha found that creep strains obtained at various temperatures can be combined to give a master curve at some standard temperature.

The parameter A, which appears in Eqs. (1), (3), and (4), describes the creep strains in ice and is taken to follow the Arrhenius activation energy law to model temperature effects below -10°C, i.e.,

$$A = A_o \exp(Q/NRT) \tag{7}$$

where T is the temperature in degrees Kelvin (0°C equals 273°K), A_o is a temperature independent constant, Q is the activation energy, and R is the universal gas constant. As the temperature reduces, the parameter A increases in value. In consequence, the effective elastic modulus tends to the Young's modulus and the nonlinear dashpot becomes highly viscous. Then ice displays a purely linear elastic material behavior with no rate or temperature sensitivity. At the same time, the model predicts that no continuum damage can occur in compression; this is realistic since at such temperatures ice behaves as a brittle material for which the transition from an undamaged state to a state with extensive macrocracking is almost instantaneous.

3. VARIABLE LOADING HISTORY SIMULATION

Governing Equations.-- The rate-sensitive damage model for the continuum behavior of sea ice assumes that the total strainrate is the sum of the effective elastic strainrate and the nonlinear viscous strainrate, i.e.,

$$\dot{\varepsilon} = \dot{\sigma}/E_{eff} + \dot{\varepsilon}_{sc} \tag{8}$$

where $\dot{\varepsilon}_{sc}$ can be expressed as $\mu\sigma$ with

$$\mu = (M/A_D)\ \dot{\varepsilon}^{1/N-1} \tag{9}$$

Alternatively, Eq. (8) can be expressed as:

$$\dot{\sigma} = E_{eff} (\dot{\varepsilon} - \dot{\varepsilon}_{sc}) \tag{10}$$

Using Eq. (2), Eqs. (8) and (10) can be rewritten in terms of Young's modulus and total creep strainrate, $\dot{\varepsilon}_{cr}$, in the form given below.

$$\dot{\varepsilon} = \dot{\sigma}/E + \dot{\varepsilon}_{cr} \tag{11}$$

and

$$\dot{\sigma} = E(\dot{\varepsilon} - \dot{\varepsilon}_{cr}) \tag{12}$$

where

$$\dot{\varepsilon}_{cr} = \dot{\sigma}/E_d + \mu\sigma \tag{13}$$

For an ideal creep test, the instantaneous stressrate at the time of stress application is a Dirac delta function. It follows from Eq. (10) that the instantaneous total strainrate is a delta function and from Eq. (1) that the instantaneous effective modulus is equal to the Young's modulus. Further for all time after application of the stress, the stressrate is zero. According to Eq. (10) this is possible only if the total strainrate equals the secondary creep strainrate for all time immediately after load application. Thus according to the model, the ideal creep curve should exhibit no primary creep strain. Tertiary creep strains may occur for large stresses as the total strain increases.

The stress-strain-strainrate behavior for loading conditions other than ideal creep cannot be obtained analytically. A numerical solution algorithm, applicable to constant strainrate, constant stressrate, and variable history loadings, is presented in what follows.

Solution Algorithm.-- An iterative solution algorithm is developed to solve the nonlinear governing equation given in Eq. (12). At first the governing equation is integrated in time between t_i and t_{i+1} to yield:

$$\Delta\sigma = E\ (\Delta\varepsilon - \Delta\varepsilon_{cr}) \tag{14}$$

where Δ signifies the increment in the variables over the time increment $t_{i+1}-t_i$. The incremental creep strain which appears in this equation is obtained from Eq. (13) with the α-method of numerical time integration, i.e.,

$$\Delta\varepsilon_{cr} = \Delta\sigma/E_d + \Delta t\ \mu_\alpha\ \sigma_\alpha \tag{15}$$

where σ_α is a weighted average of the stress over the specified time interval, i.e.,

$$\sigma_\alpha = (1-\alpha)\ \sigma_i + \alpha\ \sigma_{i+1} \tag{16}$$

and μ_α is derived from Eq. (9). A value of α greater than or equal to 0.5 results in an unconditionally stable, implicit algorithm. The well-known trapezoidal rule and backward Euler method are obtained with α=0.5 and α=1, respectively. The total strain required in the evaluation of A_D in Eq. (9) is also estimated with the α-method. However, the total strainrate required in the computation of E_d and A_D, i.e., $\Delta\varepsilon/\Delta t$, is assumed to be a constant over the specified time interval and no weighting is necessary. This assumption is reasonable for small values of Δt.

For accelerating solution convergence in problems of interest dominated by creep strains, a numerical algorithm which combines a Newton-Raphson or tangent type nonlinear equation solver with the α-method is developed. The resulting equations are listed below:

$$\left[1 + E\ \frac{\partial\Delta\varepsilon_{cr}}{\partial\sigma_{i+1}}\right]^k\ \sigma_{i+1}^{k+1} = \sigma_i + E\ (\Delta\varepsilon - \Delta\varepsilon_{cr}^{\,k}) + E\left[\frac{\partial\Delta\varepsilon_{cr}}{\partial\sigma_{i+1}}\right]^k\ \sigma_{i+1}^{k} \tag{17}$$

where $\Delta\varepsilon_{cr}{}^{k}$ is obtained by applying Eq. (15) after obtaining the stress quantities at iteration k, and similarly:

$$\left[\frac{\partial \Delta\varepsilon_{cr}}{\partial \sigma_{i+1}}\right]^{k} = 1/E_{d} + \Delta t\ \alpha\ \mu_{\alpha}{}^{k}\ N \qquad (18)$$

For a constant strainrate or strain controlled test, $\Delta\varepsilon$ and σ_i are known. Iteration using Eqs. (17) and (18) is necessary to obtain σ_{i+1} and $\Delta\varepsilon_{cr}$. In the process of computing the incremental creep strains, the primary, secondary and tertiary creep components of strain can be identified. For a constant stressrate or stress controlled test, $\Delta\sigma$ and ε_i are known. First, Eq. (14) is applied to estimate $\Delta\varepsilon$ assuming $\Delta\varepsilon_{cr}$ is zero. Then iteration with Eqs. (17) and (18) yields $\Delta\varepsilon_{cr}$ and in general an incorrect value of $\Delta\sigma$. Equation (14) is again applied with the correct value of $\Delta\sigma$ and the estimated $\Delta\varepsilon_{cr}$ to update $\Delta\varepsilon$. Iteration is then performed with Eqs. (17) and (18). This procedure is repeated until the solution converges, i.e., the stress increment predicted by Eq. (17) equals the specified stress increment. Convergence of the iterations in Eq. (17) is defined to occur when the absolute value of the relative change in stress between iterations k and k+1 is less than 0.01. Iteration is also stopped if the actual stress is zero at k and its absolute value is less than 0.01 at k+1. Application of this iterative scheme with α=1 shows that convergence is typically obtained in 4 iterations.

4. CALIBRATION WITH UNIAXIAL EXPERIMENTAL DATA

The uniaxial model is calibrated with several independent sets of experimental data obtained for example from constant strainrate, creep, and constant stressrate tests. In addition, predictions of the model with respect to (a) evolution of the damage parameter, (b) ratio of residual stress to peak stress

versus strainrate, (c) stress relaxation, and (d) unloading and reloading are also explored. This calibration is based on the following values for the nine model parameters:

$E = 9.$ GPa
$r = 0.98$
$A_o = 0.00652$ MPa $s^{1/N}$
$N = 3$
$M = 1411.2$
$Q = 65{,}000$ J mol^{-1}
$R = 8.314$ J mol^{-1} K^{-1}
$c_1 = 1.76 \times 10^5$ s
$c_2 = 882$ s

For the particular ice type in one of the tests a different value of E equal to 8.5 GPa and r=0.51 is necessary.

Experimental data on sea ice is limited in comparison to that on pure ice. One way to enlarge the data base is to recognize that sea ice differs from pure ice only in the respect that it contains brine. The salinity of sea ice, S, is typically 3-10 ppt (parts per thousand). The brine volume ν is related to the temperature (°C) and the gross salinity through a general relationship derived by Frankenstein and Garner (1967) and contained in Sanderson (1984):

$$\nu = 0.001\ S\ (0.53 - 49.2/T) \tag{19}$$

This equation breaks down for temperatures below -22.9°C and also if a significant amount of pore volume is occupied by air bubbles/gas. Brine pockets allow the ice to deform more easily and reduce the strength of the ice. Geometrical considerations (Weeks and Assur, 1967), similar to those in soil mechanics, show that for horizontal loading of ice containing vertically arranged cylindrical brine pockets the net section stress σ' is:

$$\sigma' = \sigma/[1-(\nu/\nu_o)^{1/2}] \tag{20}$$

where σ is the applied gross stress. The quantity ν_o corresponds physically to the brine volume at which sea ice loses all strength. A value of ν_o equal to 0.16 gives an optimum correction for a range of experimental observations

(Sanderson, 1984). Equations (19) and (20) as well as the Arrhenius law are used to normalize sea ice stress data when necessary during calibration.

Constant Strainrate Tests.-- The maximum stress (for convenience termed strength in this paper) observed from three independent sets of constant strainrate tests on pure columnar (S-2) ice is plotted in Fig. 2 versus strainrate. Data for columnar sea ice is combined with the pure ice data and plotted in Fig. 3. The data is widely scattered and ice strength may vary by an order of magnitude at any given strainrate. Normalizing the experimental data for temperature and salinity effects reduces the scatter by more than a factor of two. Figure 4 contains this normalized data. The solid line in the figure represents the prediction of the rate-sensitive damage model proposed here; it is obvious that the model captures the overall trend of the data very well. For strainrates greater than 10^{-2} s^{-1} the continuum model of damage is invalid and a horizontal line representing fracture is drawn at a stress of 5 MPa. The dashed line in the figure is the familiar power law model for secondary creep in ice which fails to model material damage resulting in strain-softening for strainrates between $2x10^{-4}$ s^{-1} and 10^{-2} s^{-1}.

Wang (1982) has conducted constant strainrate tests on columnar sea ice in the nominal strainrate range 10^{-6} s^{-1} to 10^{-3} s^{-1}. Examples of stress-strain curves observed by him are contained in Fig. 5, while those generated by his semi-empirical model are shown in Fig. 6. Figure 7 plots the predictions of the model proposed here up to a strainrate of 10^{-2} s^{-1}. Comparison of the three figures shows that the proposed model is able to capture the characteristics displayed by the experimental data. Further, the model correctly predicts the observed lowering of residual stress at higher strainrates as a result of strain-softening.

Creep Tests.-- Experimental limitations preclude the possibility of conducting an ideal creep test. In most cases a finite time equivalent to a few seconds is necessary to develop the nominal creep stress. This finite rise time effect may be modelled in general with a time-varying stress given by:

$$\sigma(t) = \sigma_n [1 - \exp(-at^b)] \tag{21}$$

where σ_n is the nominal creep stress, and a,b are constants. The rise time, t_r, is defined as the time required to reach 99% of the nominal creep stress. Given the rise time and b=1, the parameter a may be evaluated with:

$$a = - \ell n\ 0.01/t_r \tag{22}$$

Figure 8 presents the creep test data observed by Sinha (1978) at a stress of 0.49 MPa and temperatures of -41°C, -30°C, and -19.8°C, respectively. The predictions of creep strains and creep strain recovery associated with unloading for the model proposed here and that of Sinha (1978) are shown by the solid lines. The rise times as well as the finite times for unloading are indicated on the figures. In general the proposed model is able to describe the observed data as well if not better than Sinha's model. The tests at -30°C yield creep and recovery curves that are significantly variable under the same nominal conditions, suggesting that most of the variability associated with the model predictions may be linked to this factor, i.e., difficulty in conducting repeatable creep tests. By changing the finite rise time from 1.6 to 2.4 seconds the proposed model is able to capture some of the variability, the remainder is the uncertainty in the finite rise time model and other experimental uncertainties not accounted for. It is also possible that some of the variability may be due to model uncertainty.

Figure 9 shows the experimental creep data of Brill and Camp (1960) for randomly oriented snow ice together with the predictions of the current model

and the model of Sinhā (1978). Two of the curves correspond to tests at -5°C and one to -10°C. It must be reiterated that the Arrhenius law loses validity at -5°C. The proposed model captures the overall data trend at -10°C and for the 0.232 MPa stress case at -5°C. The prediction is poor at -5°C for the 0.125 MPa stress case. Sinha's model however appears to fit the data quite well; to some extent this is made possible by the variation of grain size, a parameter which directly influences his formulation of the primary creep component of strain.

Wang (1982) has generated creep curves using his semi-empirical model for sea ice as shown in Fig. 10. He found the curves to agree with experimental observations contained in Mellor (1980). Creep curves generated by the model proposed here are shown in Fig. 11. The proposed model provides good agreement with the curves of Wang.

Constant Stressrate Tests.-- Experimental data obtained during constant stressrate tests is limited. Figure 12 contains the "strength" versus stressrate data for sea ice obtained from two independent sources. The data normalized for temperature and salinity effects is plotted in Fig. 13. The solid line in the figure is the prediction of the proposed model. For stressrates greater than about 0.[illegible] MPa/s, a strainrate of 10^{-2} s^{-1} is reached prior to reaching the maximum stress. If the stress is greater than 5 MPa, the fracture stress at this strainrate, the material is assumed to have fractured and the maximum stress just prior to fracture is considered to be the strength. For stressrates greater than about 0.1 MPa/s the model captures the observed behavior quite well. For lower stressrates, the model over predicts the strength. A careful study of the stress-strain curves (see Fig. 14) shows that while they appear to reach their maximum asymptotic values at strain values of 1-5%, in fact the stress keeps increasing further. It is

therefore possible that experimental observations are made prematurely and as such do not reflect the actual "strength". On the other hand, it is also possible that the model predictions are unrealistic. Further research is necessary to explain this discrepancy.

The stress-strain curves predicted by the semi-empirical model of Wang (1982) under constant stressrate conditions are shown in Fig. 15. Beyond a certain strain value the solution ceases to exist. The predictions were found to agree reasonably well with his earlier test results (Wang, 1979). The curves predicted by the model proposed here and shown in Fig. 14 are in good agreement with Wang's curves.

Effective Elastic Modulus.-- Data on the strainrate variation of the effective elastic modulus is plentiful (see Mellor, 1983). The experimental data of Traetteberg, Gold, and Frederking (1975) on pure columnar-grained ice at -10°C is presented in Fig. 16. Predictions of the effective elastic modulus based on the proposed model is indicated by the solid line, which suggests an excellent match with the observed data.

Other Model Characteristics.-- The evolution of the damage parameter D with strain and strainrate is shown in Fig. 17 for a range of strainrates and strains up to 1%. For lower strainrates the accumulation of material damage is small and not of significance in modeling the behavior of sea ice. The figure also shows how damage evolves under a variable history loading.

The ratio of residual stress to peak stress ("strength") is plotted versus strainrate in Fig. 18. There is an almost exponential decay of the ratio, and the value tends to zero as strainrate approaches 10^{-2} s^{-1}.

The test in which a suddenly applied constant stress is followed by a condition in which the strain is kept constant often results in a stress reduction. This phenomenon is termed stress relaxation. Figure 19 shows the stress relaxation for the proposed model during a creep test conducted at 3

MPa. The amount of relaxation is dictated by the numerical value of the parameter r. If r=1 the effective modulus equals zero, Eq. (10) predicts the stressrate to be zero, and thus no stress relaxation is possible. A value of r less than one is necessary to model this phenomenon.

The simulation of unloading and reloading requires specification of how the unloading or reloading is to take place. In a constant strainrate test, unloading could imply a change in the sign of the constant strainrate or simply the setting of stress equal to zero. Reloading may be defined in similar terms. Figure 20a shows unloading and reloading based on controlling strainrate, while in Fig. 20b unloading is stress controlled while reloading is strainrate controlled. In both cases, the model follows the virgin loading curve once the effect of the unloading/reloading ends. Figure 20c represents a sinusoidal variation of stress between zero and a prescribed maximum value. Experimental data of Mellor and Cole (1981) suggests that hysteresis loops should be obtained for such tests. The present model will have to be extended to capture this phenomenon.

5. MULTIAXIAL MODEL FORMULATION AND CALIBRATION

Sea ice is not an isotropic material. Field observations have shown that this type of ice, which is predominantly columnar, has two sources of anisotropy: (a) the c-axis is oriented perpendicular to the axis of crystal growth, and (b) the c-axes of different crystals may show preferred azimuthal orientation in the plane on which they lie. There is strong evidence suggesting that the preferred azimuthal orientation is correlated with the instantaneous current direction just underneath a growing ice sheet (Weeks and Gow, 1978, Langhorne, 1982, and Langhorne, 1983). While such alignments are common in landfast ice, observations suggest that strong alignments can develop in pack ice when there is little rotation of the floes relative to the current direction (Cherepanov, 1971, and Kovacs and Morey, 1980).

where $\underline{C}$ is the linear elastic compliance matrix for an orthotropic material (see Appendix A), and the remaining vectors are in general of size (6x1) in engineering notation.

To derive the relationship between the creep strainrate and stress vectors, first an effective stress measure generalized for orthotropic materials with identical behavior in compression and tension is defined.

$$\sigma_e^2 = 3/\beta \left[\frac{a_1}{3} (\sigma_{xx} - \sigma_{yy})^2 + \frac{a_2}{3} (\sigma_{yy} - \sigma_{zz})^2 + \frac{a_3}{3} (\sigma_{zz} - \sigma_{xx})^2 + 2a_4 \sigma_{xy}^2 + 2a_5 \sigma_{yz}^2 + 2a_6 \sigma_{zx}^2 \right] \tag{24}$$

with $\beta = a_1 + a_2$. This may be expressed in compact form using matrix notation as:

$$\sigma_e^2 = 3/\beta \, \underline{\sigma}^T \underline{G} \, \underline{\sigma} \tag{25}$$

where $\underline{G}$ is the matrix defined in Appendix A.

The creep strainrate vector can now be related to the stress vector by defining a scalar potential function ϕ which obeys the associated flow rule, i.e.,

$$\dot{\underline{\varepsilon}}_{cr} = \frac{\partial \phi}{\partial \underline{\sigma}} \tag{26}$$

with

$$\phi = \frac{\sigma_e \dot{\sigma}_e}{E_d} + \mu \frac{\sigma_e^2}{2} \tag{27}$$

Combining Eqs. (25)-(27) yields the desired relationship:

$$\dot{\underline{\varepsilon}}_{cr} = \lambda \, \underline{S}^* \tag{28}$$

where

$$\lambda = 3/\beta \frac{1}{\sigma_e} \left[\frac{\dot{\sigma}_e}{E_d} + \mu \sigma_e^N \right] \tag{29}$$

and

$$\underline{S}^* = \underline{G}\, \underline{\sigma} \tag{30}$$

Note that $\underline{S}^*$ is not the conventional deviatoric stress vector. It may be thought of as a pseudo deviatoric stress vector for an anisotropic material.

The evaluation of μ and E_d above requires knowledge of the effective creep strainrate $\dot{\varepsilon}_{e,cr}$ which can be expressed as:

$$\dot{\varepsilon}_{e,cr} = \beta/3\, \dot{\underline{\varepsilon}}^T H\, \dot{\underline{\varepsilon}} \tag{31}$$

where $\underline{H}$ is the matrix defined in Appendix A.

Given the stress vector, the pseudo deviatoric stresses may be obtained from Eq. (30). Then applying Eqs. (25), (29), and (28) in succession leads to the creep strainrate vector. Note that if $a_1 - a_6 = 1$, these equations predict isotropic material behavior.

Estimation of Multiaxial Model Parameters.-- Five uniaxial (compression) tests at constant strainrate are necessary to obtain the five orthotropic model parameters: a_2-a_6. Note that (i) a_1 can be set equal to one without loss of generality, and (ii) there is experimental evidence which shows that the power law exponent N can be considered independent of the direction of loading. For purposes of the current derivation, it is assumed that the c-axes of the sea ice crystals lie on the y-z plane and that they are aligned in the y-direction (Fig. 22). This implies that the x-axis represents the crystal growth direction.

The tests can be conducted in the three orthogonal directions y, x, and z respectively, and along the three 45° axes on the y-z, x-y, and z-x planes respectively. It is assumed that the uniaxial model discussed earlier refers

to the y-direction. Then, let β_1-β_5 represent the experimentally determined ratios of the maximum stresses for the latter five tests, respectively, to the maximum stress in the reference y-direction at the same strainrate. The orthotropic model parameters may be determined from the following equations:

$$a_2 = - \frac{\beta_1^n - \beta_2^n (1-\beta_1^n)}{\beta_1^n - \beta_2^n (1+\beta_1^n)} \tag{32}$$

$$a_3 = - \frac{\beta_1^n + \beta_2^n (1 \beta_1^n)}{\beta_1^n - \beta_2^n (1 \cdot \beta_1^n)} \tag{33}$$

$$a_4 = \frac{\beta}{6} [4\beta_4^{-n} - \beta_2^{-n}] \tag{34}$$

$$a_5 = \frac{\beta}{6} [4\beta_3^{-n} - \beta_1^{-n}] \tag{35}$$

$$a_6 = \frac{\beta}{6} [4\beta_5^{-n} - 1] \tag{36}$$

where $n=2N/(N+1)$. Typical ranges for the β_i's (identified in the previous subsection) are 2-5 for β_1, 0.50-0.95 for β_2, and 0.25-0.60 for β_3. Values for β_4 and β_5 are not generally available in the literature. Since these two parameters determine only the out of plane shear strains and stresses in sheet ice, they have no influence on plane strain and plane stress problems. However, the parameters will have to be obtained in the case of three-dimensional boundary value problems.

For a transversely isotropic material, i.e., isotropy in the y-z plane, $\beta_2=\beta_3=1$ and $\beta_4=\beta_5$. As a result $a_1=a_3=1$, $a_4=a_6$, the parameters a_2 and a_5 are functions of only β_1, while a_4 depends on both β_1 and β_4. Only two uniaxial tests are required to obtain β_1 and β_4; one in the x-direction and one along the 45° axis on the x-y or z-x planes.

Frederking (1977) has conducted plane strain uniaxial compression tests on columnar-grained transversely isotropic freshwater ice. For his type A tests, strains in the z-direction are constrained to zero and stresses are applied in the y-direction. The ratio Γ_z of the plane strain stress to the unconfined stress at the same strainrate is directly related to β_1 by the following equation:

$$\Gamma_z = \left[\frac{4\beta_1^{2n}}{4\beta_1^{n} - 1} \right]^{1/n} \tag{37}$$

The equation predicts Γ_z to vary between 2.1-5.1 for experimentally observed values of β_1 ranging from 2 to 5, and N between 3 and 4. This is consistent with Frederking's experimental observations of Γ_z which were close to 2 at high strainrates and to 5 at low strainrates. In the type B tests, strains in the x-direction are constrained to zero while stresses are again applied in the y-direction. In this case, the stress ratio Γ_x is given by:

$$\Gamma_x = \left[1 + \frac{1}{4\beta_1^{n} - 1} \right]^{1/n} \tag{38}$$

Since β_1 is generally greater than one, Γ_x will be less than approximately 1.? for N between 3 and 4. For typical values of β_1, the predicted values of Γ_x range from 1.01 to 1.06. This is consistent with Frederking's experiments which showed negligible influence of x-direction confinement on stresses.

Triaxial tests of first-year sea ice have been conducted by Richter-Menge, Cox et al. (1985) on samples obtained from horizontal cores in the plane of the ice sheet at angles of 0°, 90°, and 45° to the preferred c-axis orientation. According to the orthotropic material model, the ratio Γ_t

of the maximum axial stress with a confining pressure equal to τ times the axial stress to the maximum stress in the unconfined state at the same strainrate should be given by:

$$\Gamma_t = \frac{1}{1-\tau} \tag{39}$$

The deviatoric stress (i.e., axial stress minus radial stress) normalized by the unconfined stress is independent of τ or confining pressure for the model and equal to one. Experimental data for this quantity is plotted versus confining pressure in Fig. 23, which shows that the sea ice data is only moderately pressure sensitive. Thus the use of a pressure insensitive model appears to be justified for sea ice. The figure also includes data obtained by Hausler (1981) on columnar-grained saline ice at a strainrate of 2×10^{-4} s^{-1} using a so-called "true" triaxial testing machine.

No general conclusions can be drawn as yet concerning the pressure insensitivity of sea ice since the results of Panov and Fokeev (1977) for natural and artifical sea ice seem to indicate an appreciable increase in deviatoric stress with confining pressure. However their tests were carried to the "breaking point" of ice, and as such the data represents the fracture surface and not the yield surface prior to fracture. On the other hand, the triaxial behavior of pure (non-saline) polycrystalline ice has been studied by Jones (1978) and Durham et al. (1982). The tests by Jones performed at strainrates of 10^{-6} to 5×10^{-3} s^{-1} indicate up to a factor of two increase in deviatoric stress due to confining pressure. Durham et al.'s tests were conducted at temperatures of -78°C to -196°C where ice is expected to behave more as a brittle material and to very high pressures (up to 350 MPa). Very high yield stresses were recorded, and phase transitions to higher density polymorphs were reached. Both these sets of data for pure ice have limited applicability for calibration of sea ice models since no equivalence in the

triaxial behavior of pure and sea ice has been established. It must be noted that the plasticity based pressure sensitive parabolic yield function of Reinicke and Ralston (1977) has been justified with the help of Frederking's (1977) data (which has been shown in this paper to follow a pressure insensitive model very well) and that the three parameter extension of their yield function by Reinicke and Remer (1987) has been justified on the basis of Jones' triaxial data for pure polycrystalline ice.

6. CONCLUSIONS

This paper has presented a rate-sensitive damage model for describing the continuum behavior of sea ice under variable loading conditions. The model, based on a nonlinear generalization of the Maxwell differential formulation, is characterized by its ability to (a) decompose the various recoverable and irrecoverable components of strain, (b) represent continuously damaging or strain-softening material behavior in the ductile to brittle transition region, (c) capture the rate-dependent behavior of sea ice with rate-independent model parameters, and (d) describe materially anisotropic mechanical behavior. Further, the model shows strong dependency of the creep and constant strainrate behavior. Calibration of the model is achieved with several independent sets of data, particularly those for first-year sea ice. The following specific conclusions can be drawn from the work reported in this paper:

1. The uniaxial model developed here is described by 9 parameters. For comparable models, i.e., those of Sinha and Michel, the number of parameters is 8 and 10 respectively. It must be recognized that Sinha's model does not capture material damage while calibration of Michel's model with experimental data has been very limited.

2. All parameters of the proposed model, i.e., 9 for the uniaxial model and 5 for the orthotropic generalization, can be determined from conventional

tests conducted on ice. The experimental data base is generally adequate to determine the model parameters. In particular, normalization of the uniaxial strength data for salinity and temperature is a useful way of including test results for pure polycrystalline ice in model calibration.

3. Material damage that can be described by the continuum model proposed here is significant in the strainrate range of 2×10^{-4} s^{-1} to 10^{-2} s^{-1}. At higher strainrates the presence of macrocracks precludes a solely continuum description of ice behavior.

4. According to the proposed model, an ideal creep test does not lead to primary creep strains. However if the finite rise time required to reach the nominal stress in a creep test is taken into account, primary creep strains are simulated by the model. Experimental evidence appears to support this conclusion.

5. The pressure-insensitive orthotropic model proposed here predicts very well the plane strain uniaxial compression tests conducted by Frederking. Further, experimental data of Richter-Menge et al. on first-year sea ice and that of Hausler on saline ice indicate that sea ice is only moderately pressure sensitive in comparison with pure ploycrystalline ice which is highly pressure-sensitive.

Additional research is needed to resolve several questions; including (a) the presence or lack thereof of primary creep strains in ideal creep tests, (b) the adequacy of the incremental damage accumulation model based on Miner's rule particularly for variable history loading, (c) the generation of hysteresis loops during unloading/reloading and cyclic loading, (d) the presence or lack thereof of a peak stress in tests conducted at low stressrates (i.e., lower than 0.1 MPa/s), (e) the extent of stress relaxation in sea ice, and (f) equivalence, if any, in the triaxial behavior of pure and sea ice. Both experimental and theoretical research is very much needed to

better characterize the multiaxial behavior of sea ice particularly under cyclic loading.

7. ACKNOWLEDGEMENTS

This research on the Numerical Modeling of Ice-Structure Interaction is funded by The Standard Oil Company (Ohio) through MIT's Center for Scientific Excellence in Offshore Engineering, and cosponsored by the U.S. Department of the Interior, Minerals Management Service.

REFERENCES

Brill, R. and Camp, P.R. (1961), Properties of Ice, U.S. Army Snow, Ice and Permafrost Research Establishment, Research Report 68, 48 p.

Brown, E. (1926), Experiments on the Strength of Ice, St. Lawrence Waterway Project, Report to the Joint Board of Engineering, Appendix F, Ottawa, 423 p.

Butkovich, T.R. (1959), On the Mechanical Properties of Sea-Ice, U.S. Army Snow, Ice and Permafrost Research Establishment, Thule, Greenland.

Croasdale, K.R. (1977), Indentation Tests to Investigate Ice Pressures on Vertical Piers, Journal of Glaciology, 19(81), 301-312.

Cherepanov, N.V. (1971), Spatial Arrangement of Sea Ice Crystal Structure, Problemy Arktiki i Antarktiki, 3~, 171-181.

Durham, W.B., Heard, H.C. and Kirby, S.H. (1982), Deformation of Ice at Pressures to 350 MPAa at 77 to 195 K, EOS, 63(45), 1094p, T51B-01.

Frankenstein, G. and Garner, R. (1967), Equations for Determining the Brine Volume of Sea Ice from -0.5° to -22.9°C, Journal of Glaciology, 6(48), 943-944.

Frederking, R. (1977), Plane-Strain Compressive Strength of Columnar-Grained and Granular-Snow Ice, Journal of Glaciology, 18(80), 505-516.

Frederking, R. (1983), Ice Engineering I, Lecture Notes.

Glen, J.W. (1955), The Creep of Polycrystalline Ice, Proceedings, Royal Society London, Series A, 228(1175), 519-538.

Gold, L.W. (1960), The Cracking Activity in Ice During Creep, Canadian Journal of Physics, 38, 1137-1148.

Gold, L.W. (1972), The Process of Failure of Columnar-Grained Ice, Philosophical Magazine, 26(2), August, 311-328.

Grant, N.J. (1971), Fracture Under Conditions of Hot Creep Rupture, Fracture - An Advanced Treatise, H. Liebowitz (Ed.), Academic Press, New York, ?, 483-533.

Hausler, F.V. (1981), Multiaxial Compressive Strength Tests on Saline Ice with Brush-Type Loading Platens, Proceedings, IAHR Ice Symposium, Quebec, Canada, 526-536.

Jones, S.J. (1978), Triaxial Testing of Polycrystalline Ice, Proceedings, Third International Conference on Permafrost, Edmonton, Alberta, Canada, July, 670-674.

Karr, D.G. (1984), Applications of Continuous Damage Models in Ice Mechanics, Proceedings, Fourth International Conference on Applied Numerical Modeling, Taiwan, December.

Karr, D.G. (1985a), A Damage Mechanics Model for Uniaxial Deformation of Ice, Proceedings, Fourth International Symposium on Offshore Mechanics and Arctic Engineering, Dallas, TX, February.

Karr, D.G. (1985b), Constitutive Equations for Ice as a Damaging Material, Proceedings, ASCE Speciality Conference: ARCTIC '85 - Civil Engineering in the Arctic Offshore, San Francisco, CA, March.

Kovacs, A. and Morey, R.M. (1980), Investigations of Sea Ice Anisotropy, Electromagnetic Properties, Strength, and Under-Ice Current Orientation, U.S. Army Cold Regions Research and Engineering Laboratory, Hanover, NH, Research Report No. [illegible], [illegible] p.

Langhorne, P.J. (1982), Crystal Alignment in Sea Ice, Ph.D. Thesis, University of Cambridge, U.K.

Langhorne, P.J. (1983), Laboratory Experiments on Crystal Orientation in NaCl Ice, Annals of Glaciology, 4, 163-169.

Mellor, M. (1980), Mechanical Properties of Polycrystalline Ice, Proceedings, IUTAM Symposium on Physics and Mechanics of Ice, Copenhagen, 1979, P. Tryde (Ed.), Springer-Verlag, Berlin, 117-128.

Mellor, M. (1983), Mechanical Behavior of Sea Ice, U.S. Army Cold Regions Research and Engineering Laboratory, Hanover, NH, Monograph No. 83-1, June.

Mellor, M. and Cole, D. (1981), Cyclic Loading and Fatigue in Ice, Cold Regions Science and Technology, 4, 41-53.

Michel, B. (1981), Advances in Ice Mechanics, Proceedings, 6th International Conference on Port and Ocean Engineering Under Arctic Conditions.

Michel, B. and Toussaint, N. (1977), Mechanisms and Theory of Indentation of Ice Plates, Journal of Glaciology, 19(81), 285-300.

Morland, L.W. and Spring, U. (1981), Viscoelastic Fluid Relation for the Deformation of Ice, Cold Regions Science and Technology, 4, 255-268.

Panov, V.V. and Fokeev, N.V. (1977), Compression Strength of Sea Ice Specimens Under Complex Loading, Problemy Artiki i Antarktiki, 49, 81-86.

Peyton, H.R. (1966), Sea-Ice Strength, University of Alaska, Geophysical Institute, Research Report No. UAG R-182.

Peyton, H.R. (1968), Ice and Marine Structures, Ocean Industry, 3(3), March, 40-41; 3(9), September, 59-65; 3(12), December, 51-58.

Ralston, T.D. (1979), Sea Ice Loads, Exxon Technical Seminar, Houston, TX.

Reinicke, K.M. and Ralston, T.D. (1977), Plastic Limit Analysis with an Anisotropic, Parabolic Yield Function, International Journal of Rock Mechanics and Mining Sciences, 14, 147-154.

Richter-Menge, J.A. et al. (1985), Triaxial Testing of First-Year Sea Ice, U.S. Army Cold Regions Research and Engineering Laboratory, Hanover, NH, Internal Research Report No. 877.

Saeki, H., Nomura, T. and Ozaki, A. (1978), Experimental Study on the Testing Methods of Strength and Mechanical Properties of Sea Ice, Proceedings, IAHR Ice Symposium, 135-149.

Sanderson, T.J.O. (1984), Theoretical and Measured Ice Forces on Wide Structures, Proceedings, IAHR Ice Symposium, Hamburg, August, 32 p.

Schwarz, J. and Weeks, W.F. (1977), Engineering Properties of Sea Ice, Journal of Glaciology, 19(81), 499-531.

Shapiro, L.H. (1978), Development of Hardware and Procedures for In-Situ Measurement of Creep in Sea Ice, OCSEAP Annual Report, Research Unit 265, Contract No. 03-5-022-55, March.

Sinha, N.K. (1978), Rheology of Columnar-Grained Ice, Experimental Mechanics, 464-470, December.

Sinha, N.K. (1979), Grain Boundary Sliding in Polycrystalline Materials, Philosophical Magazine A, 40(6), 825-842.

Sinha, N.K. (1983a), Field Tests on Rate Sensitivity of Vertical Strength and Deformation of First-Year Columnar-Grained Sea Ice, Proceedings, 7th International Conference on Port and Ocean Engineering Under Arctic Conditions, Helsinki, 1, April, 909-919.

Sinha, N.K. (1983b), Creep Model of Ice for Monotonically Increasing Stress, Cold Regions Science and Technology, 8, 25-33.

Spring, U. and Morland, L.W. (1982), Viscoelastic Solid Relations for the Deformation of Ice, Cold Regions Science and Technology, 5, 221-234.

Spring, U. and Morland, L.W. (1983), Integral Representations for the Viscoelastic Deformation of Ice, Cold Regions Science and Technology, 6, 185-193.

St. Lawrence, W.F. and Cole, D.M. (1982), Acoustic Emissions from Polycrystalline Ice, Cold Regions Science and Technology, 5, 183-199.

Traetteberg, A., Gold, L.W. and Frederking, R. (1975), The Strain Rate and Temperature Dependence of Young's Modulus of Ice, Proceedings, IAHR/AIRH Third International Symposium on Ice Problems, August, 479-486.

Vaudrey, K.D. (1977), Ice Engineering - Study of Related Properties of Floating Sea-Ice Sheets and Summary of Elastic and Viscoelastic Analyses, Naval Civil Engineering Laboratory, Port Hueneme, CA, Technical Report No. R860.

Vittoratos, E.S. (1979), Existence of Oriented Sea Ice by the Mackenzie Delta, Proceedings, 5th International Conference on Port and Ocean Engineering Under Arctic Conditions, Trondheim, Norway, August, 643-650.

Vivatrat, V. and Chen, V. (1985), Ice Load Prediction with the Use of a Rate-Dependent Anisotropic Constitutive Law, Proceedings, ASCE Speciality Conference: ARCTIC '85 - Civil Engineering in the Arctic Offshore, San Francisco, CA, March, 942-952.

Wang, Y.S. (1979a), Sea Ice Properties, Exxon Technical Seminar, Houston, TX.

Wang, Y.S. (1979b), Crystallographic Studies and Strength Tests of Field Ice in the Alaskan Beaufort Sea, Proceedings, 5th International Conference on Port and Ocean Engineering Under Arctic Conditions, Trondheim, Norway, August, 651-666.

Wang, Y.S. (1982), A Rate-Dependent Stress-Strain Relationship for Sea Ice, Proceedings, First International Symposium on Offshore Mechanics and Arctic Engineering, New Orleans, LA, 243-248.

Weeks, W.F. and Assur, A. (1967), The Mechanical Properties of Sea Ice, U.S. Army Cold Regions Research and Engineering Laboratory, Hanover, NH, Monograph No. II-C3.

Weeks, W.F. and Gow, A.J. (1978), Preferred Crystal Orientations Along the Margins of the Arctic Ocean, Journal of Geophysical Research, 84(C10), 5105-5121.

Zaretsky, Y.K., Chumichev, B.D. and Solomatin, V.I. (1979), Ice Behavior Under Load, Engineering Geology, 13, 299-309.

GENERALIZED MAXWELL MODEL

RATE-DEPENDENT SPRING

NONLINEAR DASHPOT

INSTANTANEOUS ELASTICITY

+

DELAYED ELASTICITY OR PRIMARY CREEP

SECONDARY CREEP

+

DAMAGE OR TERTIARY CREEP

Fig. 1

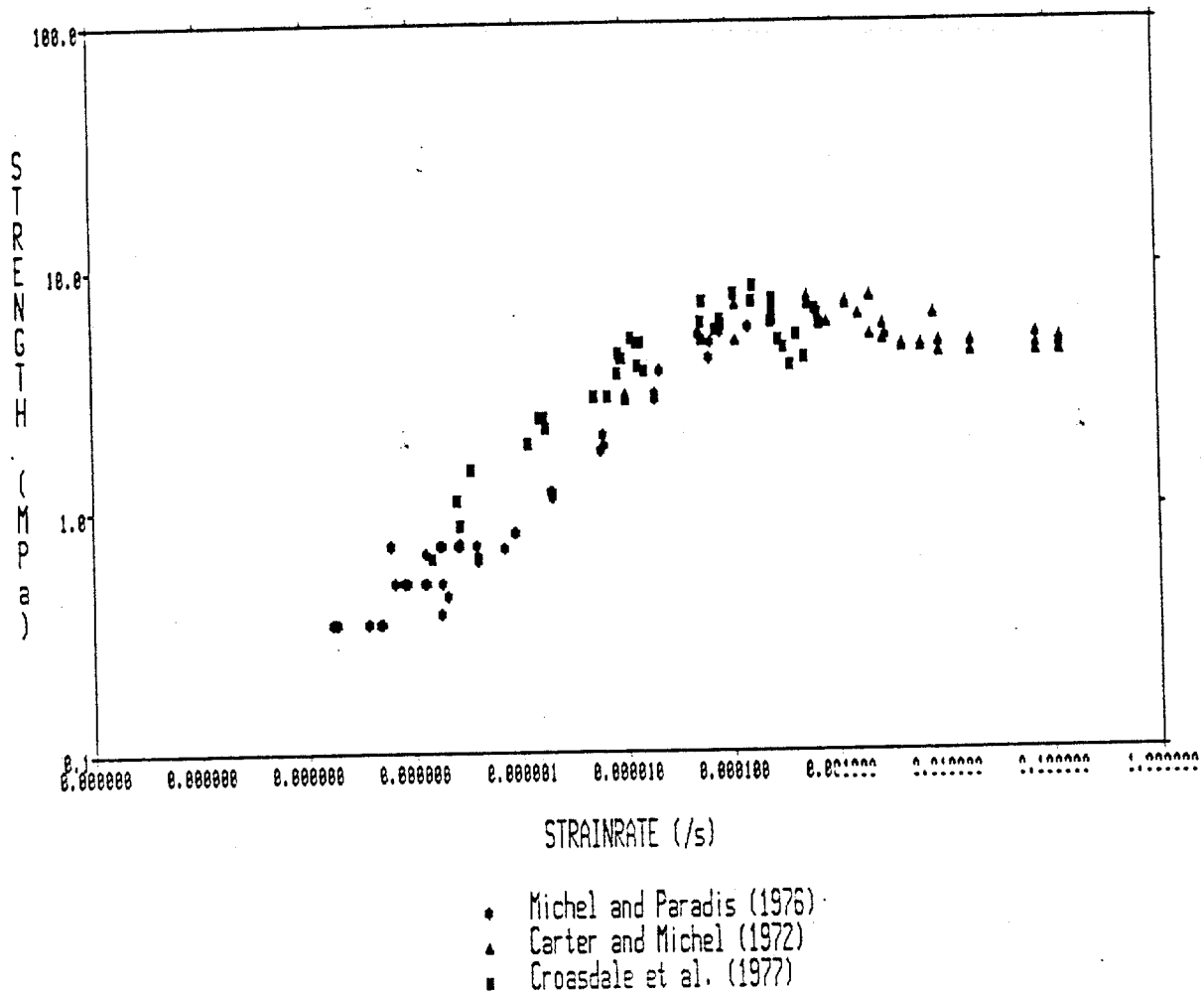

Fig. 2 Strength of Columnar Pure Ice as a Function of Strainrate.

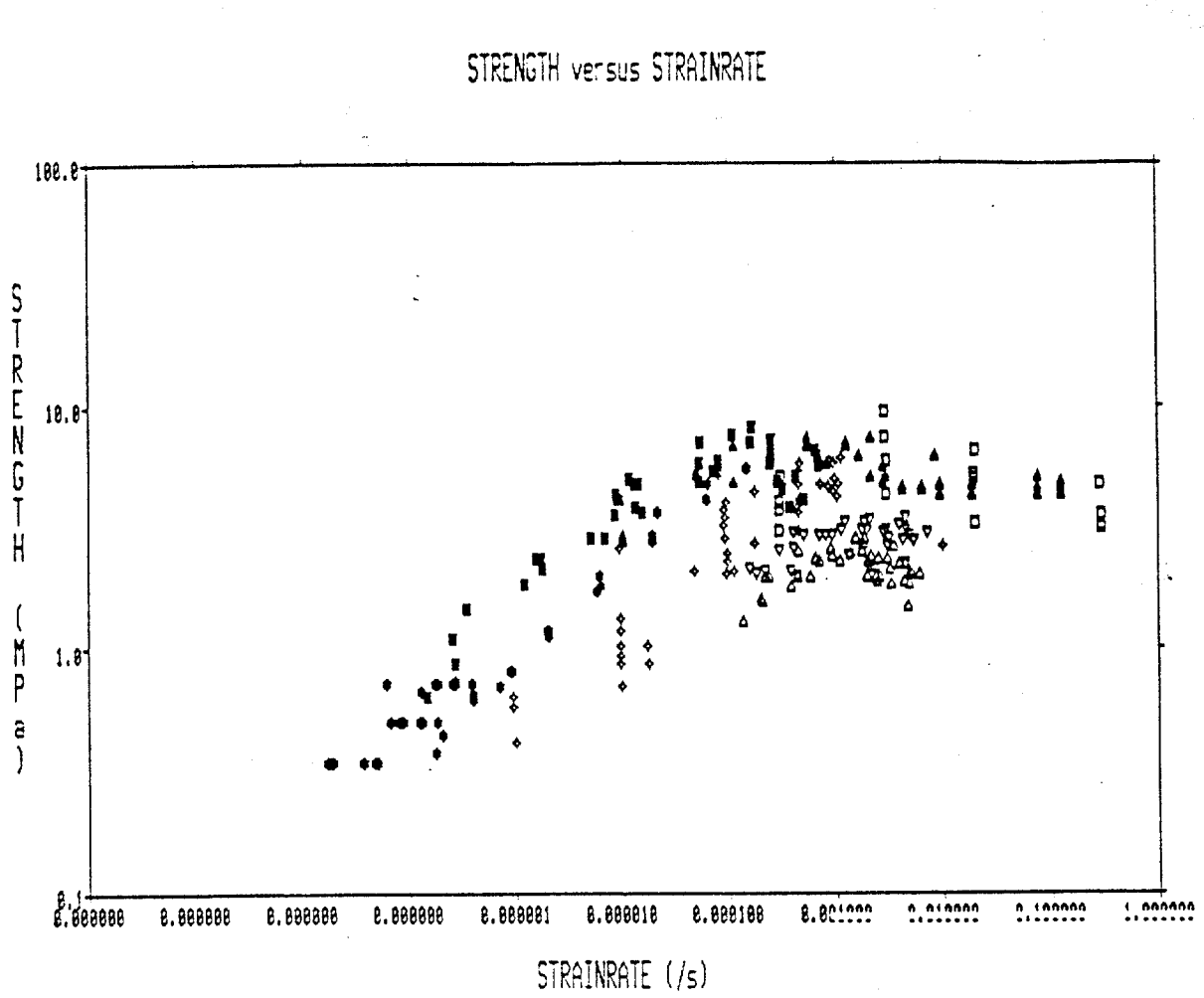

Fig. 3 Strength of Columnar Pure and Sea Ice as a Function of Strainrate.

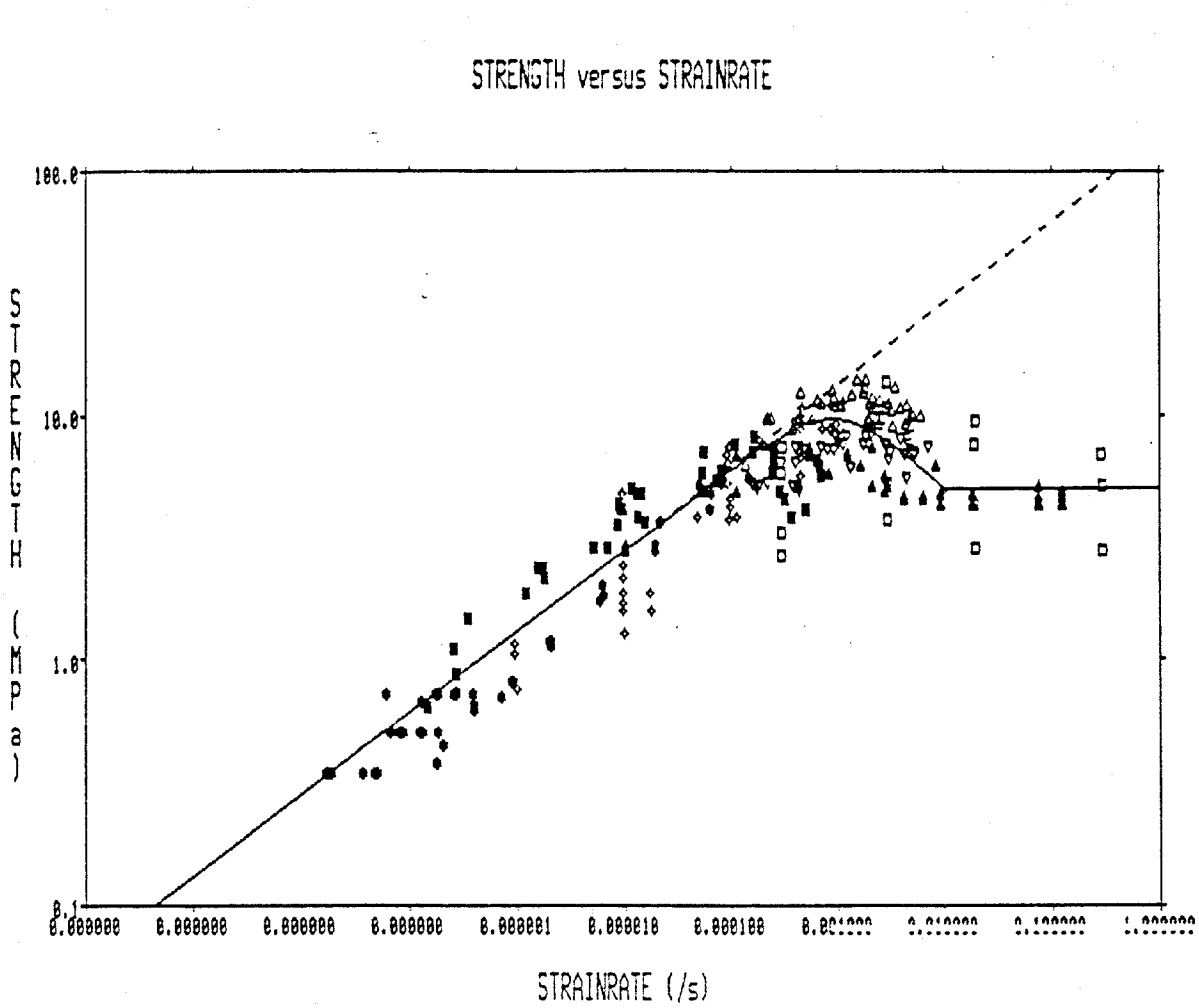

Fig. 4 Strength of Columnar Pure and Sea Ice Corrected for the Effects of Brine Volume.

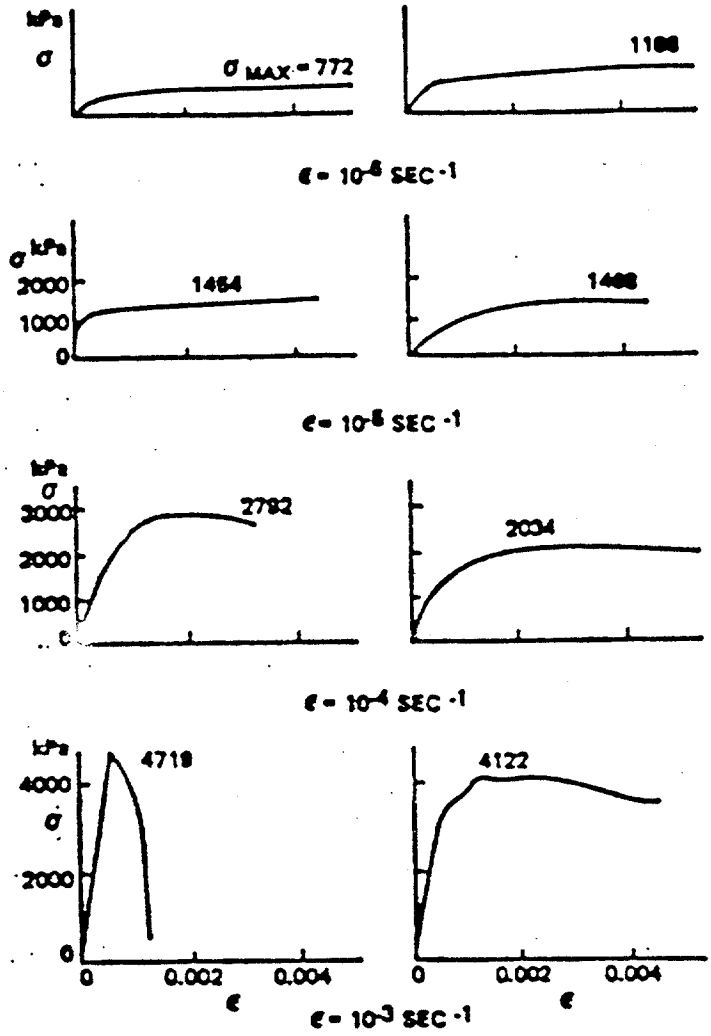

Fig 5 Stress-Strain Curves for Arctic Sea Ice Under Constant Strain Rate Loading (Wang, 1982)

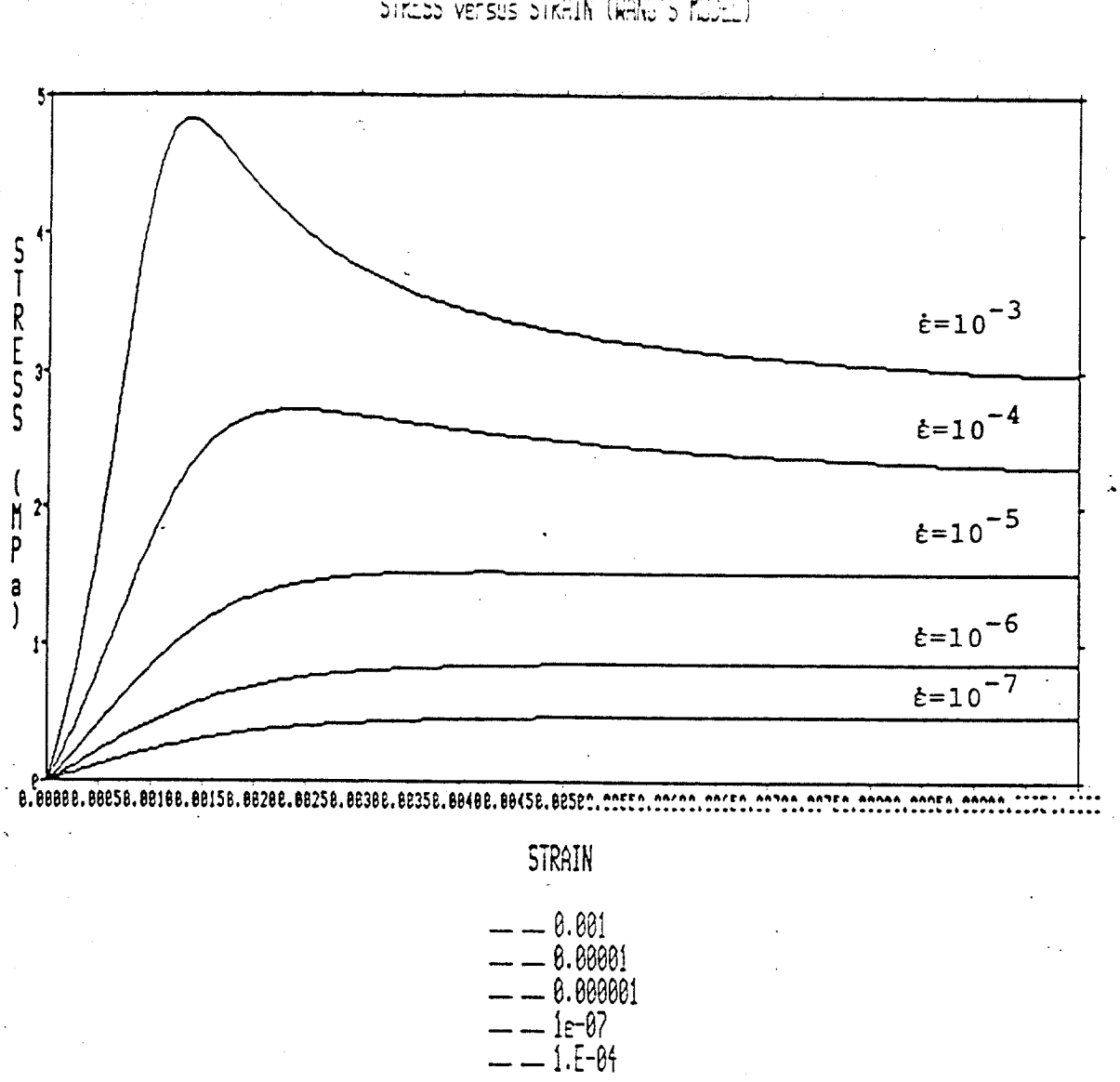

Fig. 6 Stress-Strain Plots for Wang's (1982) Model for Different Strainrates.

STRESS versus STRAIN (Sea Ice)

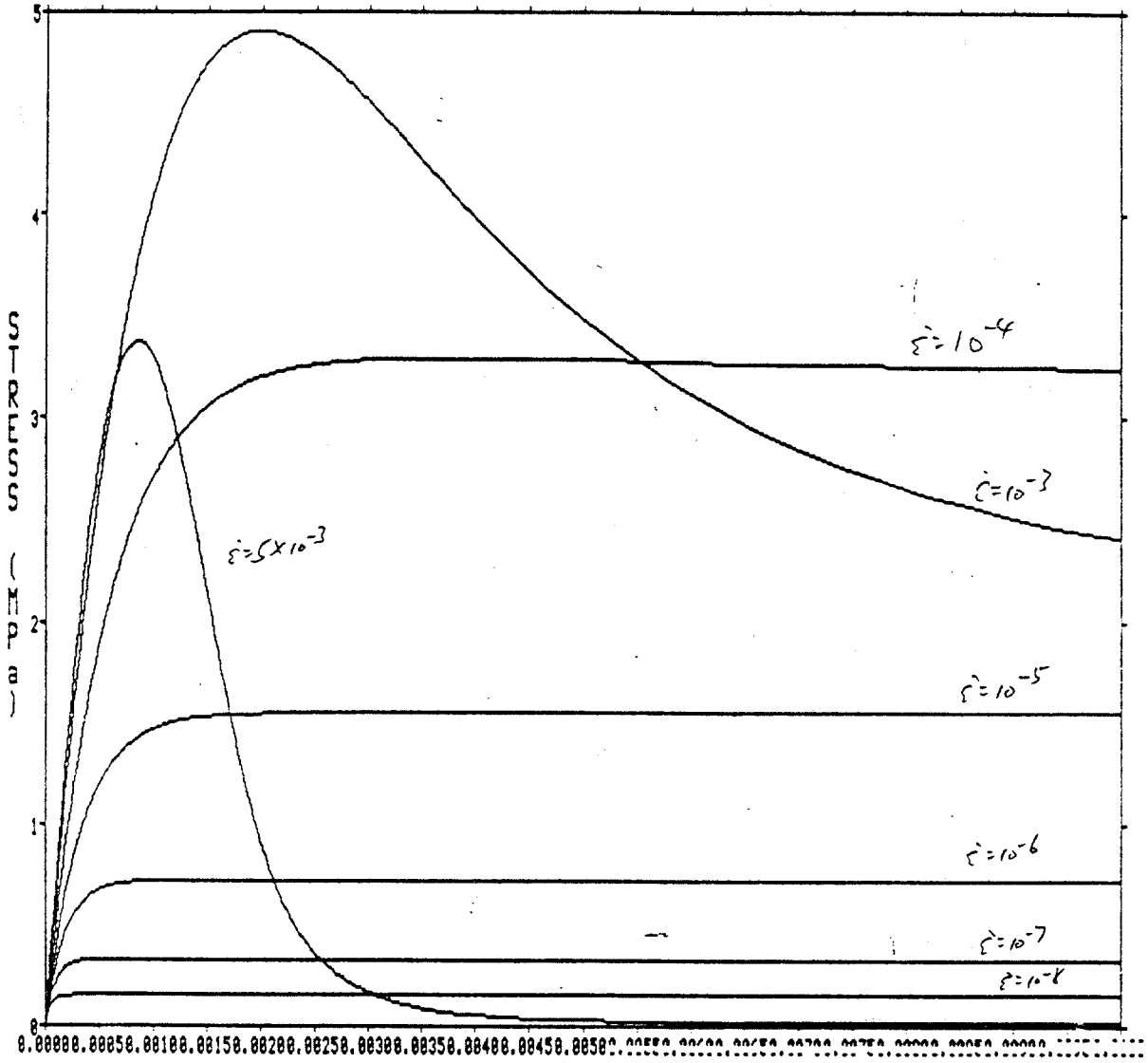

Fig. 7

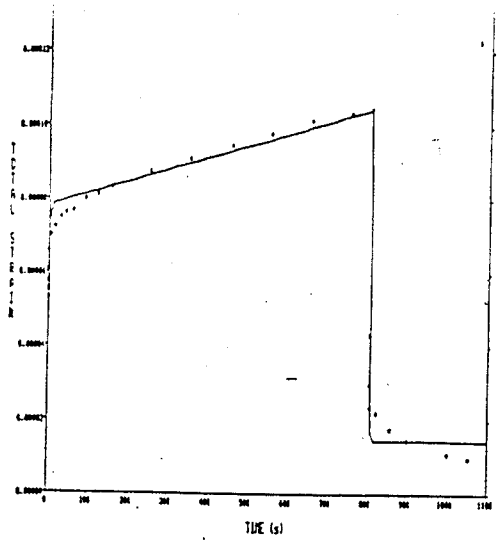

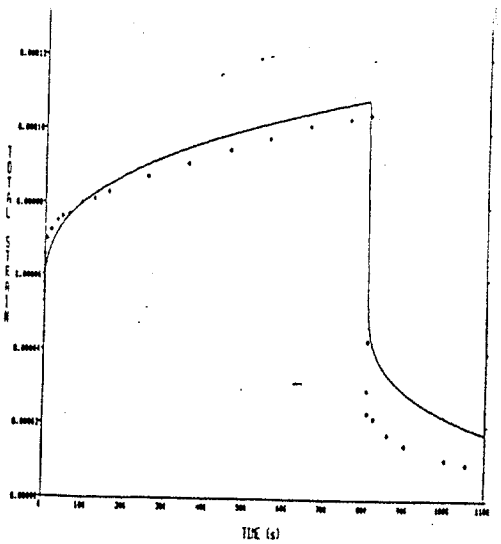

STRESS=0.49 MPa, -30 C

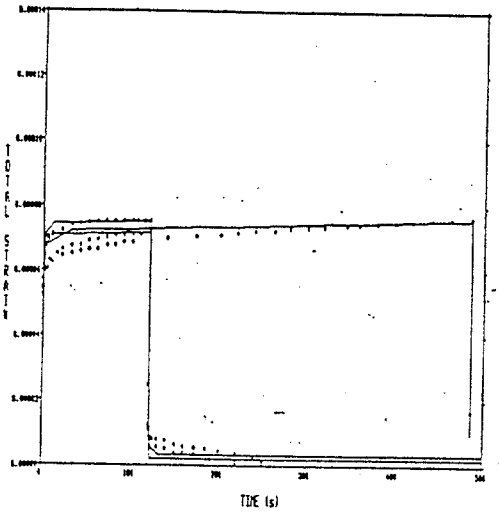

STRESS=0.49 MPa -30 C SINHA'S PLOT

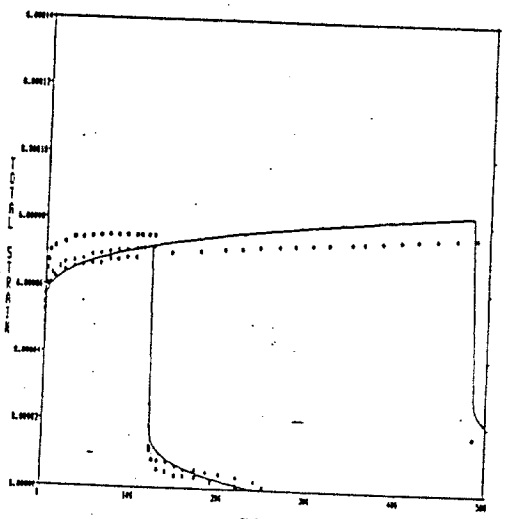

STRESS=0.49 MPa, -41 C

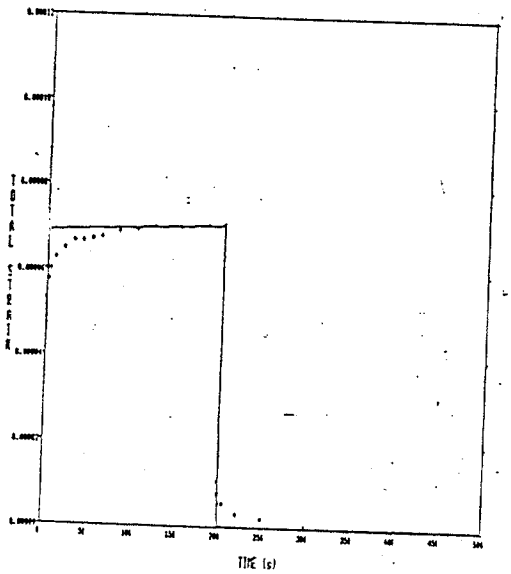

STRESS=0.49 MPa -41 C SINHA'S PLOT

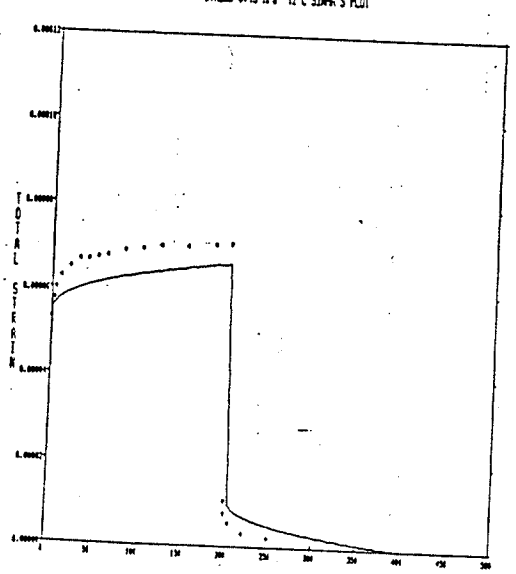

Fig. 9

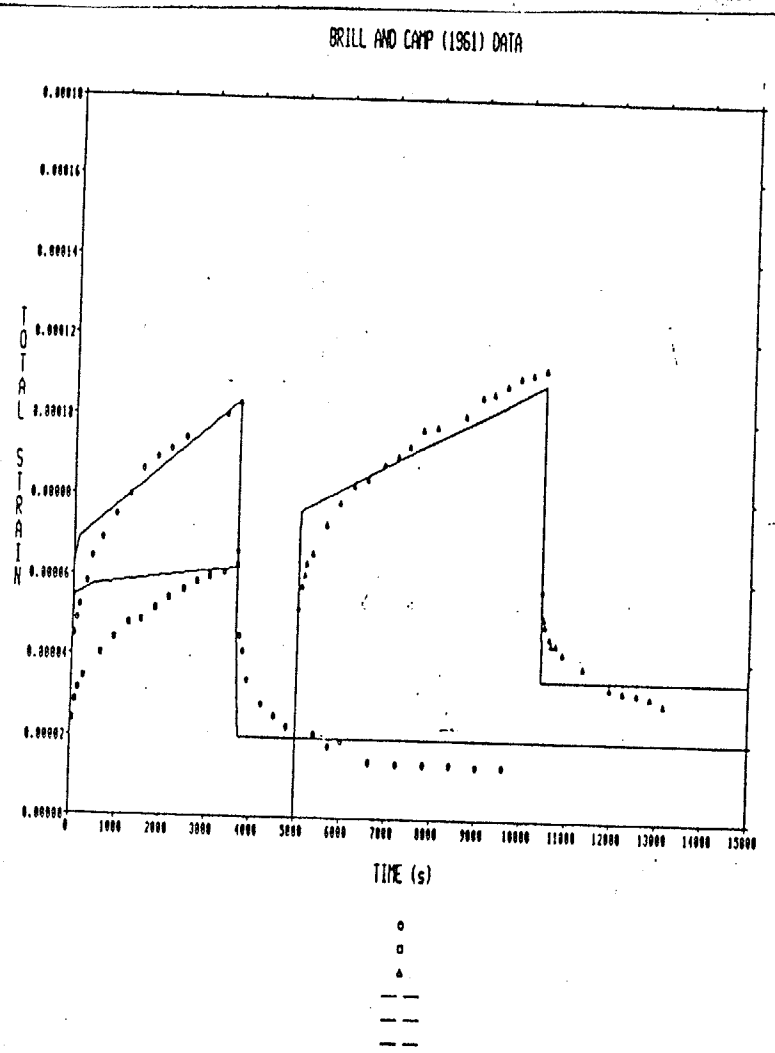
BRILL AND CAMP (1961) DATA
TOTAL STRAIN
TIME (s)

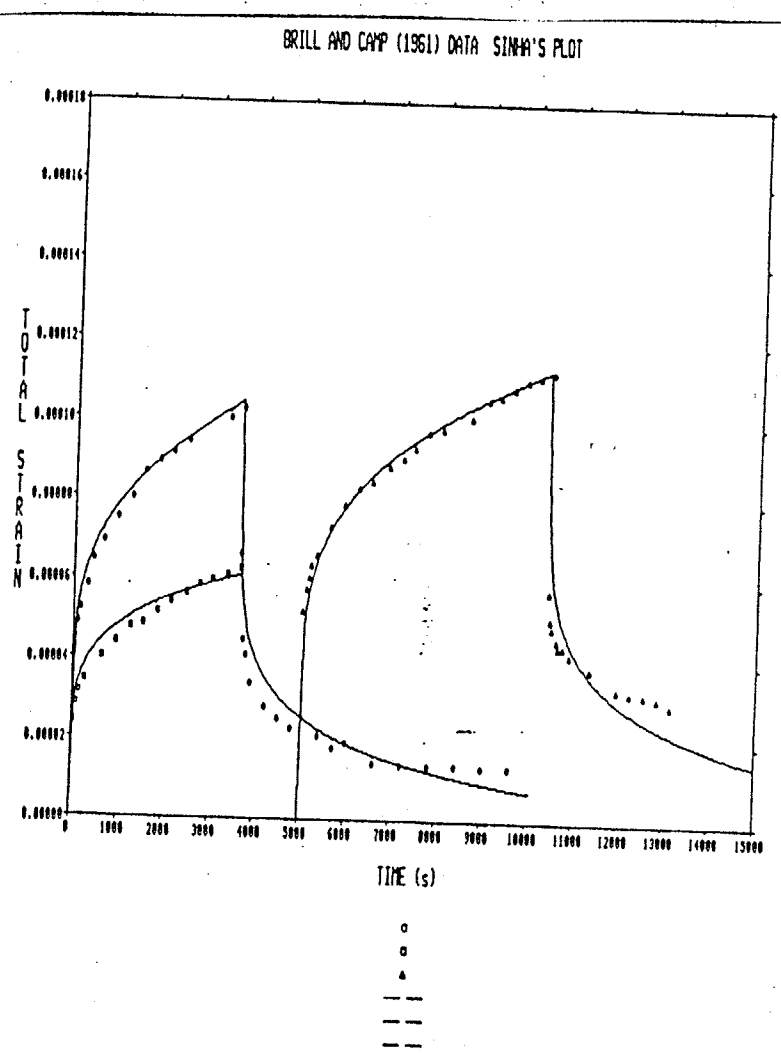
BRILL AND CAMP (1961) DATA SINHA'S PLOT
TOTAL STRAIN
TIME (s)

Fig 9

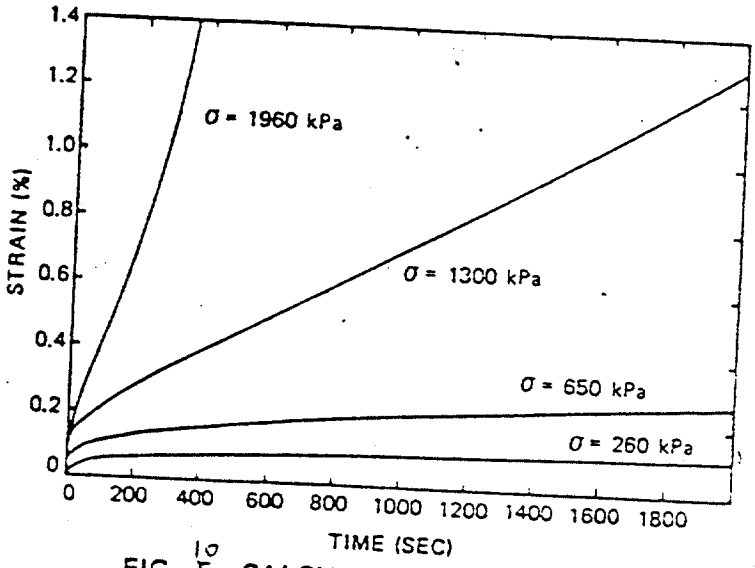

FIG. 5. CALCULATED CREEP CURVES.

CREEP CURVES

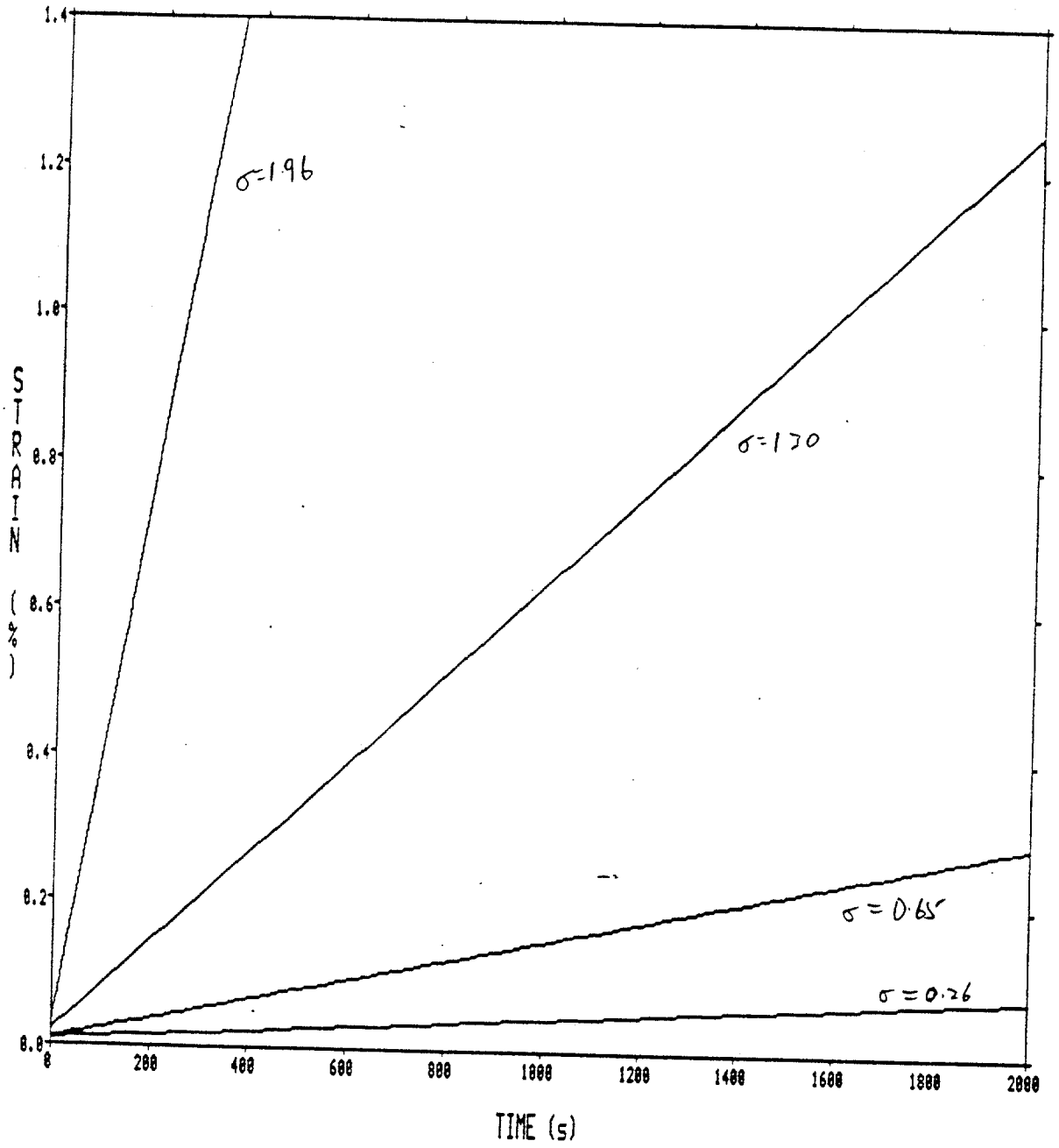

Fig. 11

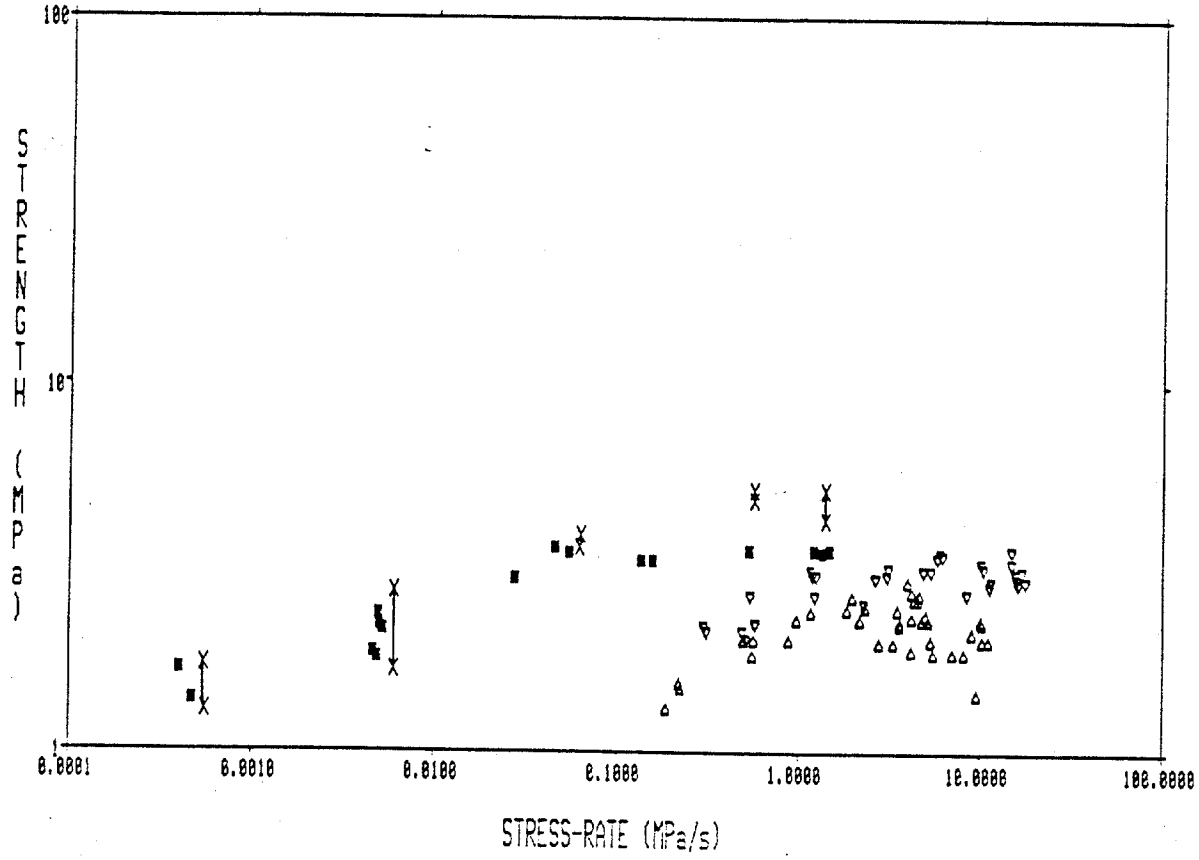

Fig. ~~15~~ 12 Strength of Sea Ice
as a Function of Stress-Rate.

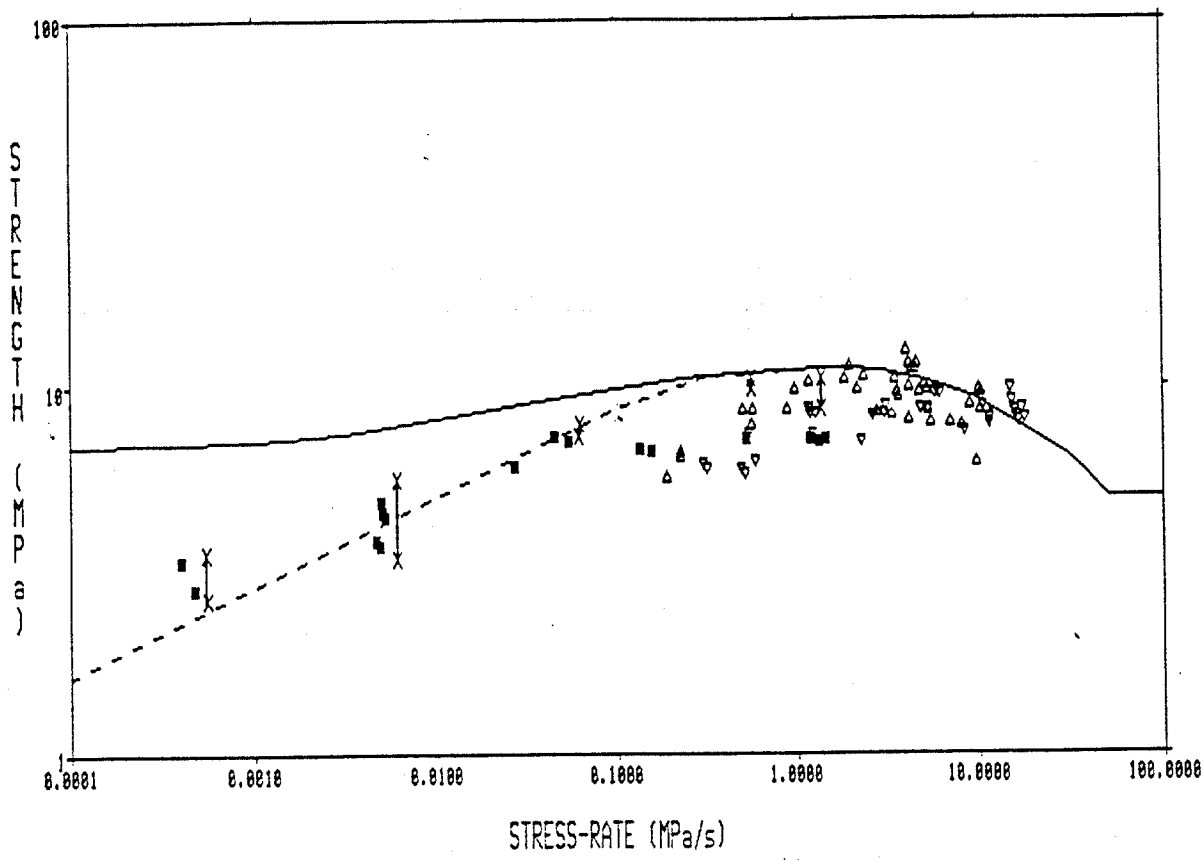

Fig. 13 Strength of Normalized Ice as a Function of Stress-Rate

STRESS versus STRAIN (Sea Ice - Constant Stress-Rate)

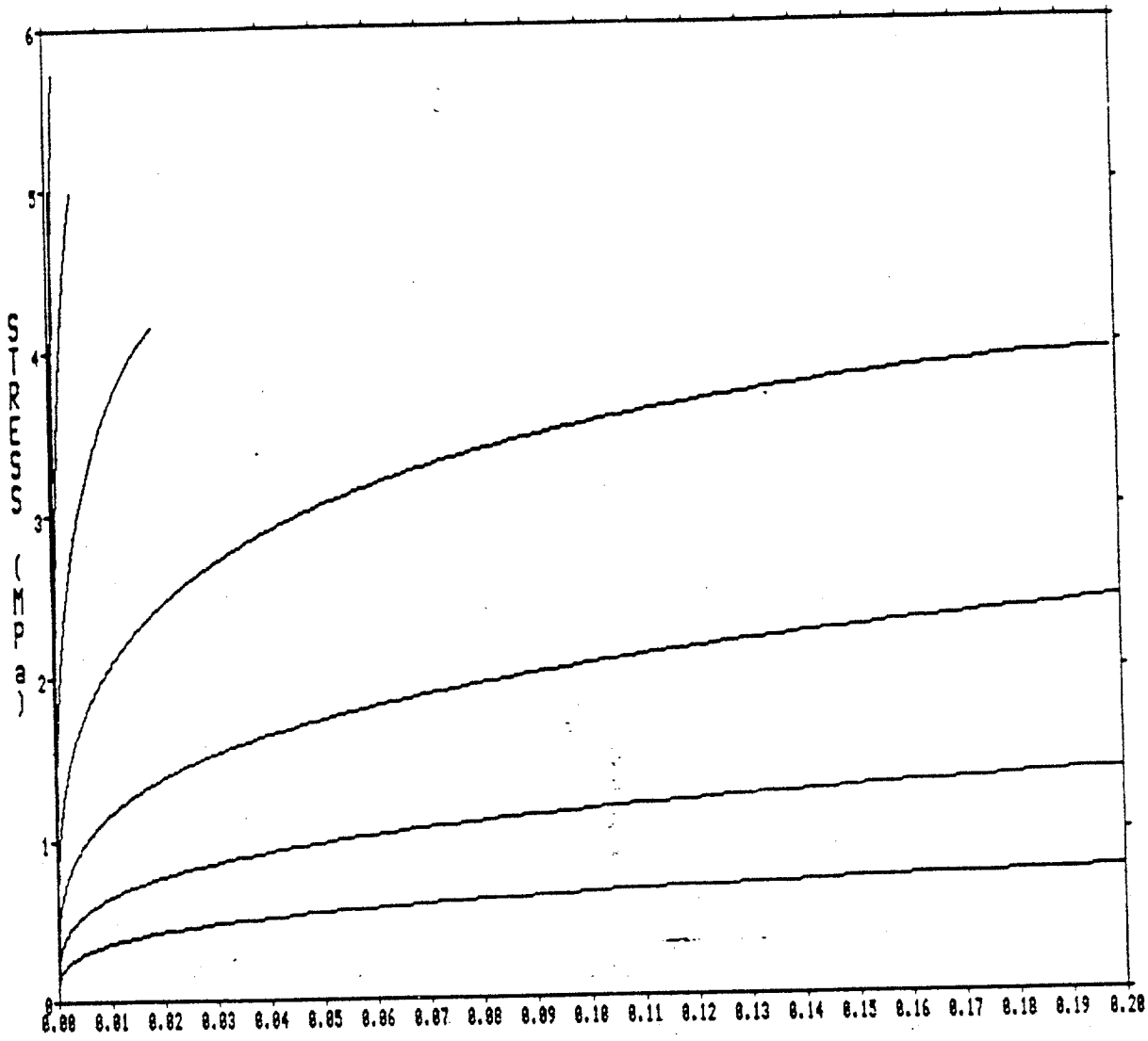

Fig 13a

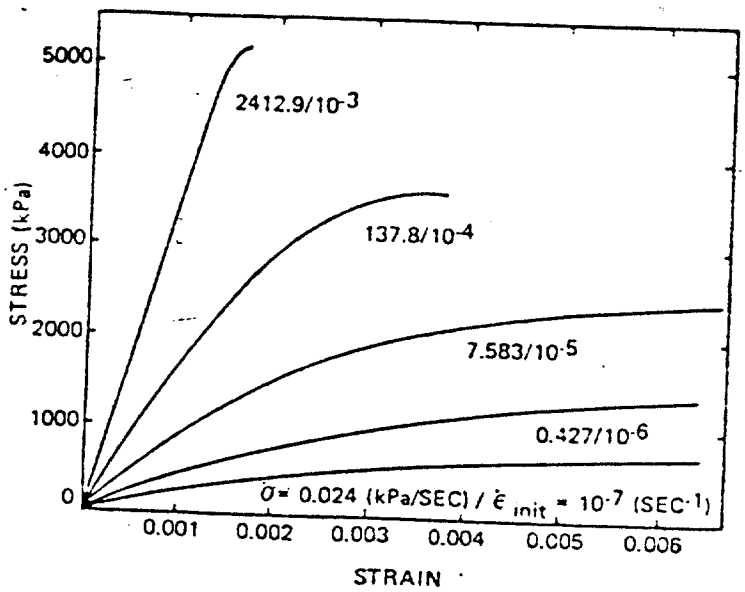

FIG. 14. CALCULATED STRESS - STRAIN CURVES FOR UNORIENTED COLUMNAR SEA ICE UNDER CONSTANT STRESS RATE LOADING.

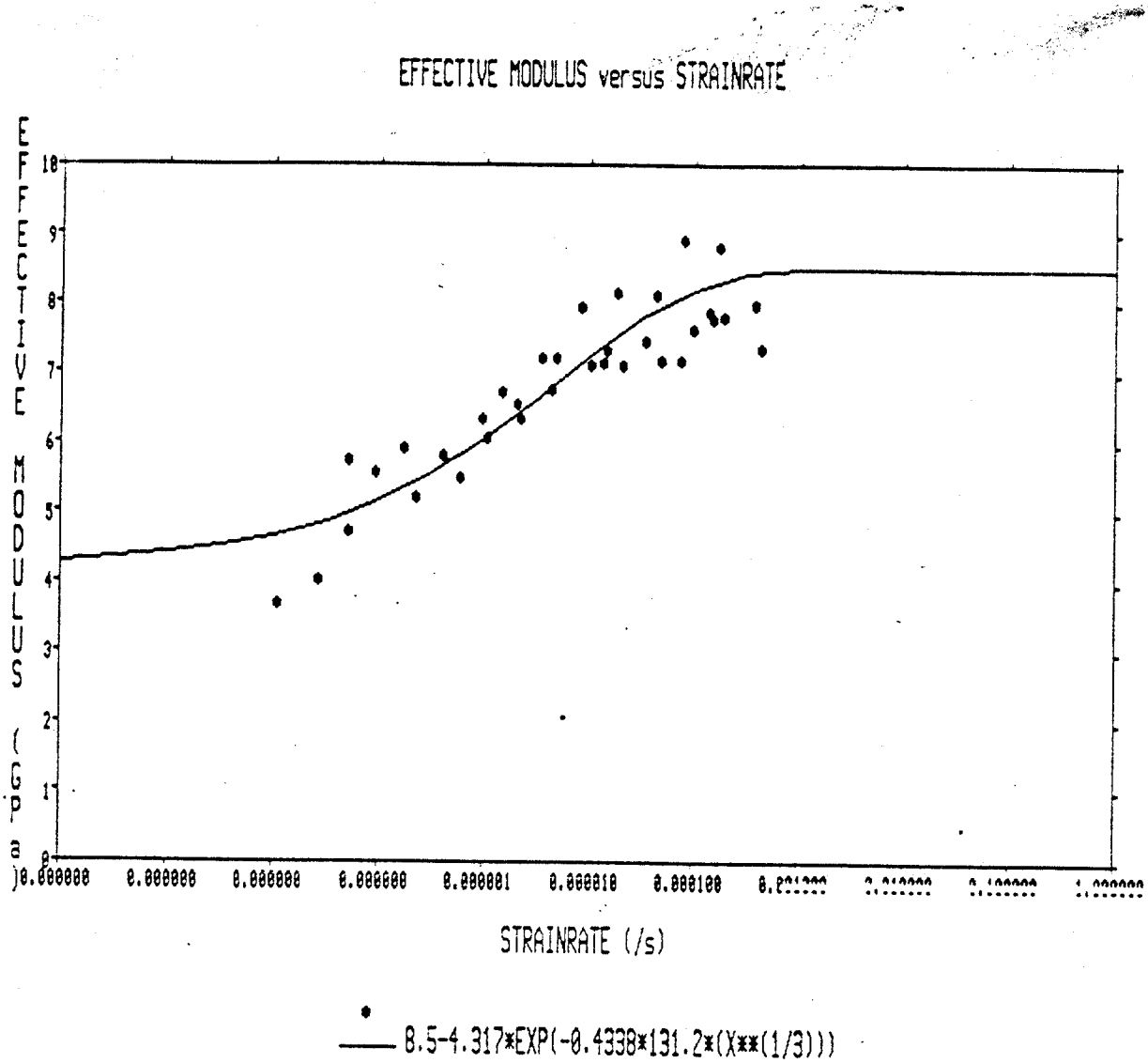

Fig.15 Effective Modulus versus Strainrate
(Traetteberg, Gold and Frederking, 1975).

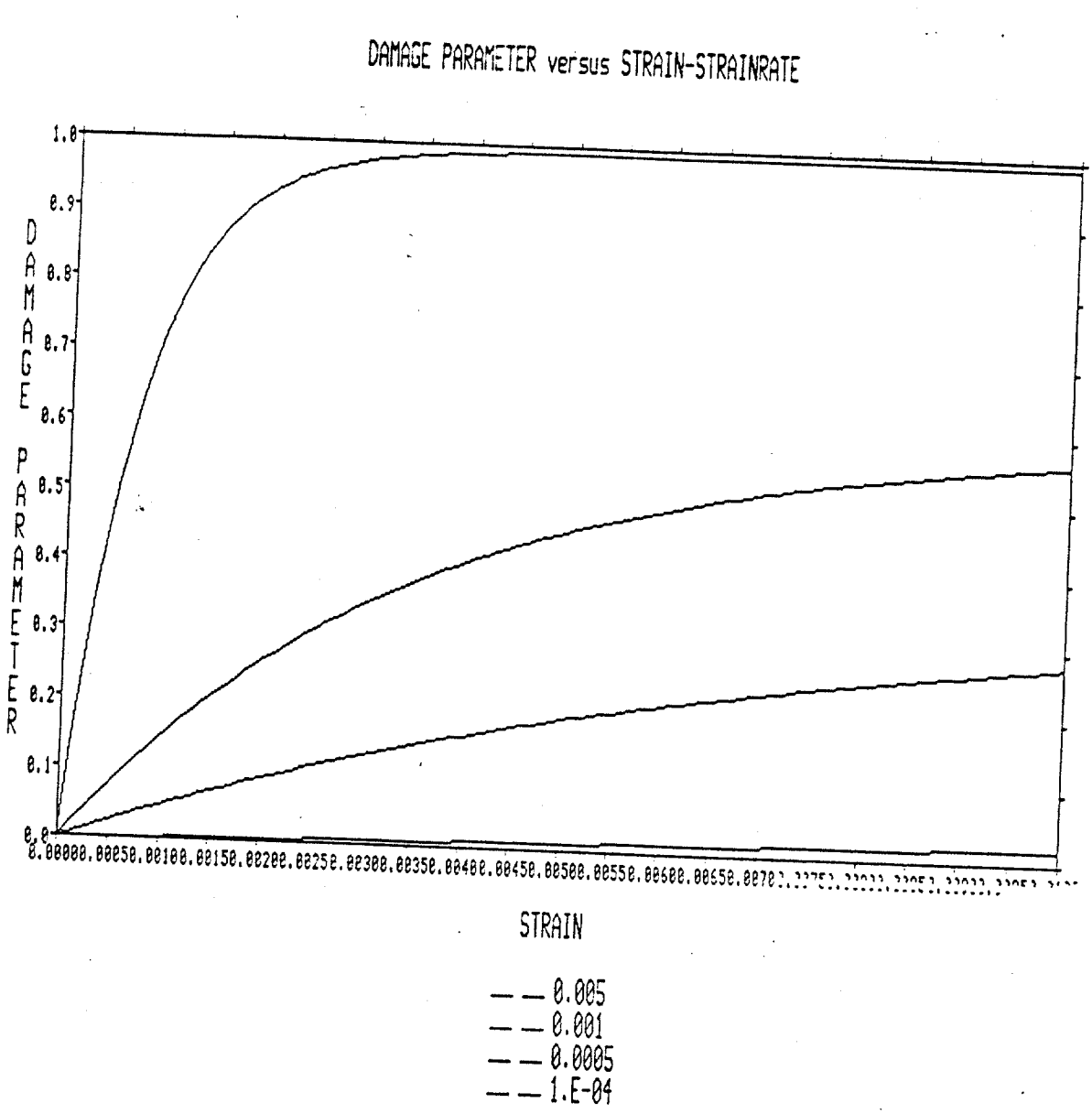

Fig.16 Damage Parameter as a Function of Strain and Strainrate.

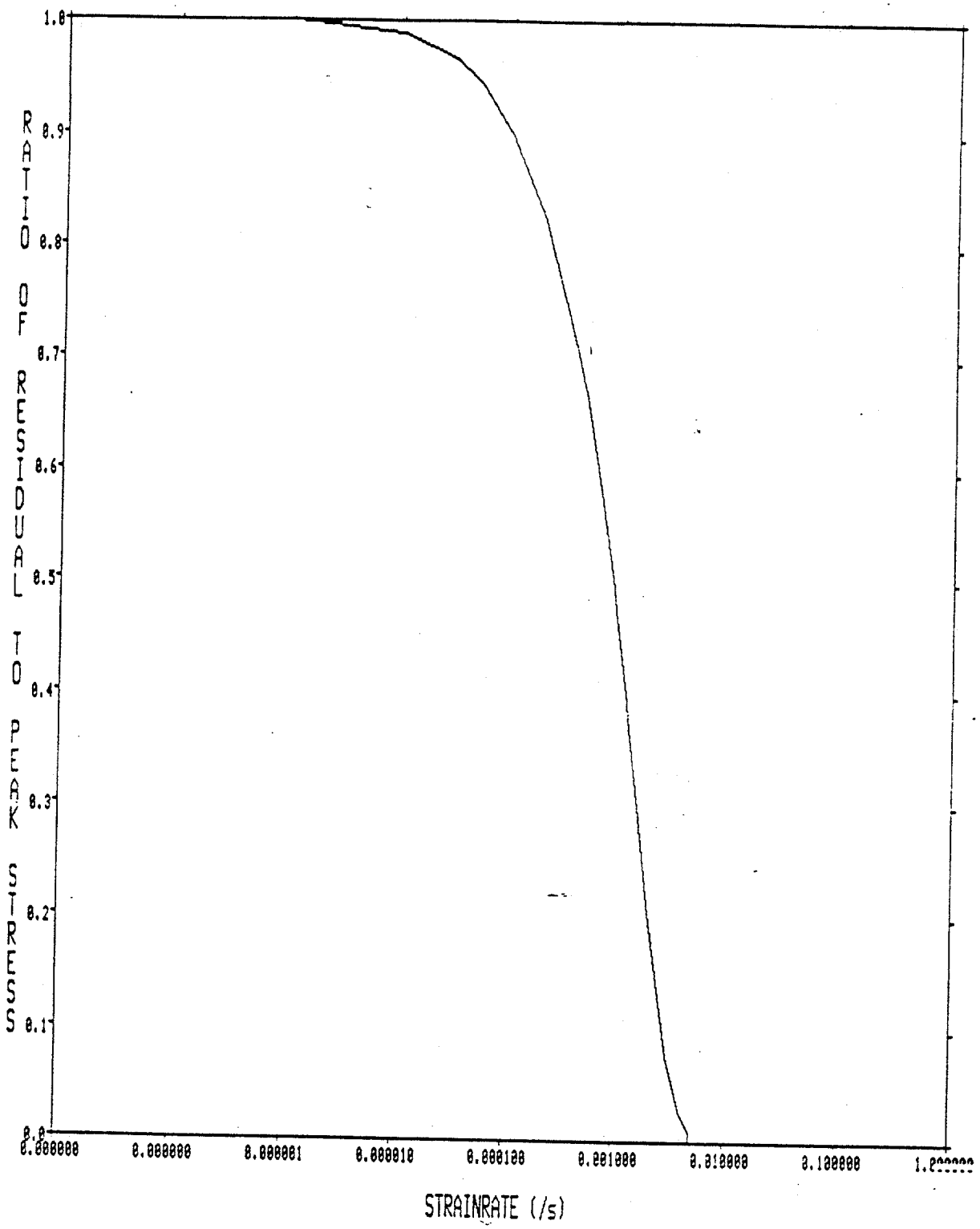

Fig. 17 Ratio of residual stress to stress at maximum versus strainrate

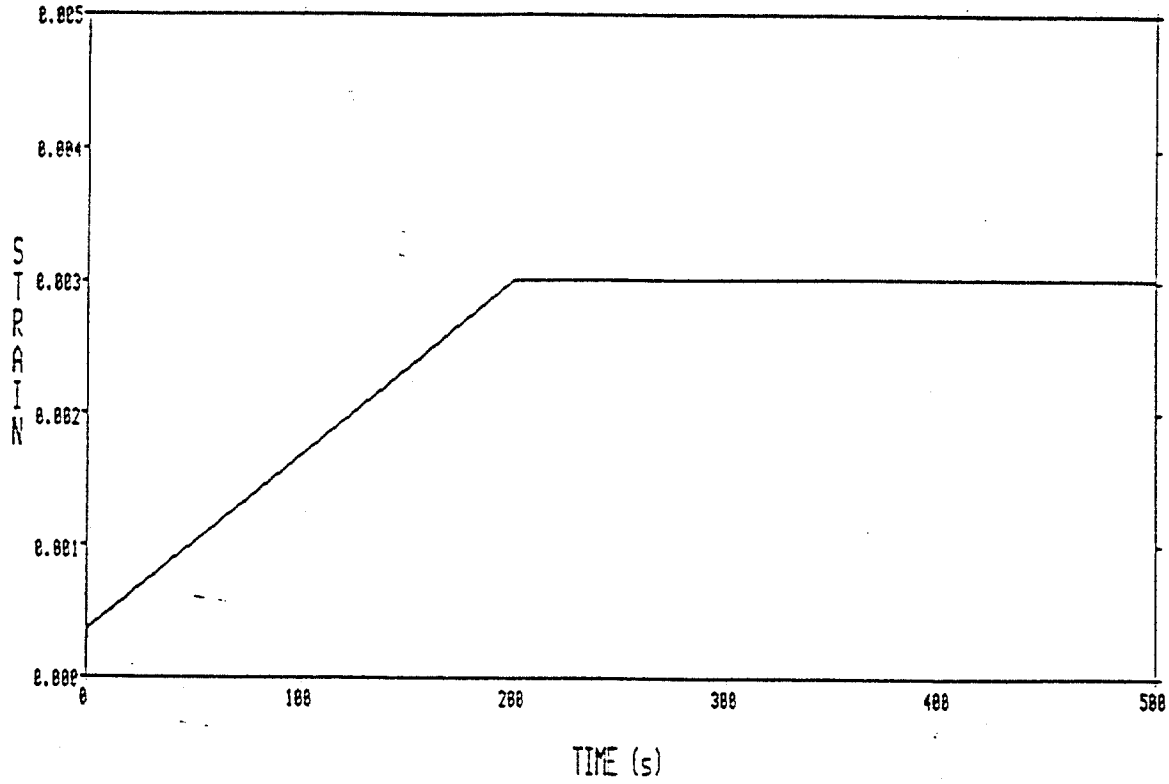

STRESS HISTORY

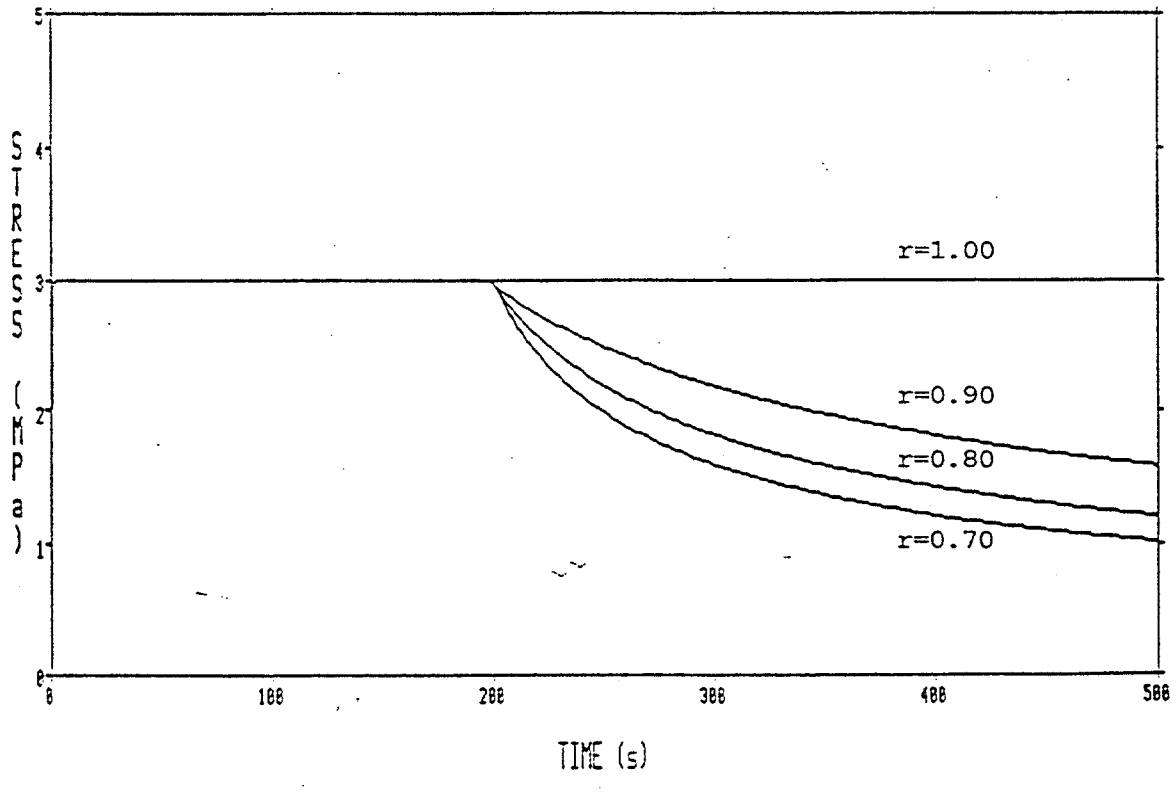

— — r=1.00
— — r=0.90
— — r=0.80
— — r=0.70

Fig. 19 Stress Relaxation

STRESS versus STRAIN

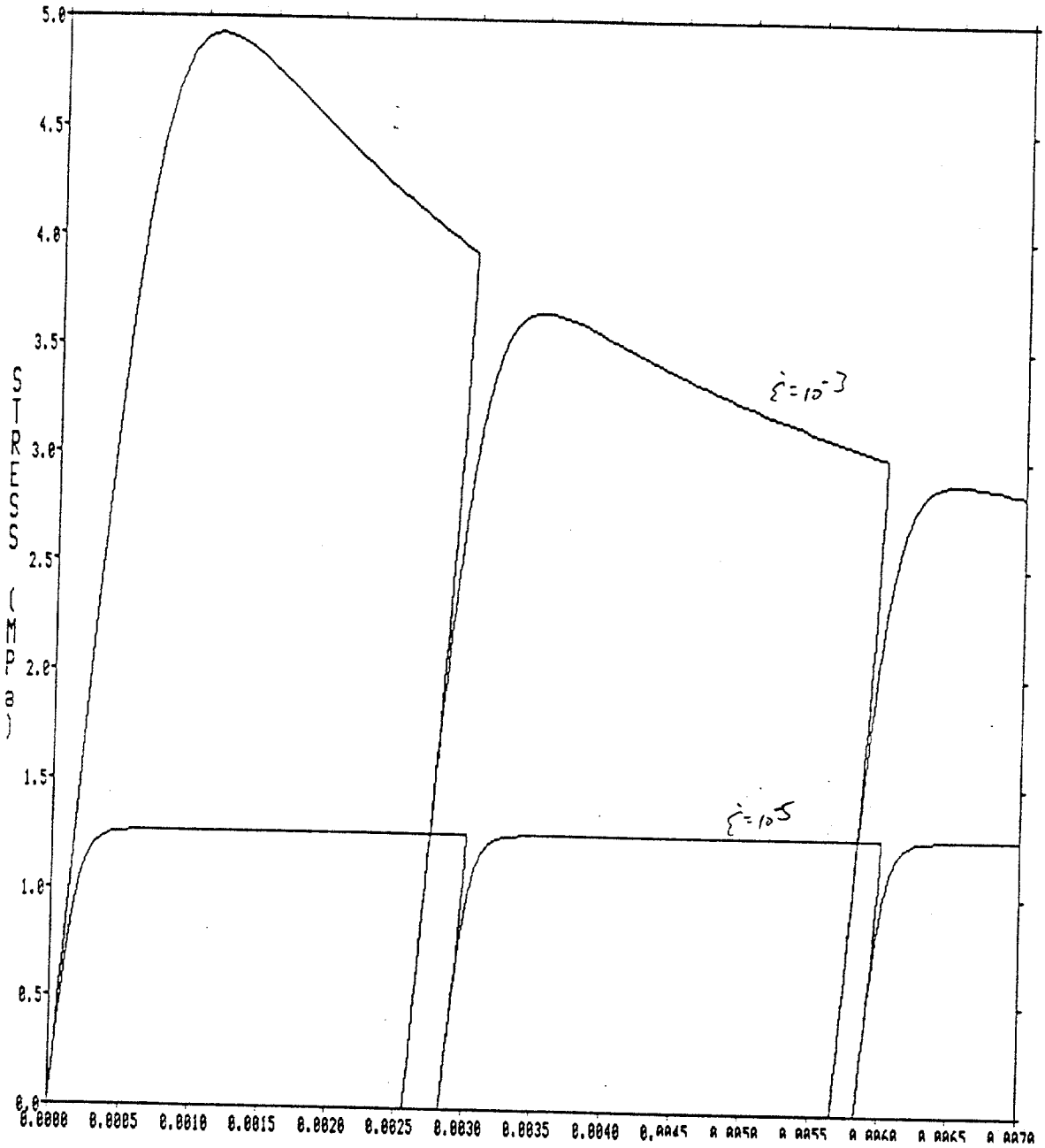

Fig 19

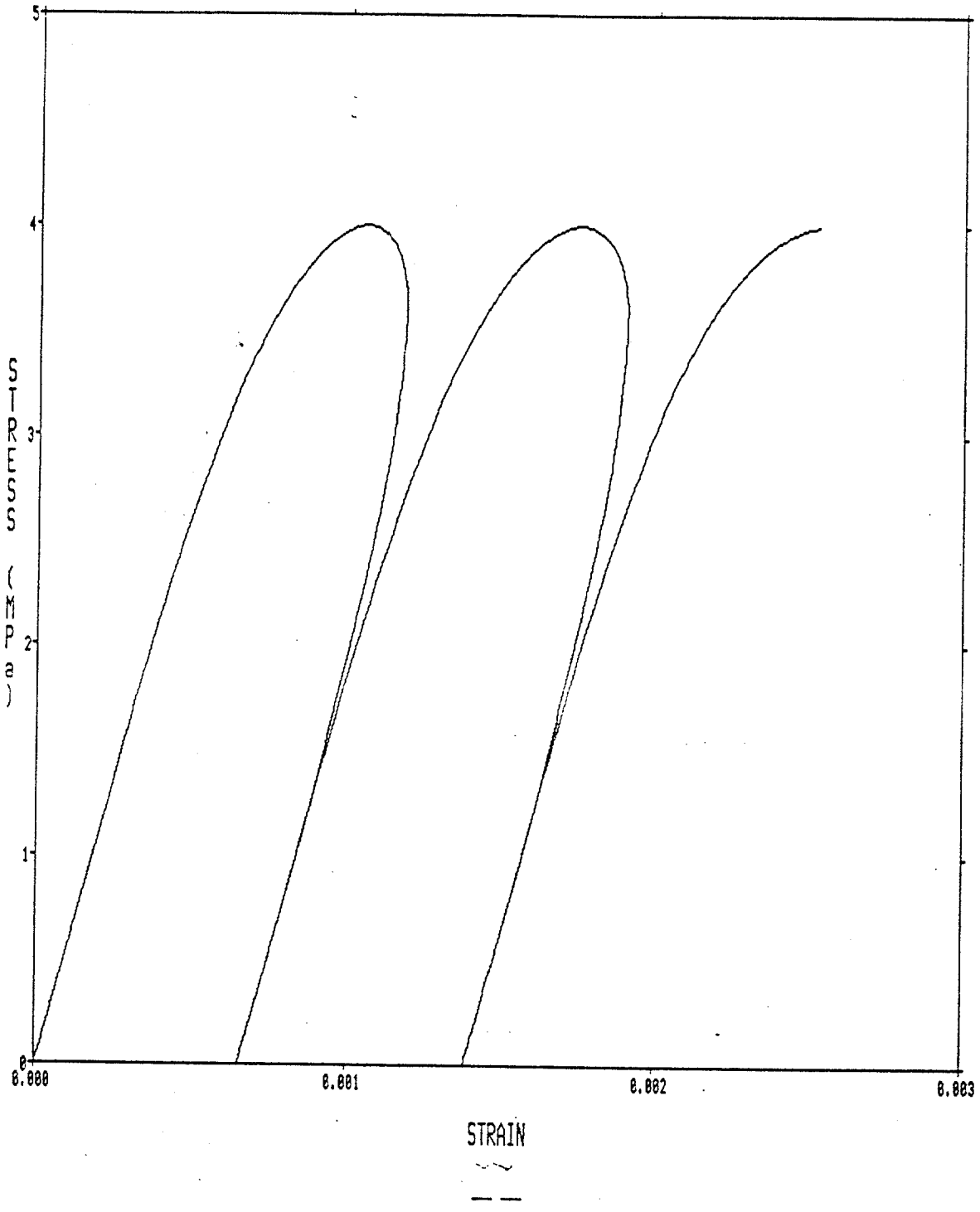

Fig 20 Cyclic stress loading.

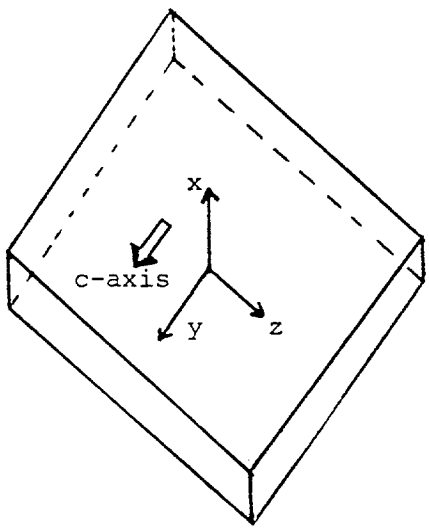

Fig. 22 C-axis Orientation.

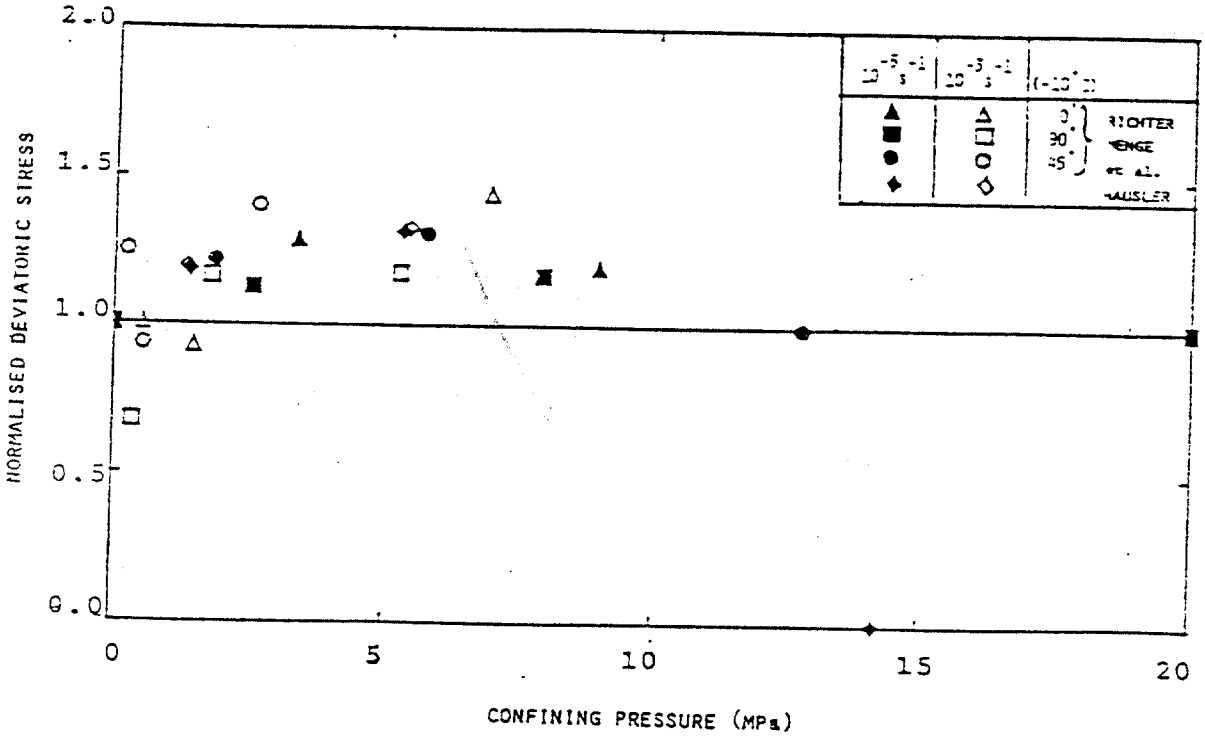

Fig. 22 - Normalised Deviatoric Stress Versus Confining Pressure